"*Considerate la vostra semenza:*
fatti non foste a viver come bruti,
ma per seguir virtute e canoscenza".

(Dante Alighieri, Divina Commedia)

Abstract

This Ph.D. thesis focuses on two main topics:

A) Resorc[4]arene ω-Undecenyl Esters as Preorganized Synthons for Olefin Metathesis.

The preparation of *C*-alkylated resorc[4]arenes by tetramerization in the presence of ethereal BF$_3$ of opportunely substituted 2,4-dimethoxycinnamates prompted us to study both the versatility of the reaction and the chemical and physical properties of the new macrocycles obtained, as depending on the variation of the side chains. We previously designed, synthesized and studied C-alkylresorc[4]arenes able to form a complex with cations such as Cu(II), Fe(III) or Ga(III), to recognize chiral amino acids and to entrap nitrosonium (NO$^+$) cation and to interact with protein surfaces. As an extension of our studies on NOx entrapment, with the aim of coupling the complexation feature of the upper rim with the anchorage of the macrocycle to a solid support, we planned to synthesize resorc[4]arenes featuring long aliphatic side chains ending with a vinylidene group. Looking at the terminal double bonds as suitable active sites we planned to submit the new resorcarenes to an olefin metathesis which currently represents a powerful tool in the formation of carbon-carbon bonds, in order to incorporate the macrocycles into polymeric architectures with intriguing mechanical properties. Resorc[4]arene ω-undecenyl esters **1a** (*chair* conformation), **1b** (*cone* conformation), and **1c** (*1,2-alternate* conformation) were synthesized and afterwards submitted to olefin metathesis, using the second-generation Grubbs complex as the catalyst. Different intra- and inter-molecular products with intriguing architectures were obtained. To ascertain the optimal reaction conditions, several experiments were run with resorc[4]arene **1a** as the substrate, in which a variation in the substrate concentration and the catalyst loading was performed.

B) Self-Assembly and Encapsulation Studies of Fullerenes C_{60} and C_{70}. The design and synthesis of preorganized bowl-shaped macrocyclic hosts which can have applications in supramolecular and material chemistry has been of considerable interest in recent years. In particular, calix[n]arenes, resorcarenes, cyclodextrins, and similar macrocyclic frameworks have been studied, all providing efficient shape complementarity to spherical, mostly C_{60} fullerene, guests. We focused our attention on basket-like resorc[4]arene **3b**, obtained by olefin metathesis of the *cone* resorc[4]arene ω-undecenyl ester **1b** synthesized as described in Part A.

X-ray diffraction analysis of **3b** revealed an auto-complexing ability culminated in the formation of a *trio* of molecules as a brick unit. Notably, the three-some arrangement is responsible for a peculiar chiral behaviour that is the loss of a symmetry element by the (relative) position of the univocally blocked side chains. This trimeric arrangement of basket resorc[4]arene **3b** is an example of supramolecular chirality. To indentify the supramolecular interaction involved, the aggregates have been investigated by UV-vis spectroscopy in solution and in binary (THF/H_2O) solution, **3b** exhibits a strong tendency to self-aggregation, provided that the Hildebrand polarity index, δ, of the solvent is higher than about 15.

The optimal behavior of the resorc[4]arene **3b** in the self-assembly process suggested us to promote its supramolecular interaction with fullerenes C_{60} and C_{70} as guests. We report an exhaustive computational study, with the aim to investigate the type of supramolecular recognition involved in the host–guest complexation. The interaction of **3b** with C_{60} and C_{70} has been experimentally demonstrated by UV measurements.

Table of Contents

Part A

Resorc[4]arene ω-Undecenyl Esters as Preorganized Synthons for Olefin Metathesis

Part B

Part A

Resorc[4]arene ω-Undecenyl Esters

as Preorganized Synthons for Olefin Metathesis

Chapter A1

General Introduction

A1.1 Emerging class of macrocyclic receptors

A1.1.1 Calixarenes

Calixarenes are macrocyclic molecules containing phenolic rings bridged by methylene groups and are among the most ubiquitous host molecules in supramolecular chemistry (Arduini et al., 2001; Casnati et al., 2003; Gutsche, 1998; Katsuhiko and Toyoki, 2006; Ludwig, 2005; Mandolini and Ungaro, 2000). The basic molecular scaffolds are, in general, simple to prepare in high yields from cheap starting compounds: they derive from the condensation of phenols and formaldehyde. These compounds are characterized by an hydrophobic cavity which allows the interactions with neutral molecules (Arduini et al., 2001), but they can also be derivatized in the lower rim or in para positions on the aromatic nuclei (upper rim) with catalytic centers or other functional groups which favor interactions with ions (Figure 1.1) (Dalla Cort and Mandolini, 2000).
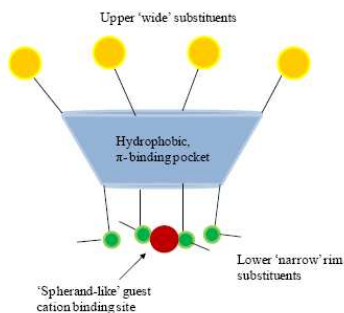
3

Figure 1.1 Anatomy of a calix[4]arene in the *cone* conformation.

The parent calixarenes are flexible during their high temperature synthesis, the rotation of the phenolic moieties about the bridging CH_2 groups possible, but the smallest members of the class "freeze out" upon cooling to ambient temperatures (Steed and Atwood, 2009). This is an important consideration when working with calix[4]arenes, macrocyclic molecules consisting of four phenol units connected via methylene bridges in the *ortho* position with respect to the hydroxyl group. They exist in different conformers that are hard to interconvert and become immobilized in a particular case if substituents are bound in the lower rim, even if re-heated to relatively high temperatures. Four principal conformers are observed at room temperature (Fig 1.2). If all four upper rim substituents are in the same orientation, then a *cone* conformer results, which is the average C_{4v} symmetry structure resulting from a

fast equilibrium between two equivalent C_{2v} *flattened cone* conformers (Abis et al., 1988). If one phenolic group is inverted with respect to the others, a *partial cone* conformer is found. Finally, two possibilities exist when two phenol rings are inverted: *1,3-alternate* and *1,2-alternate*. Similar descriptions exist also for larger calixarenes, although these compounds are often conformationally dynamic and only frozen out in the solid state or in low temperature experiments.
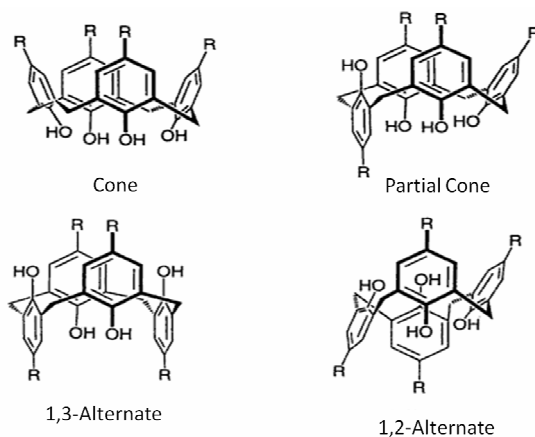

Figure 1.2 Calix[4]arene conformers.

A1.1.2 Resorcarenes

Condensation products obtained from the reaction between aliphatic aldehyde and resorcinol were first reported in the XIX

5

century (Baeyer, 1872a; Baeyer, 1872b), but only in 1968 their structure was finally proved by Erdtman and co-workers by a single crystal X-ray analysis (Erdtman et al., 1968). A suitable trivial name for these molecules was not found earlier, but recently the term resorc[4]arene (or resorcarene, in a shorter version) seems to be generally accepted to indicate cyclic tetramers made by resorcinol units connected with methylene bridges. A simplified general structure of a resorcarene is shown in Figure 1.3 with typical atoms (Botta et al., 2005).
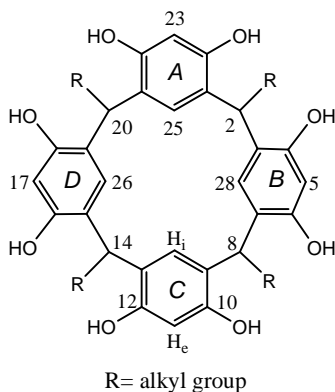

R= alkyl group

Figure 1.3 General structure of resorcarenes.

❖ *Conformations of resorcarenes*

The stereochemistry of resorcarenes may be defined as the combination of three elements (Timmerman et al., 1996):

1. The conformation of the macrocyclic ring, which can adopt five extreme symmetrical arrangements: *crown* or *cone* (C_{4v} symmetry), *boat* or *flattened cone* (C_{2v}), *diamond* or *1,2-alternate* (C_s), *saddle* or *1,3-alternate* (D_{2d}), and *chair* (C_{2h}). The five architectures are presented both in 3D (Fig. 1.4) and in sketched representations (Fig. 1.5). The most common conformation of resorc[4]arenes (*cone*) is very close in solution to the one of calixarenes, but it is, in reality, the result of the equilibrium between two equivalent forms (Högberg, 1980a, Högberg, 1980b). Only one form (namely, *flattened cone*) characterizes the structure of the macrocycle in solid (Erdtman et al., 1968) and gas (Botta et al., 1994) phases.
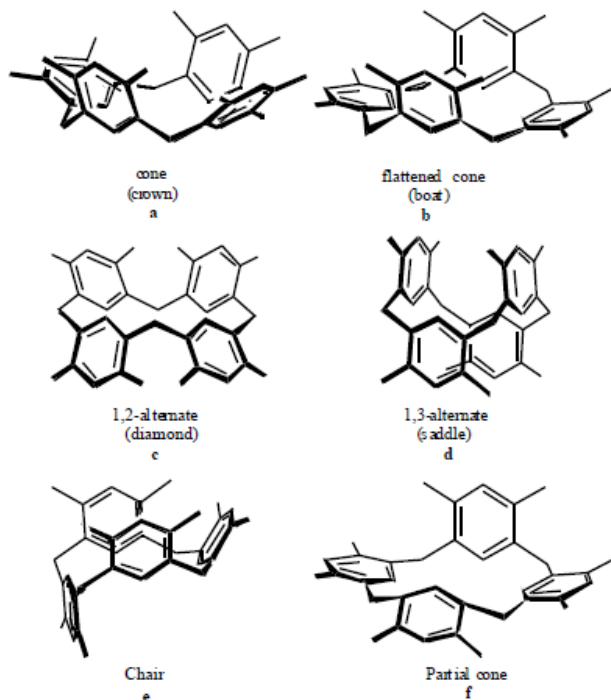
Figure 1.4 Principal conformations (and symmetry) for the resorc[4]arene.
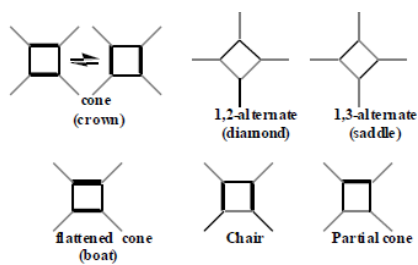

Figure 1.5 Sketched conformations.

Octamethoxyresorcarenes have also been found in two different *chair*-like forms, named *flattened partial cone 1* (**f**) (Botta et al., 1994) and *flattened partial cone 2* (Botta et al., 1997), coincident with the previously reported "*chair*" (**e**) (Abis et al., 1988).

2. The relative configurations of the side chains at the methylene bridges: the arrangements of the substituents were ruled by Högberg (Fig 1.6), who took as a reference the side chain on the C-2 methine (*r*) and considered the relative positions (*cis* or *trans*, i.e. *c* or *t*) of the other CH in the sequence (C-8, C-14, C-20). The substituents of the *cone* and 1,3-*alternate* forms are all cis (or *rccc*). The substitution pattern of *1,2-alternate* is *rctc*, where it is evidenced the anomalous position of the C-14 substituent. The substitutions found for *flattened partial cone* 1 and *chair* were *rccc* and *rctt*, respectively, but other arrangements cannot be excluded.
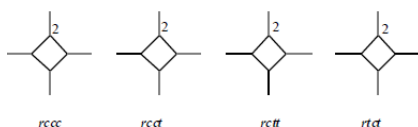

Figure 1.6 Substituents distribution pattern.

3. The individual configuration of the substituents at the methylene bridge, which, in conformations of the macrocycle with C symmetry,

9

may be axial or equatorial. In the sketched structures of figure 1.5, axial substituents are represented with a dotted line.

❖ *Synthesis of resorcarenes*

Condensation of resorcinol with aldehydes

The acid-catalyzed condensation reaction between resorcinol and an aliphatic or aromatic aldehyde (Scheme 1.1) is generally carried out by heating the constituents to reflux in a mixture of ethanol and concentrated HCl for several hours (Egberink et al., 1992; Tunstad et al., 1989; Thoden van Velzen et al., 1994). Each aldehyde, in an almost unlimited range of R options, requires different optimal conditions, while unsubstituted resorcinol (1,3-dihydroxybenzene, X=H) is the mostly used counterpart. 2-Methylresorcinol (X=Me) (Konishi et al., 1990) or pyrogallol (1,2,3-trihydroxy benzene, X=OH) (Cometti et al., 1992) have been preferentially used in the reaction with formaldehyde to obtain better yields. A number of different 5,11,17,23-tetrahydroxyresorc[4]arenes (pyrogallo[4]arenes) have been obtained *via* acidic condensation of 2-hydroxyresorcinol with the appropriate aldehyde in mixtures of HCl, ethanol, and water. Tetra-*n*-nonyl-, tetra-*n*-octyl-, tetra-isobutyl-, tetraethyl-, tetramethyl-, and tetrakis(biphenylyl)-hydroxyresorcarenes has been prepared in this way (Gerkensmeier et al., 2001). The substituents, with some exceptions, presented an axial all-*cis*

10

configuration, which forced the cyclic tetramer to assume a bowl-like shape and form polarity-induced double layers (Gerkensmeier et al., 2001), in the solid state. Resorcinol derivatives carrying electron-withdrawing substituents, like NO_2 or Br at C-2 or featuring partially alkylated hydroxyl groups do not give cyclization. The resorcarenes synthesized throughout the years till the end of 1994 are listed in a review by Reinhoudt and co-workers (Timmerman et al., 1996).
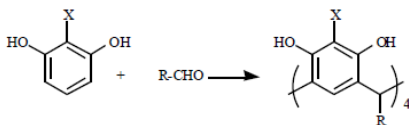
Scheme 1.1 Classical synthesis of resorcarenes X=H, Me,OH.

Tetramerization of resorcinol dimethyl ether derivatives by Lewis acid

It has been seen that treatment of (*E*)-2,4-dimethoxycinnamic acid esters **1** (R = COOMe, COOEt, COOiP) with $BF_3 \cdot Et_2O$ in $CHCl_3$ at reflux (Scheme 1.2) gives after 15 min the corresponding octamethylated resorcarene **2** (R=COOMe, COOEt, COOiP) in 75% overall yield, as a mixture of *cone*, *1,2-alternate* and *1,3-alternate* forms (Botta et al., 1992).

11
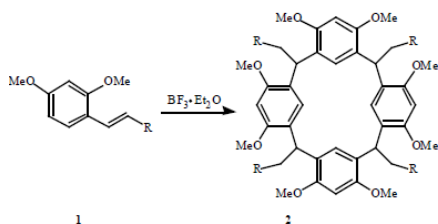
Scheme 1.2 Tetramerization of cinnamic acid derivatives.

Indeed, this simple reaction allows the design of several new structures: the versatility of the reaction does not depend only on the variability of R group in the monomer, but also on the possible modifications of the side chains, CH_2R. Each new structure is a potential owner of characteristics that may introduce into a novel research avenue.

As an example Botta *et al.* synthesized double-spanned resorc [4]arenes treating octamethylated resorc[4]arenes with glutaroyl, adipoyl and pimeloyl dichlorides in the presence of triethylamine (Botta *et al.*, 1997). The insertion of two polymethylene bridges led to the formation of a cavity-shaped architecture resembling a basket which gave the name to these molecules (Fig 1.7). NMR characterization showed a C_{2v} symmetry with two parallel bridges: the formation of the bridge froze one of the two *flattened cone* conformations, which are normally in fast equilibrium to get the *cone* conformation as average (Figure 1.7).
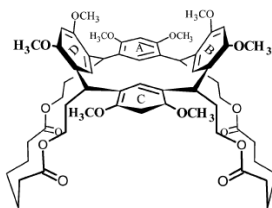
Figure 1.7 Chemical structure of a basket resorc[4]arene with two polymethylene bridges.

Analogously, when 2,4-dimethoxybenzyl alcohol **6** was treated with trifluoroacetic acid (5% in CHCl$_3$), the unsubstituted resorcarene **7a** was obtained in 95% yield (Scheme 1.3) (Falana et al., 1994). Notably, compound **7a** cannot be synthesized by the acid-catalyzed condensation of resorcinol and formaldehyde, since this reaction gives only polymeric products (Gutsche et al., 1983; Gutsche et al., 1989; Gutsche et al., 1995; Böhmer, 1995; Mandolini and Ungaro, 2000; Asfari et al., 2001). Lewis acid catalyzed also the condensation (Scheme 1.3) of 1,3-dimethoxybenzene (**8**) with isovaleraldehyde (**9**), to give **7b**; in particular, SnCl$_4$ led to selective formation in high yield of the *rccc* isomer.
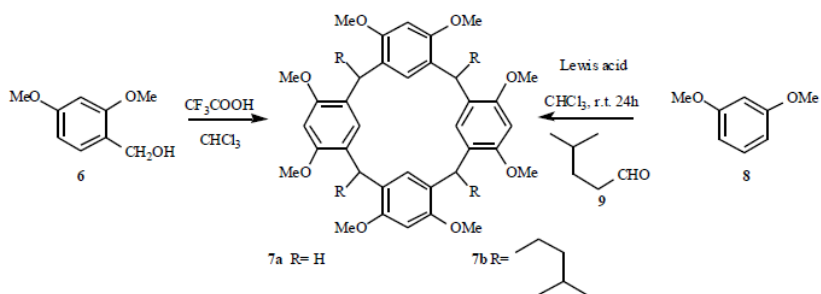
Scheme 1.3 Octamethoxyresorcarenes by Lewis acid catalyzed reaction.

A1.2 The metathesis reactions: from a historical perspective to recent developments

Metathesis, with its multiple aspects, has become one of the most important chemical reactions and is now extremely useful. This area has gone beyond the research stage in inorganic and organometallic chemistry to develop in organic, medicinal, polymer and materials chemistry to such an extent that it has now become a familiar tool for the specialists of these fields (Astruc, 2005).

A1.2.1 Metathesis: fragments changing place

The etymology of the word metathesis comes from the Greek μεταθεσιζ (metathesis) that means transposition. Thus, metathesis is invoked when, for instance, ions are exchanged in a solution containing two ion pairs in order to produce the most stable ion pairs [eqn. (1)] (Loupy et al., 1992). In the same way, two carbenes of an olefin can be exchanged to give, if they are different, another recombination leading to the two symmetrical olefins [eqn. (2)] or the two carbynes of an alkyne to give the two symmetrical alkynes [eqn. (3)].

$$A^+B^- + C^+D^- \rightleftharpoons A^+D^- + C^+B^- \qquad (1)$$

(2)

(3)
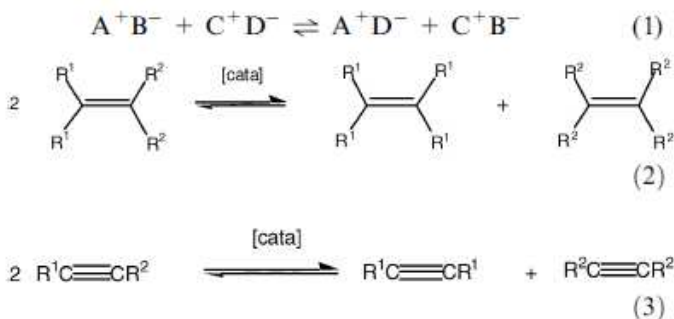
Although the name metathesis was given for the first time to this reaction by Calderon in the seventies (Calderon, 1967; Calderon, 1972) the first observation of the metathesis of propene at high temperature was reported in 1931. Twenty years later, industrial chemists at Du Pont, Standard Oil and Phillips Petroleum reported that propene led to ethylene and 2-butenes when it was heated with molybdenum (in the form of the metal, oxide or [Mo(CO)$_6$] on alumina) (Banks and Bailey 1964; Rouhi 2002). The first polymerization of norbornene by the system WCl$_6$/AlEt$_2$Cl was independently reported in 1960 by Eleuterio (Eleuterio, 1960; Eleuterio, 1991) and by Truett (Truett et al., 1960), but it was recognized only in 1967 that ROMP (*ring opening metathesis polymerization*) and the disproportionation of acyclic olefins were the same reaction. A detailed historic account was reported by Eleuterio (Eleuterio, 1991). The metathesis reactions are in principle

16

under thermodynamic control, that is they are equilibrated, which clearly is an inconvenience. In fine chemical synthesis, this problem can be circumvented by choosing to carry out metathesis of a terminal alkene or alkyne. The formation of ethylene (or respectively, acetylene) displaces the reaction towards the product. This strategy also applies to olefins terminated by an ethylidene group, because metathesis then produces 2-butenes whose volatility also displaces the reaction towards the products. Operating under reduced pressure insures elimination of the volatile olefin in order to displace the metathesis reaction [eqns. (4) and (5)]. In fact, many metathesis reactions are under kinetic control. Notably alkene metathesis is most often complicated by the formation of both Z and E isomers [eqn. (4)], whereas this problem does not exist in alkyne metathesis [eqn. (5)], disclosed for the first time by Blanchard, Mortreux and coworkers (Blanchard and Mortreux, 1972; Blanchard and Mortreux, 1975; Mortreux et al., 1977; Mortreux et al. 1978; Mortreux et al., 1995; Bunz, 2002; Bunz, 2003; Grela and Ignatowska, 2002; Zhang, 2003; Zhang et al., 2004; Zhang and Moore 2004).

$$2 \quad \overset{R^1}{\underset{R^2}{>}} = \quad \xrightarrow{[cata]} \quad = + \overset{R^1}{\underset{R^2}{>}}\overset{R^1}{\underset{R^2}{<}} + \overset{R^1}{\underset{R^2}{>}}\overset{R^2}{\underset{R^1}{<}} \tag{4}$$

$$2 \ R^1C{\equiv}CH \quad \xrightleftharpoons{cata} \quad HC{\equiv}CH \ + \ R^1C{\equiv}CR^1 \tag{5}$$
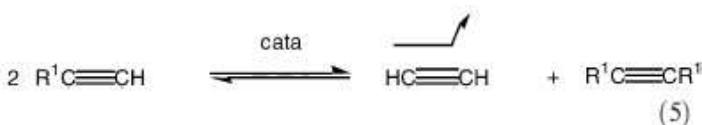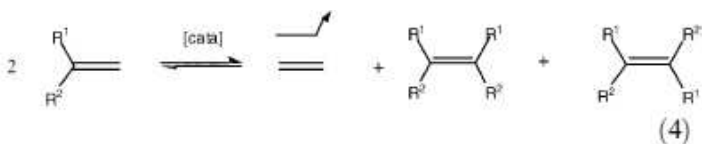
A1.2.2 The Chauvin mechanism

At the end of the 1960's, the metathesis reaction was very mysterious. Catalytic systems were either oxides such as WO_3/ SiO_2 used in industry for the transformation of propene to ethylene and butenes or Ziegler–Natta derived systems such as WCl_6 (or $MoCl_5$) + AlX_nR_{3-n} or (SnR_4). Mechanistic ideas had appeared, but they did not match the results of some metathesis experiments. In the process of thinking about the metathesis mechanism, Yves Chauvin from the Institut Français du Pètrole, had taken into account the report of Fischer on the synthesis of a tungsten-carbene complex (Fischer, 1964), that of Natta on the polymerization of cyclopentene by ring opening catalyzed by a mixture of WCl_6 and $AlEt_3$ (Natta, 1964) and that of Banks and Bailey on the formation of ethylene and 2-butene from propene catalyzed by [$W(CO)_6$] on alumina (Banks and Bailey, 1964). Consequently, Chauvin and his student Jean-Louis Hérisson

published their proposition of metathesis mechanism in 1971 (Scheme 1.4) (Hérisson and Chauvin, 1971). The latter involves a metal-carbene species (or more precisely metal-alkylidene), the coordination of the olefin onto the metal atom of this species, followed by the shift of the coordinated olefin to form the metallocyclobutane intermediate, and finally the topologically identical shift of the new coordinated olefin in the metallocyclobutane in a direction perpendicular to the initial olefin shift. This forms a metal-alkylidene to which the new olefin is coordinated, then liberated. This new olefin contains a carbene from the catalyst and the other carbene from the starting olefin. The new metalalkylidene contains one of the two carbenes of the starting olefin and it can re-enter into a catalytic cycle of the same type as the first one. In fact, depending on the orientation of the coordinated olefin, the new catalytic cycle can give two different metallacyclobutenes, one leading to the symmetrical olefin and the other one leading the starting olefin. This latter cycle is said to be degenerate olefin metathesis. Thus, the catalytic cycles alternatively involves both metal-alkylidene species resulting from the combination of the metal with each of the two carbenes of the starting olefin. Hérisson and Chauvin not only suggested the metallacyclobutane mechanism, but also published several experiments to confirm it.

1°) INITIATION

2°) PROPAGATION

degenerate metathesis

degenerate metathesis
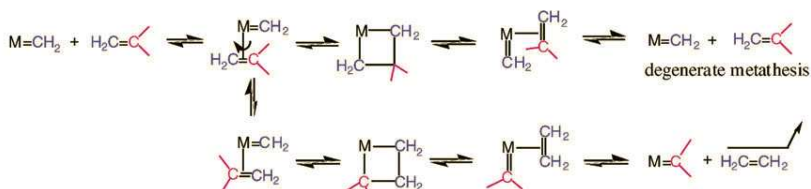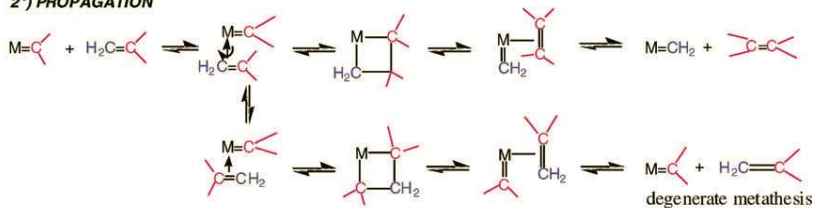
Scheme 1.4 Chauvin's mechanism, proposed in 1971, for the catalyzed olefin metathesis involving metal alkylidene and metallacyclobutane intermediates.

Chauvin's mechanism introduced several new ideas. First, it proposed the implication of a metal-carbene complex to initiate the catalysis of the metathesis reaction. This idea first suggested that

one could just synthesize metal-alkylidene complexes and let them react as catalysts with olefins to carry out the metathesis reaction.

It was in 1980 that Dick Schrock's group at MIT reported a tantalum-alkylidene complex, [Ta(=CH–t-Bu)Cl(PMe$_3$)(O–t-Bu)$_2$], which catalyzed the metathesis of cis-2-pentene (Schrock et al., 1980). This provided the very first proof for Chauvin's mechanism of olefin metathesis with a well-defined high oxidation state alkylidene complex, almost a decade after Chauvin's proposal. Molybdenum and tungsten, however, were obviously the most active metals in alkene metathesis and, around 1980, Schrock and his group considerably increased their efforts in the search for stable molecular alkylidene and alkylidyne complexes of these metals that would catalyze the metathesis of unsaturated hydrocarbons. This search was successful (Wengrovius et al., 1980) and eventually produced a whole family of molybdenum- and tungsten-alkylidene complexes of the general formula [M(=CHCMe$_2$Ph)(=N–Ar)(OR$_2$), R being bulky groups. These compounds presently are the most active alkene metathesis catalysts (Fig. 1.8) (Schrock et al., 1990; Bazan et al., 1990; Bazan et al., 1991).

The advantage of Schrock's catalysts, whose most efficient members were reported in 1990, was that even though they are extremely active, they are molecular (without additives) and also provided a commercial catalyst and chiral versions for the first

21

examples of asymmetric metathesis catalysis (Aeilts et al., 2001; Teng X. Et al, 2002; Tsang et.al., 2003a; Tsang et.al., 2003b).

Schrock's closely related Mo-alkylidyne complexes do not react with olefins, but they selectively and efficiently metathesize alkynes without the need for a co-catalyst.
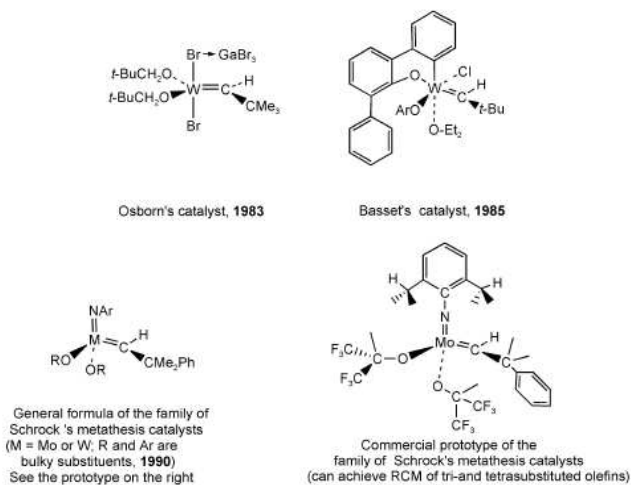
Figure 1.8 Main families of molecular Mo and W metathesis catalysts.

A1.2.3 Transition metal catalysts

Two classes of metal-alkylidene complexes are usually distinguished: those containing a nucleophilic carbene of the Schrock type and those with an electrophilic carbene of the Pettit type (Guerchais and Astruc, 1985). A related Fischer-type ruthenium complex, [RuCp{=C(Me)OMe}(CO)(PCy$_3$)][PF$_6$], stabilized by a methoxy group on the carbene carbon, was synthesized by Malcolm Green's group at Oxford in 1971. This was the first reported ruthenium-carbene complex (Green et al., 1971). The reactivity of this type ruthenium complexes towards olefins is again cyclopropanation, because of the strongly electrophilic character of the carbene ligand due to the positive charge, further increased by the electron-withdrawing carbonyl ligands (Fig. 1.9). Grubbs had been interested for a long time in the metathesis reaction, as indicated by his mechanistic proposal of a metallocyclopentane intermediate (Grubbs, 1972). He had noticed Natta's 1965 publication on the catalysis by RuCl$_3$ of the polymerization of cyclobutene and 3-methylcyclobutene by ring opening (Natta et al., 1965; Grubbs and Tumas, 1989). This process (in butanol) had been developed by Norsorex. In this context, the Ziegler–Natta polymerization of olefins under mild conditions obviously had a considerable impact on polymer chemistry. The delineation of a

23

new polymerization mechanism, however, was not a simple task. Wellinspired by this approach, Grubbs published in 1988 the polymerization of 7-oxanorbornene into a high molecular weight monodisperse polymer (Mw = 1.3 x 106 g mol⁻1; Mw/ Mn = 1.2) by $RuCl_3$ or $[Ru(H_2O)_6]$ $(OTs)_2$ (OTs = toluene sulfonate). This catalysis was all the more remarkable as it was conducted in water (Novak and Grubbs, 1988).
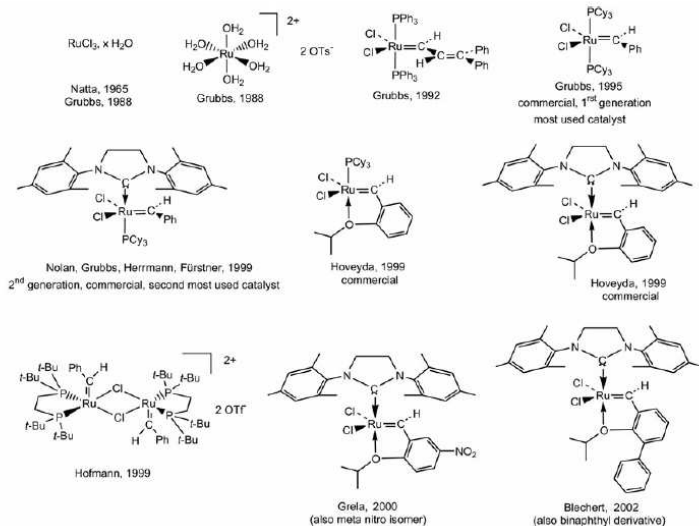
Figure 1.9 Grubbs-type (or derived) ruthenium metathesis catalysts, air-stable and compatible with most functional groups.

Shortly afterwards, he could show, in the course of the same reaction, the formation of a Ru-alkylidene intermediate, then the polymerization of cyclooctene, an olefin with little constraints,

24

when the alkylidene ligand source was ethyl diazoacetate added to the aqueous solution of [Ru(H$_2$O)$_6$] (OTs)$_2$ (France, 1993; Nguyen, 1992; Nguyen, 1992; Schwab, 1998). Consecutively and according to the same logic, a great step forward was accomplished by Grubbs in 1992. He reported the first molecularly well-defined ruthenium-carbene complex that promoted the *ring opening metathesis polymerization* (ROMP) of low-strain olefins as well as the catalytic *ring-closing metathesis* (RCM) of functionalized dienes. Grubbs showed that these vinylidene complexes, [RuCl$_2$(PR$_3$)(=CH–CH=CPh$_2$)] (R = Ph or Cy), were efficient molecular catalysts for these polymerization reactions (Scheme 1.5) and other metathesis reactions such as those involving ring closing of terminal diolefins.
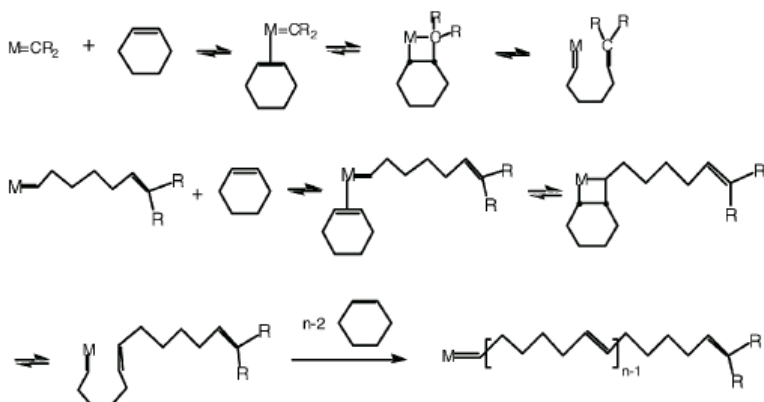
Scheme 1.5 Metathesis mechanism for the ring-opening metathesis polymerization (ROMP) of a cyclic olefin.

25

In 1995, the new molecularly well-defined catalysts [Ru(=CHPh)Cl$_2$(PR$_3$)$_2$], R = Ph or Cy, whose structures are closely related to the vinylidene ones published three years earlier, appeared and were commercialized with R = Cy (Fig. 1.9). [Ru(=CHPh)Cl$_2$(PCy$_3$)$_2$] is now known as the **first generation Grubbs** catalyst and is still today the most used metathesis catalyst by organic chemists, because of its stability to air and compatibility with a large variety of functional groups (except for amines and nitriles and basic media).

Fine mechanistic studies with this catalyst led Grubbs' group to conclude that the mechanism first involved the dissociation of one phosphine to generate the reactive 14-electron ruthenium intermediate. In order to accelerate this dissociative step, Grubbs introduced, in place of one phosphine, one of Arduengo's cyclic bis-amino carbene ligands that are relatively stable, even in the free forms obtained by deprotonation of the corresponding imidazolium cation (Arduengo, 1999; Herrmann and Köcher, 1997; Bourissou et al., 2000; Wetskamp T. et al., 1998). It is Herrmann's group that first synthesized ruthenium complexes with two such carbene ligands in the context of the catalysis of olefin metathesis, but their catalytic activity was shown to be modest. In **first generation Grubbs catalysts** containing only one such ligand, they increase the electron density at the ruthenium center, however, and their trans effect

labilizes the ruthenium-phosphine bond, favoring phosphine dissociation. Thus, the **second generation Grubbs catalysts** [RuCl$_2${C(N(mesityl)CH$_2$)$_2$}(PCy$_3$)(=CHPh)] and its catalytic activity in metathesis were successively proposed within a few months by the groups of Nolan (Ackermann et al., 1999), Grubbs (Scholl et al., 1999a; Scholl et al., 1999b; Trnka et al., 2003; Love et al., 2003; Chatterjee et al, 2003; Morril and Grubbs, 2003), and Fürstner and Herrmann (Ackermann et al., 1999). It is presently the most used catalyst for efficient cross-metathesis reactions, although it is not tolerant to amines and nitriles (for instance, with acrylonitrile, Schrock's catalyst is efficient, in contrast to the ruthenium catalysts). On the contrary, this new, commercially available, catalyst is even more active although it is also more thermally stable than the first one. Along this line, Hoveyda (Kingsbury et al., 1999; Grela et al., 2002), Hofmann (Hansen et al., 1999; Volland et al., 2004), Grela and Blechert (Connon et al., 2002; Wakamatsu and Blechert, 2002a; Wakamatsu and Blechert, 2002b; Dunne et al., 2003) reported other related, very active, stable and functional-group tolerant ruthenium metathesis catalysts. The first Hoveyda metathesis catalyst is derived from Grubbs' first generation catalysts. It bears only one phosphine and a chelating carbene ligand. The second one bears, in addition, Arduengo's carbene instead of the phosphine. Both catalysts are now commercially

available, although expensive. Grela recently reported variations of the Hoveyda catalyst with increased efficiency (active even at 0 °C) when the aryl group of the benzylidene ligand bears a nitro group in the meta or para positions or two methoxy substituents (Fig. 1.9). Grela's successful idea was to destabilize the Ru–O(ether) bond in order to favor the ether decoordination that generates the catalytically active 14-electron species (Grela et al., 2002). The family of Hoveyda catalysts, whose activity compares with that of the second generation Grubbs catalyst, are especially useful for difficult cases of metathesis of polysubstituted olefins and selective cross metathesis (CM) in which homo-coupling needs be avoided (Kingsbury et al., 1999; Honda et al., 2004). The most successful variation of these Ru-benzylidene catalysts so far was reported by Blechert whose strategy to sterically destabilize the Ru–O(ether) bond was to introduce an aryl (phenyl or naphthyl) substituent on the benzylidene aryl in the ortho position relative to the O(ether) (Connon et al., 2002; Wakamatsu and Blechert, 2002a; Wakamatsu and Blechert, 2002b; Dunne et al., 2003). The catalytic efficiency and stability of Blechert complexes surpasses those of all the other Ru catalysts, although it has been shown several times that the catalytic efficiency depends on the type of metathesis reaction examined and the tolerance towards the required functional group.

28

A1.2.4 Intra- and intermolecular olefin metathesis

Olefin metathesis is a metal-catalyzed transformation, which acts on carbon-carbon double bonds and rearranges them via cleavage and reassembly. According to the mechanism, first introduced by Chauvin, the coordination of an olefin to a metal carbene catalytic species leads to the reversible formation of a metallacyclobutane (Scheme 1.6). This intermediate then proceeds by cycloreversion via either of the two possible paths: 1) non-productive—resulting in the re-formation of the starting materials or 2) product-forming— yielding an olefin that has exchanged a carbon with the catalyst's alkylidene. Since all of these processes are fully reversible (Scheme 1.6), only statistical mixtures of starting materials as well as all of possible rearrangement products are produced in the absence of thermodynamic driving forces.
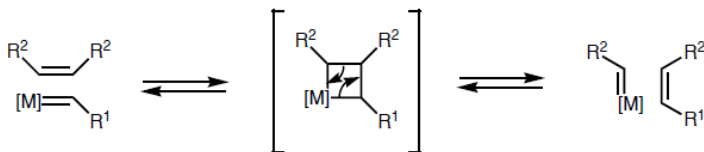
Scheme 1.6 General mechanism of olefin metathesis.

The most important olefin metathesis subtypes are presented in Scheme 1.7. They are currently employed in the synthesis of a large

varierty of small, medium and polymeric molecules, as well as novel materials.
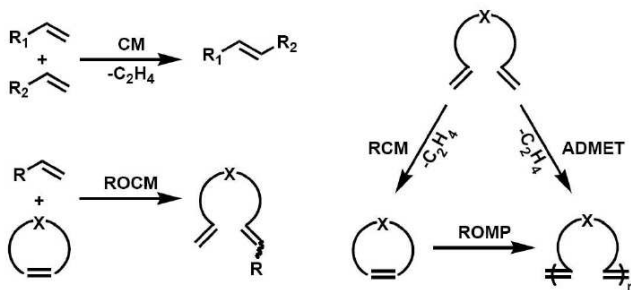
Scheme 1.7 Different types of olefin metathesis, all proceeding according to the Chauvin mechanism and catalyzed by Schrock-type or Grubbs-type catalysts.

Ring-Closing Metathesis (RCM)

Construction of rings is one of the fundamental processes in organic synthesis. Of the various strategies available, cyclization is the most straightforward way of obtaining rings. Commonly employed cyclization methods involve reactions of cationic, anionic or radical species. Common rings such as 5–7 membered ones are easily available by these methods. However, formation of medium or large rings by these methods either proceeds with low yields or does not proceed at all due to unfavourable enthalpic and entropic factors. In recent years, olefin metathesis has emerged as a powerful tool for carbon–carbon bond formation and has enabled the synthesis of rings of different sizes (Ghosh et al., 2006). The construction of

macrocycles by ring-closing metathesis (RCM) is often used as the key step in the synthesis of natural products containing large rings (Conrad and Fogg, 2006). The Chauvin mechanism for olefin metathesis (Chauvin and Hérisson, 1971) involves a sequence of [2+2] cycloadditions and retroadditions, in which the key intermediate is a metallacyclobutane species. Each step of the catalytic cycle is in principle reversible, resulting in an equilibrium mixture of olefins unless a bias can be exerted to drive the reaction in a chosen direction. Ring-closing metathesis of dienes is entropically favoured by the formation of two olefinic products from a single diene precursor (Scheme 1.8). When both olefinic groups in the diene are terminal, one equivalent of ethylene is formed for each cycloalkene, and ring-closing is driven by loss of volatile ethylene.
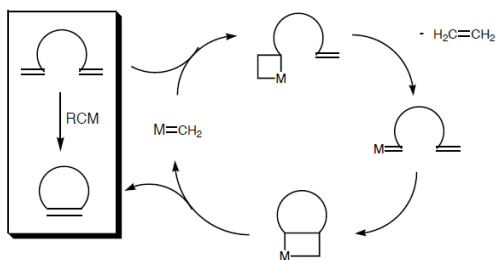
Scheme 1.8 Intramolecular RCM metathesis of a diene to form a cyclic olefin.

Steric parameters favour metathesis of α,ω-olefins over internal olefins, as does the decreased volatility and increased solubility

(Atiqullah et al., 1998) of olefinic coproducts heavier than ethylene. The rate, products, and selectivity of RCM processes are determined by a subtle interplay of substrate and catalyst parameters. Substrate parameters, of course, determine whether a target reaction is thermodynamically feasible. Reaction rates and product selectivity are determined by the interaction of catalyst and substrate properties: the structure-activity relationships are very complex and remain poorly understood.

Cross-metathesis (CM) *and Ring-Opening Cross-Metathesis (ROM-CM)*

Olefin cross-metathesis (CM) can be formally described as the intermolecular mutual exchange of alkylidene (or carbene) fragments between two olefins promoted by metal-carbene complexes (Grubbs and Chang, 1998; Randall and Snapper, 1998). There are two main variations on this theme (Scheme 1.9): a) cross-metathesis (CM) and b) ring-opening cross-metathesis (ROM-CM).

CM is not yet in such widespread laboratory use as the more entropically favorable RCM reaction. However, the development of a second generation of active and robust ruthenium catalysts (see Section A1.2.3), which combine the high activity previously only associated with molybdenum-based catalysts with an impressive functional-group tolerance, has recently allowed many groups to

breathe new life into what were previously in many cases little more than unselective mechanistic curiosities (Hérisson and Chauvin, 1971).
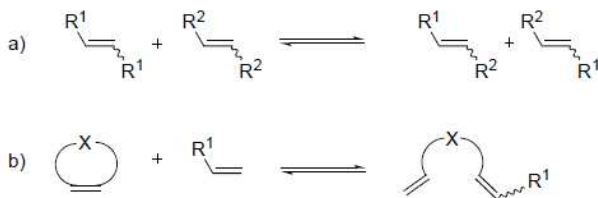
Scheme 1.9 Variations of cross-metathesis (CM).

A general mechanistic scheme for the CM of two symmetrically substituted olefins (in practice, this is quite difficult) is presented in Scheme 1.10. The first step in the catalytic cycle (after the first catalyst turnover to produce A) is a [2+2] cycloaddition reaction between olefin B and a transition metal carbene A to give a metallacyclobutane C. The latter undergoes subsequent collapse in a productive fashion to afford a new olefin product D and a new metal carbine (alkylidene) E, which carries the alkylidene fragment R1. Similarly, E can react with a molecule of F via G to yield D and A, which then re-enters the catalytic cycle. The net result is that D is formed from B and F with A and E as catalytic intermediates.
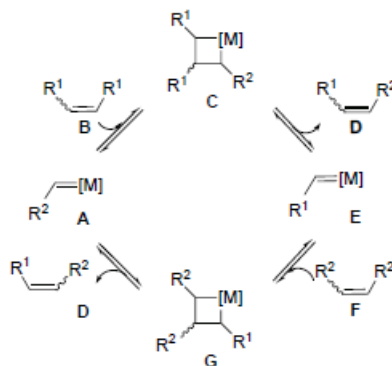
Scheme 1.10 General mechanistic scheme for the CM of the two symmetrically substituted olefins B and F.

The highly efficient and atom-economic ROM–CM reaction has been the subject of much recent investigation. The presumed catalytic cycle for this reaction is shown in Scheme 1.11.
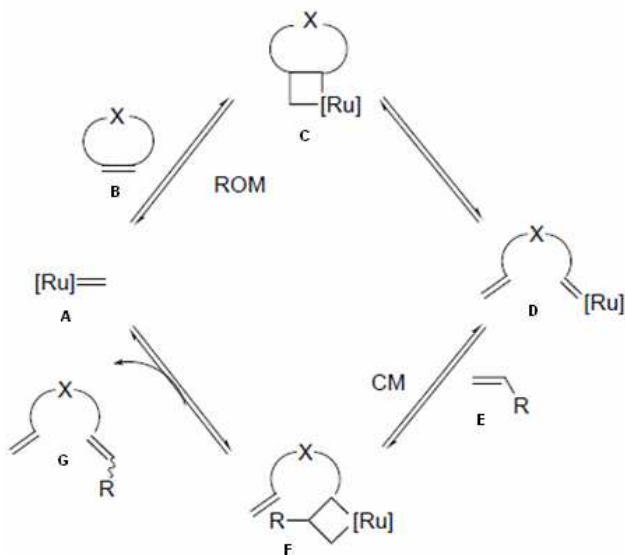
Scheme 1.11 ROM–CM catalytic cycle.

The reaction of ruthenium methylidene A and olefin substrate B furnishes metallacyclobutane intermediate C, which on collapse gives ring-opened alkylidene D. This step is most efficient for highly strained cyclic olefin substrates, in which relief from ring strain provides an energetic counterweight to the entropically favored reverse *ring-closing* reaction (D→A). It is hardly surprising, therefore, that norbornenes, oxanorbornenes, (Schneider and Blechert, 1996a; Schneider and Blechert, 1996b; Schneider et al., 1997a; Schneider et al., 1997b) and cyclobutenes (Randallet al.,

1995; Tallarico et al., 1997; Snapper et al., 1997) are generally excellent substrates for ROM–CM reactions. CM between D and terminal olefin E (internal olefins may also serve as CM partners) then affords ROM–CM product G via intermediate F with loss of the ruthenium methylidene, which then reenters the catalytic cycle. An important condition for ROM–CM to be efficient is that CM between D and E must be faster than the reaction between D and B (a competing ROMP pathway), a factor which very much depends on the nature of the cyclic olefin B and the CM partner E used. However, in the majority of cases, ROM–CM competes effectively with ROMP, particularly under high dilution conditions.

Acyclic diene metathesis polymerization (ADMET)

Traditionally, acyclic diene metathesis (ADMET) is considered to be a step-growth polycondensation-type polymerization, which makes strictly linear chains from unconjugated dienes (Allcock et al., 2001; Wagener et al., 1997).
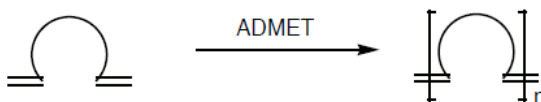
As such, ADMET requires very high monomer conversion rates to produce polymer chains of considerable size. Therefore, the more

36

active 2nd generation catalysts are usually better suited for ADMET than bisphosphine ones. Since the loss of ethylene is the main driving force behind the cross metathesis of terminal olefins, the efficient removal of this volatile gas from the reaction vessel is also crucial. Consequently, although olefin metathesis with ruthenium catalysts is, in general, very mild and does not require stringent air removal, ADMET greatly benefits from conditions which promote the diffusion and expulsion of ethylene (i.e., higher reaction temperatures, application of vacuum, and rigorous stirring). In addition, the use of concentrated or even neat solutions of monomers is usually helpful to polycondensation reactions but, in the case of ADMET, a very viscous solution might be detrimental to efficient stirring and ethylene removal. Furthermore, as a consequence of the poor molecular weight control of stepgrowth reactions, the polydispersity index (PDI) of polymers obtained by this method is usually quite large. However, an important advantage of ADMET is that it allows a large variety of monomers to be polymerized since terminal olefins are quite easy to install. Many functional groups and moieties of interest can be incorporated into such polymers directly through monomer design, due to the excellent tolerance of ruthenium catalysts.

Ring-Opening Metathesis Polymerization (ROMP)

Ring opening metathesis polymerization (ROMP) exhibits very different reaction kinetics from the ADMET approach to polymeric materials. ROMP is a chain-growth type polymerization which relies on monomer ring strain and, thus, it can be efficiently controlled by catalyst loading.
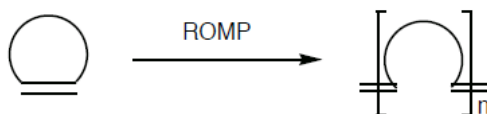
The equilibrium molecular weight of the resulting polymer chains is, therefore, essentially independent of the extent of conversion. Moreover, a variety of olefin metathesis catalysts effect ROMP and sufficiently fast initiating ones can even lead to a living polymerization of appropriately chosen monomers. For example, the polymerization of norbornenes with the fast initiating bispyridine species produces well-defined polymers with PDIs close to 1.0 (Choi and Grubbs, 2003). The employment of these strained, bi-cyclic alkenes as monomers ensures that both depolymerization via competing RCM and chain fragmentation via "back-biting" of the catalyst into the growing chain are significantly suppressed. However, the limited availability of suitable monomers is the main disadvantage of this method. Although a variety of backbones can

be created through monomer functionalization, such alterations sometimes negatively affect the ring strain and, thus, success of ROMP.

A1.3 Metathesis reaction of calixarenes

When ring-closing metathesis (RCM) was utilized as a novel route to synthesize calix[4]arenes with upper and lower alkenyl bridges (Pitarch et al., 1998), both intramolecular and intermolecular metathesis occurred between distal (1,3)-alkenyls of the lower rim, depending on the length of the substituents, the nature of the vicinal phenolic groups, and the concentration of the precursors (Scheme 1.12). By contrast, the simple *p*-allyl derivatives of the upper rim gave merely intermolecular (dimer, trimer and cyclodimer) products.
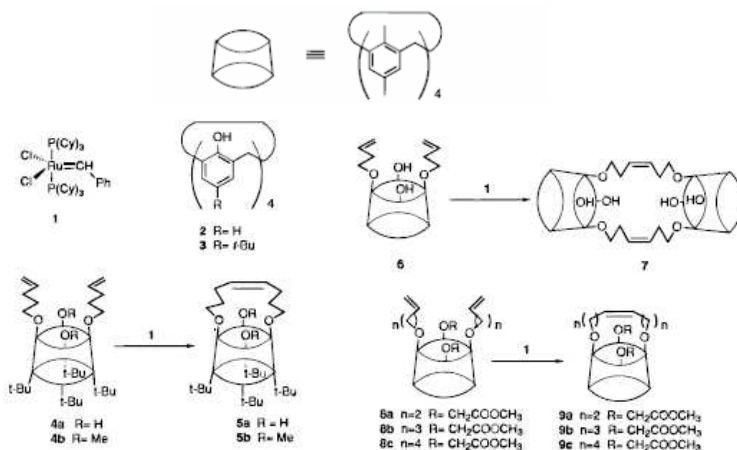
Scheme 1.12 synthesis of calix[4]arenes with upper and lower alkenyl bridges.

40

Two successive RCM reactions on different template calixarenes led instead to the cyclization of eight alkenyl units and the formation of huge macrocycles with more than one hundred atoms (Scheme 1.13) (Cao et al., 2005; Vysotsky et al., 2004).
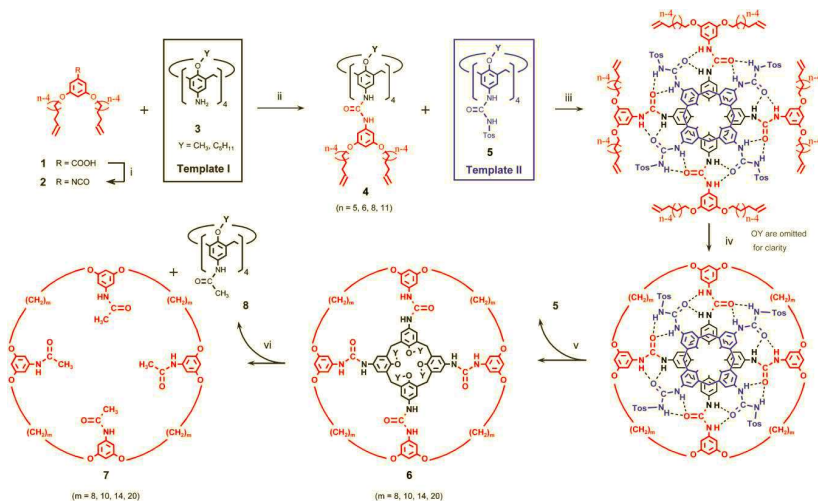
Scheme 1.13 Synthesis of huge macrocycles.

Alkene-bridged calix[4]arene monomers were synthesized by ring-closing metathesis. All the three possible conformers (*cone*, *partial cone*, and *1,3-alternate*) were used as comonomers with cyclooctene and norbornene in ring-opening metathesis polymerization (Scheme 1.14) (Yang and Swager, 2007). The resultant polymers were high-molecular weight, transparent and

stretchable materials with high calixarene incorporation (up to 25 mol % or 70 wt %) and low glass transition temperatures.
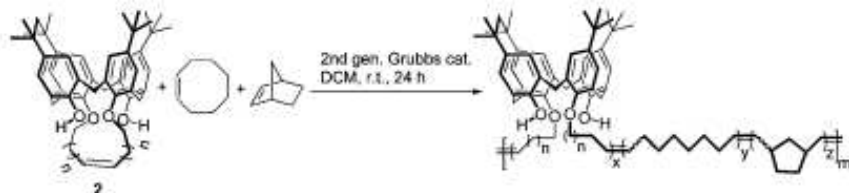
Scheme 1.14 Synthesis of Polymers

Resorcarene-encapsulated gold nanoclusters have been encaged in non-desorptive shells by olefin metathesis, yielding a mechanically robust cross-linked surfactant layer (Scheme 1.15). (Wei, 2006; Pusztay et al., 2002)
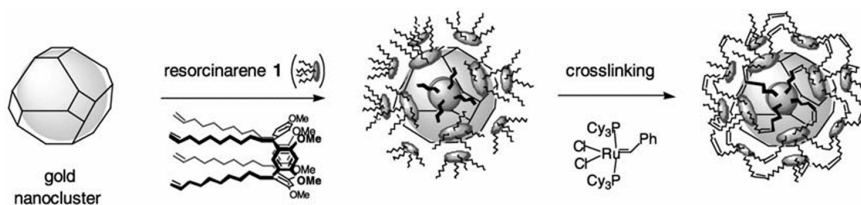
Scheme 1.15 Schematic of nanocluster encapsulation by resorcinarene 1, followed by encagement via olefin metathesis.

Chapter A2

Synthesis of Resorc[4]arene
ω-Undecenyl Esters 1a–1c

A2.1 Results and discussion

A2.1.1 Synthesis of resorc[4]arene ω-undecenyl esters 1a–1c

The preparation of C-alkylated resorc[4]arenes by tetramerization in the presence of ethereal BF_3 of opportunely substituted 2,4-dimethoxycinnamates prompted us to study both the versatility of the reaction and the chemical and physical properties of the new macrocycles obtained, as depending on the variation of the side chains. In this Phd thesis we planned to synthesize resorc[4]arenes featuring long aliphatic side chains ending with a vinylidene group which provides the possibility for cross-linking reactions.

(E)-2,4-Dimethoxycinnamic acid was quantitatively converted into the corresponding acid chloride (Scheme 2.1) by reaction with thionyl chloride in dry dichloromethane (DCM), and then converted into the corresponding ester by reaction with ω-undecenyl alcohol in dry THF, in the presence of diisopropylethylamine (DIPEA). Purification by silica gel column chromatography (chloroform as eluent) yielded the ω-undecenyl ester as a yellow oil (yield 81%). Treatment of (E)-2,4-dimethoxycinnamic acid ω-undecenyl ester with $BF_3 \bullet Et_2O$ (molar ratio 1:2) in chloroform at reflux afforded in 60% yield three stereoisomeric resorc[4]arene ω-undecenyl esters, which were shown to be in the *chair* (**1a**), *cone* (**1b**), and *1,2-alternate* (**1c**) configuration. The structure of stereoisomers **1a–1c** was confirmed by ^{1}H and ^{13}C NMR

spectroscopy and by electrospray ionization high-resolution mass spectrometry (ESI-HRMS).
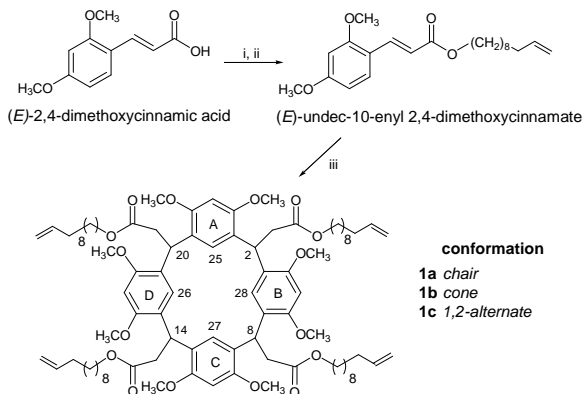
Scheme 2.1 Synthesis of resorc[4]arene ω-undecenyl esters 1a–1c. Reagents and conditions: (i) thionyl chloride, dry DCM, reflux, 2 h and 40 min; (ii) 10-undecen-1-ol, DIPEA, dry THF, reflux, 3 h. (iii) BF$_3$.Et$_2$O (molar ratio 1:2), CHCl$_3$ (stabilized with amylene), reflux, 20 min.

Conformation in solution of resorc[4]arenes **1b** (*cone* with a C4v symmetry) and **1c** (*1,2-alternate* with a Cs symmetry) could easily be assigned by the distribution pattern of NMR spectral data. (Abis et al., 1988) On the contrary, the NMR spectral data of resorc[4]arene **1a** were in agreement with both the D$_{2d}$ symmetry of the *1,3-alternate* conformation (Botta et al., 2005) and the C$_{2h}$ symmetry of a *chair* conformer. (Högberg, 1980a; Högberg, 1980b) This ambiguity was

solved by X-ray diffraction analysis of a crystal of resorc[4]arene **1a** (solvent, ethyl acetate): the results obtained fit very likely with a *chair* conformation (vide infra).

In the three forms, the side chains have different arrangements, i.e., two cis and two *trans* (rctt) in the *chair* **1a**, all-*cis* (rccc) in the *cone* **1b**, three *cis* and one *trans* (rctc) in the *1,2-alternate* **1c**.
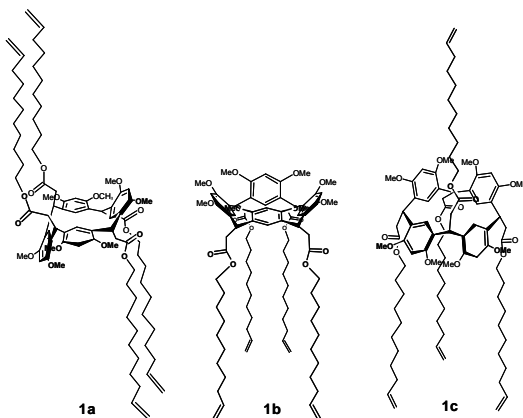
Figure 2.1 Chemical structures of resorc[4]arene ω-undecenyl esters **1a** (*chair*), **1b** (*cone*), and **1c** (*1,2-alternate*).

A2.1.2 X-Ray diffraction analysis of resorc[4]arene 1a

The molecular structure of resorc[4]arene **1a** is illustrated in Fig. 2.2. Taking as a reference the weighed least squares plane, namely R, passing through the four bridging carbon atoms of the macrocycle, the calculated dihedral angles δ values (Perrin and Oehler, 1991)(collected in Table 2.1) show that the B and D aromatic rings are almost coplanar with the plane R, whereas A and C are almost orthogonal to it, but on opposite sides. Following a procedure already adopted, (Botta et al., 2007) the molecular conformation of the macrocycle was given by the conformational parameters ϕ and χ, which account without ambiguities for the reciprocal orientations between adjacent aromatic rings (see Table 2.1). The sequence of signs (+-,+-,-+,-+) of the calculated values of ϕ and χ fits very likely with a *chair* conformation. The four ester chains attached to the bridging methine groups of the aromatic pocket point towards the exterior of the macrocycle and are segregated in pairs on opposite sides of the R plane. Such arrangement in the solid state makes resorc[4]arene **1a** a preorganized synthon undergoing a peculiar type of self-assembly which produces zigzag one-dimensional ribbons as those depicted in Fig. 2.4.
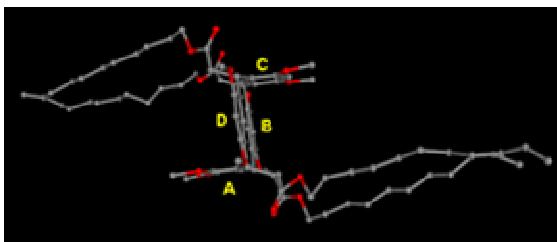
Figure 2.2 X-Ray structure of undecenyl resorc[4]arene **1a** showing the *chair* conformation adopted by the macrocycle. Colors are as follows: C, grey; O, red. Hydrogen atoms are omitted for clarity.

In the novel "secondary structure", two pairs of aliphatic arms from two neighbouring resorcarenes are inserted as in a sandwich by two pairs of aromatic methoxyl groups. The driving force for such self-assembly seems to be CH/π interactions between the terminal methylene hydrogen atoms of one molecule and the π systems of two adjacent molecules (evidenced by green lines in Fig. 2.3). In such a way, resorc[4]arene **1a** can behave at the same time as donor and acceptor of CH/π interactions, whose geometrical parameters are collected in Table 2.2.

Table 2.1 Dihedral angles (δ) and conformational parameters (ϕ and χ) for resorc[4]arene **1a**.

Rings	δ [°][a]	Rings	ϕ [°][a]	χ [°][a]
R^A	90.23 (3)	A–B	76.8 (4)	-151.4 (2)
R^B	178.02 (4)	B–C	-147.9 (2)	78.3 (1)
R^C	270.48 (4)	C–D	-70.3 (1)	152.2 (2)
R^D	177.13 (4)	D–A	145.9 (1)	-75.5 (1)

[a] Estimated standard deviations (ESD) are reported in parentheses. R is the weighed least squares plane passing through the four bridging carbon atoms of the macrocycle.

As it can be seen, strong CH/π interactions could be expected, as judged by three intermolecular distances (i.e., 2.619 (2), 2.716, (2) and 2.797 (2) Å) significantly shorter than the corresponding value of 3.6 Å found by high-level ab initio calculations on a benzene-ethylene complex (Tsuzuki et al., 2000). Drawing inspiration from these findings, we envisaged to carry out high-level ab initio calculations when resorcinol replaced benzene in the complex with ethylene. To this purpose, interaction energies were calculated using 6-311++G**, aug-cc-pVDZ, and aug-cc-pVTZ basis sets, for each of the two model complexes shown in Fig. 2.3, namely (A) and (B), where resorcinol and ethylene are in the same two reciprocal orientations observed in the crystal structure, i.e., at the same intermolecular distances [2.797 and 2.716 Å in complex (A), and 2.619 and 2.955 Å in complex (B)].
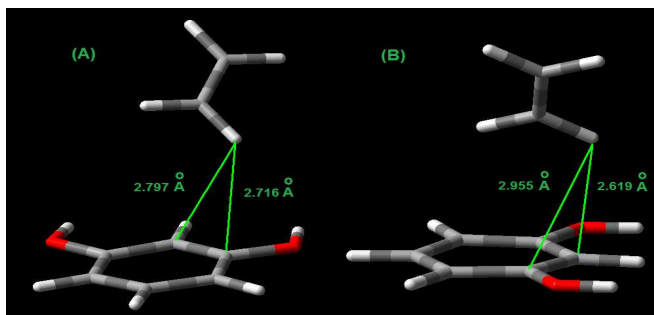
Figure 2.3 Resorcinol-ethylene complexes (A) and (B) considered for high-level *ab initio* calculations of CH/π interactions. The intermolecular distances are the same as those found in the crystal structure of resorc[4]arene **1a**.

The calculated interaction energies of (A) and (B) complexes (summarized in Table 2.3) proved to be dependent on the basis set used, becoming more negative (the mutual attraction increases) as the set is enriched with correlation-consistent polarized basis sets. Moreover, reciprocal resorcinol-ethylene attraction is always larger (the interaction energy is more negative) in complex (A) than in complex (B), where ethylene is tilted with respect to the resorcinol plane. In any case, the calculations were in agreement with the experimentally observed short contacts in the crystal of resorc[4]arene **1a** and support the hypothesis of a pivotal role exerted by the CH/π interactions in the detected self-assembly.
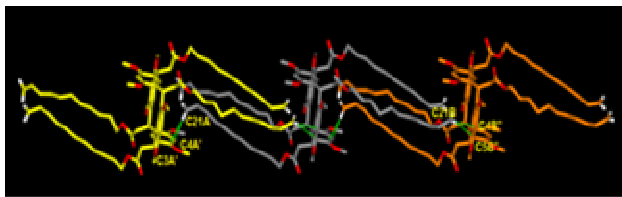
Figure 2.4 Perspective view of a zigzag one-dimensional ribbon in resorc[4]arene **1a** showing CH/π interactions (green lines) occurring between the terminal methylene hydrogen atoms of one molecule and the π systems of two adjacent molecules.

Notably, along each ribbon, polar surfaces (due to the resorcarene core, the calculated dipole moment being 3.046 D) are alternated to apolar surfaces (due to the aliphatic chains). A peculiar "tertiary structure" was indeed detected in the crystal lattice for resorc[4]arene **1a**, where a lamellar-type crystalline organization is built-up by the face-to-face exposition of polar-with-polar and apolar-with-apolar surfaces. The result is a multilayer structure containing hydrophilic (ca 7 Å thick) and hydrophobic (ca 6 Å thick) layers intercalated. Such structure might give a chance of intercalating resorc[4]arene **1a** inside biological membranes (Fig. 2.4).

51

Table 2.2 Geometrical parameters for the CH/π interactions in resorc[4]arene **1a**.

Carbon number	$C \bullet \bullet \bullet C_\pi$ (Å)[a]	$H \bullet \bullet \bullet C_\pi$ (Å)[a]	$CH \bullet \bullet \bullet C_\pi$ (°)[a]
C21A-H⋯C3A′	3.509 (3)	2.716 (2)	136.6 (2)
C21A-H⋯C4A′	3.248 (3)	2.797 (2)	108.4 (2)
C21B-H⋯C5B″	3.197 (3)	2.955 (3)	94.7 (2)
C21B-H⋯C4B″	3.199 (3)	2.619 (2)	117.0 (2)

[a] Estimated standard deviations (ESD) are reported in parentheses.

Table 2.3 Calculated interaction energies (kJ mol⁻¹) of the resorcinol-ethylene complexes (A) and (B).

Basis set	(A)[a]	(B)[a]
MP2/6-311++G** (290)[b]	−4.52	−0.72
MP2/aug-cc-pVDZ (320)[b]	−7.14	−4.60
MP2/aug-cc-pVTZ (690)[b]	−8.41	−6.48

[a] The geometry of complexes (A) and (B) is shown in Fig. 3. [b] Basis functions are given in parentheses.

A2.2 Experimental section

<u>NMR measurements</u>

NMR spectra were recorded at 300 K on a Bruker AVANCE AQS600 spectrometer operating at the proton frequency of 600.13 MHz and equipped with Bruker a multinuclear z-gradient inverse probe head capable of producing gradients in the z-direction with a strength of 55.4 G cm^{-1}. ^{1}H and ^{13}C NMR spectra were always referenced to residual CHCl$_3$ signal (^{1}H, δ = 7.26 ppm; ^{13}C, δ = 77.20 ppm). The ^{1}H NMR spectra were acquired using the following experimental conditions: number of scans 16–32, recycle delay 5 s, $\pi/2$ pulse 9.0 µs, and 32K data points. ^{1}H diffusion filter-edited NMR spectra were obtained using a double stimulated echo pulse sequence incorporating a longitudinal eddy current delay (Jerschow and Mueller, 1997) with a Δ of 160 ms, a δ of 2.6 ms, and a longitudinal eddy current delay of 25 ms. A gradient pulse recovery time of 0.1 ms, 2% and 60% of the maximum gradient intensity were used. Sixty-four scans were accumulated in time domain with 32768 points.

A2.2.1 Synthesis of ω-undecenyl (E)-2,4-dimethoxycinnamate

A solution of (*E*)-2,4-dimethoxycinnamic acid (6.0 g, 28.8 mmol) in dry DCM (60 mL) was treated with $SOCl_2$ (3.1 mL, 42.6 mmol) and the mixture was held at reflux for 2 h and 40 min. After removing the solvent under vacuum, the residue was dissolved in dry THF (32 mL) and diisopropylethylamine (DIPEA; 5.4 mL, 31.2 mmol) was added under nitrogen. After 20 min stirring at room temperature, 10-undecen-1-ol (7.0 mL, 34.1 mmol) was added to the solution and the mixture was heated under reflux for 3 h. Purification of the crude residue by silica gel chromatography with chloroform as eluent afforded the title compound (8.4 g, 81%, yellow oil). ^{1}H NMR (600 MHz, CDCl$_3$, 300 K): δ (ppm) = 7.89 (d, *J* = 16 Hz, 1H, H–α), 7.43 (d, *J* = 8.6 Hz, 1H, H-6), 6.49 (dd, *J* = 8.6, 2.4 Hz, 1H, H-5), 6.44 (d, *J* = 2.4 Hz, 1H, H-3), 6.42 (d, *J* = 16 Hz, 1H, H-β), 5.80 (m, 1H, =CH), 4.98 (br d, *J* = 17 Hz, 1H, =CH$_A$H$_B$), 4.91 (br d, *J* = 10 Hz, 1H, =CH$_A$H$_B$), 4.16 (t, *J* = 6.7 Hz, 2H, ω-CH$_2$), 3.86, 3.83 (s, 3H each, 2 × OCH$_3$), 2.03 (q, *J* = 7.5 Hz, 2H, α-CH$_2$), 1.68 (m, *J* = 7 Hz, 2H, θ-CH$_2$), 1.36 (m, 2H, η-CH$_2$), 1.28 (m, 8H, 4 × CH$_2$); ^{13}C NMR (100 MHz, CDCl$_3$, 300 K): δ (ppm) = 168.0 (s, C=O), 162.6, 159.8 (s each, C-4, C-2), 139.9 (d, CH-α), 139.2 (d, =CH), 130.4 (d, CH-6), 116.7 (s, C-1), 116.2 (d, CH-β), 114.1 (t, =CH$_2$), 105.2 (d, CH-5), 98.4 (d, CH-3), 64.4 (t, ω-CH2), 55.5 (q, OCH$_3$), 33.8 (t, α-CH2), 29.5–29.1 (t, 4 × CH$_2$), 28.9 (t, β-CH$_2$), 28.8 (t, θ-CH$_2$), 26.0 (t, η-CH$_2$). HRMS (ESI):

m/z calcd for $C_{22}H_{32}O_4+Na^+$: 383.21928 [*M*+Na]$^+$ (monoisotopic mass); found: 383.21910.

A2.2.2 Synthesis of resorc[4]arene ω-undecenyl esters 1a–1c

$BF_3 \bullet Et_2O$ (1.5 mL; 11.25 mmol) was added to a solution of ω-undecenyl (E)-2,4-dimethoxycinnamate (2.0 g, 5.55 mmol) in $CHCl_3$ (stabilized with amylene, 5 mL) under stirring and the mixture was held under reflux for 20 min. After addition of ice-water, the stirring was continued until the chloroform phase turned to fuchsia. The chloroform layer was dried over Na_2SO_4 and the solvent was removed under vacuum. The residue was purified by silica gel column chromatography (DCM and DCM-ethyl acetate, 97:3) to yield resorc[4]arene ω-undecenyl esters, in the order of elution, **1b** (130 mg, 26%), **1a** (120 mg, 24%), and **1c** (45 mg, 9%).

*Resorc[4]arene ω-undecenyl ester **1a** (chair)*

White solid, 24% overall yield. Mp: 137 ± 0.3 °C. ^{1}H and ^{13}C NMR signals are reported in Table 2.4. HRMS (ESI): *m/z* calcd for $C_{88}H_{128}O_{16}^+Na^+$: 1463.90946 [M+Na]$^+$ (monoisotopic mass); found: 1463.91035. FT-IR (KBr): 2918, 2852, 1734, 1612, 1585, 1468, 1299, 1201 cm^{-1}. In Fig. 2.5 is reported a rapresentative ^{1}H-NMR spectrum of resorc[4]arene **1a**.

Table 2.4. ^{1}H NMR and ^{13}C NMR signals* of undecenyl resorc[4]arene **1a** (*chair*).

Carbon	^{13}C	^{1}H
C=O	172.4	-
C_{Ar}–O	156.6	-
	155.8	
=CH	139.2	5.82 ddt (17.2, 10.2, 6)
CH_i (26,28)	126.6	6.19 s
CH_i (25,27)	125.7	6.82 s
C_{Ar}–C	125.3	-
	122.6	
=CH$_2$	114.3	4.99 br d (17.2)
		4.92 br d (10.2)
CH_e (5,17)	97.1	6.47 s
CH_e (11,23)	95.3	6.39 s
OCH$_2$	64.3	3.98 br t
		3.92 t
OMe	56.0	3.88 s
	56.0	3.64 s
CH$_2$-(CO)	39.6	2.73 dd (14.5, 10.5)
		2.65 dd (14.5, 6.5)
CH$_2$-(CH=)	34.0	2.05 q (6)
CH	33.0	5.04 dd (10.5, 6.5)
CH$_2$-(CH$_2$-CH=)	29.1	1.46 m
CH$_2$-(CH$_2$O)	28.7	1.38 m
CH$_2 \times 5$	29.6	1.24 br m
	29.6	
	29.5	
	29.3	
	26.0	

* 600 MHz (^{1}H) and 100 MHz (^{13}C), CDCl$_3$, T = 300 K; coupling constants J (Hz) are given in parentheses.

Figure 2.5 ^{1}H NMR spectrum of undecenyl resorc[4]arene **1a** (*chair*). 600 MHz, CDCl$_3$, 300 K.

*Resorc[4]arene ω-undecenyl ester **1b** (cone)*

Yellow solid, 26% overall yield. Mp: 101 $\pm$ 0.9 °C. ^{1}H and ^{13}C NMR signals are reported in Table 2.5. HRMS (ESI): *m/z* calcd for C$_{88}$H$_{128}$O$_{16}^+$Na$^+$: 1463.90946 [M+Na]$^+$ (monoisotopic mass); found: 1463.91035. FT-IR (KBr): 2918, 2852, 1734, 1612, 1585, 1468, 1299, 1201 cm^{-1}. In Fig. 2.6 is reported a rapresentative ^{1}H-NMR spectrum of resorc[4]arene **1b**.

57

Table 2.5 ^{1}H NMR and ^{13}C NMR signals* of undecenyl resorc[4]arene **1b** (*cone*).

Carbon	^{13}C	^{1}H
C=O	172.5	-
C_{Ar}–O	156.2	-
=CH	139.3	5.82 ddt (17.2, 10.2, 6.5)
CH_i (25,26,27,28)	126.0	6.51 s
C_{Ar}–C	124.2	-
=CH_2	114.3	4.99 br d (17.2)
		4.93 br d (10.2)
CH_e (5,11,17,23)	96.4	6.30 s
OCH_2	64.4	3.95 t (6.8)
OMe	56.0	3.63 s
CH_2-(CO)	39.2	2.83 d (7.6)
CH_2-(CH=)	34.0	2.03 m (6.5)
CH	33.2	4.96 t (7.6)
CH_2-(CH_2-CH=)	29.1	1.35 br m
CH_2-(CH_2O)	28.8	1.49 br m
$CH_2 \times 5$	29.7	1.27 br m
	29.6	
	29.5	
	29.3	
	26.0	

* 600 MHz (^{1}H) and 100 MHz (^{13}C), CDCl$_3$, *T* = 300 K; coupling constants *J* (Hz) are given in parentheses.

Figure 2.6 ^{1}H NMR spectrum of undecenyl resorc[4]arene **1b** (*cone*). 600 MHz, CDCl$_3$, 300 K.

*Resorc[4]arene ω-undecenyl ester **1c** (1,2-alternate)*

Yellow solid, 9% overall yield. Mp: 86 ± 0.9 °C. ^{1}H and ^{13}C NMR signals are reported in Table 2.6. HRMS (ESI): *m/z* calcd for C$_{88}$H$_{128}$O$_{16}$$^+Na^+$: 1463.90946 [M+Na]$^+$ (monoisotopic mass); found: 1463.91035. FT-IR (KBr): 2918, 2852, 1734, 1612, 1585, 1468, 1299, 1201 cm^{-1}. In Fig. 2.7 is reported a rapresentative ^{1}H-NMR spectrum of resorc[4]arene **1c**.

Table 2.6 ^{1}H NMR and ^{13}C NMR signals* of undecenyl resorc[4]arene **1c** (*1,2-alternate*).

Carbon	[13]C	[1]H
C=O	172.7 × 2 172.3 172.2	-
C_{Ar}–O (6,22) C_{Ar}–O (4,24) C_{Ar}–O (10,18) C_{Ar}–O (12,16)	156.4 156.3 156.1 156.1	-
=CH	139.2	5.79 ddt (17.2, 10.2, 6.5)
CH_i (25,28) CH_i (26,27)	127.6 126.5	7.25 s 6.36 s
C_{Ar}–C (7,21) C_{Ar}–C (1,3) C_{Ar}–C (13,15) C_{Ar}–C (9,19)	124.7 124.4 124.0 123.4	-
=CH_2	114.4	4.97 br d (17.2); 4.91 br d (10.2)
CH_e (11,17) CH_e (5,23)	96.7 96.0	6.38 s 6.40 s
OCH_2 (2) OCH_2 (14) OCH_2 (8,20)	64.4 63.1 64.4 × 2	4.00 t (7.0) 3.97 t (7.0) 3.91 t (7.0)
OMe	56.4; 56.1; 55.9; 55.9	3.83 s; 3.82 s; 3.75 s; 3.64 s
CH_2-(CO) (2) CH_2-(CO) (14) CH_2-(CO) (8,20)	41.2 40.3 39.4 × 2	2.87 d (8.0) 2.33 d (8.0) 2.88 dd (15.1)
CH_2-(CH=)	34.0	2.03
CH (2) CH (14) CH (8,20)	34.0 33.6 34.0 × 2	5.46 t (8.0) 5.10 t (8.0) 5.06 dd (9.6, 6.5)
CH_2-(CH_2-CH=)	29.1	1.38 br m
CH_2-(CH_2O)	28.8	1.45 br m
CH_2 × 5	29.7; 29.7; 29.7; 29.6; 26.0	1.27 br m

* 600 MHz (^{1}H) and 100 MHz (^{13}C), CDCl$_3$, *T* = 300 K; coupling constants *J* (Hz) are given in parentheses.
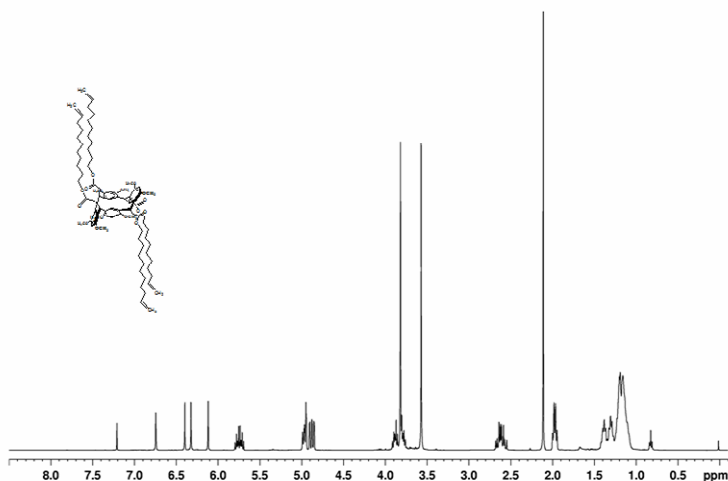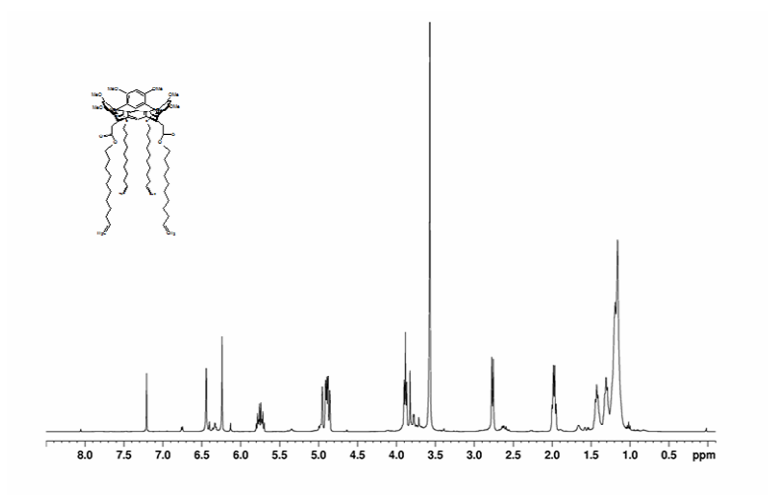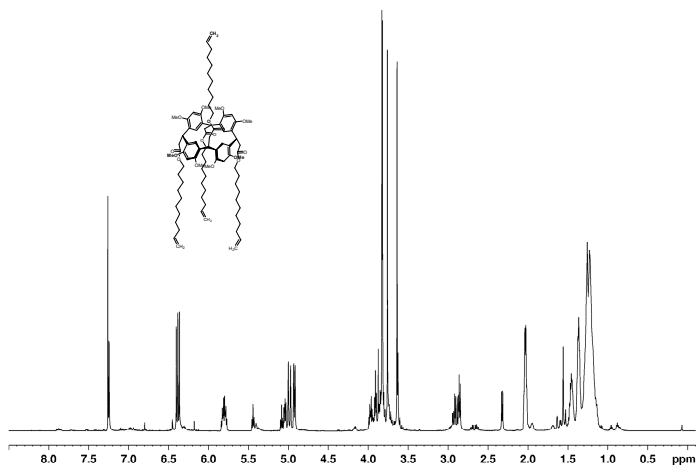
Figure 2.7 ^{1}H NMR spectrum of undecenyl resorc[4]arene **1c** (*1,2-alternate*). 600 MHz, CDCl$_3$, 300 K.

A.2.2.3 Crystallographic data of resorc[4]arene 1a

C$_{88}$H$_{128}$O$_{16}$, M = 1441.97, crystal system: triclinic, space group: P1, a = 12.297(5), b = 17.946(5), c = 10.559(5) Å, α = 100.610(5)°, β = 102.440(5)°, γ = 105.110(5)°, volume: 2124(1) Å3, Z = 1, T = 293 K, ρ (calcd.) = 1.127 g $\times$ cm–3, 8039 total reflections collected, 7989 unique reflections (R$_{int}$ = 0.00). These data can be obtained free of charge from The Cambridge Crystallographic Data Centre via www.ccdc.cam.ac.uk/data_request/cif.

61

Chapter A3

Metathesis Reaction of Resorc[4]arene ω-Undecenyl Esters:
the *Chair* Form

A3.1 Results and discussion

A3.1.1 Olefin metathesis reaction on resorc[4]arene 1a

The field of olefin metathesis is currently in a period of renaissance, largely because of the development in the early 1990s of well-defined ruthenium catalysts (Scholl et al., 1999). When we started our investigation on olefin metathesis, we faced with the problem of the selection of the appropriate catalyst. Second-generation Grubbs and Grubbs-Hoveyda complexes were tested, with a starting catalyst loading of 10 mol%. (Fig. 3.1)
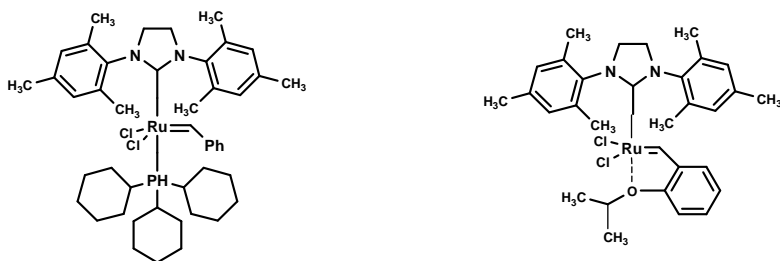
Figure 3.1 The structure of the second-generation Grubbs and Grubbs-Hoveyda complexes.

To ascertain the optimal reaction conditions, several experiments (summarized in Table 3.1) were run with resorc[4]arene **1a** as the

substrate, in which a variation in the substrate concentration and the catalyst loading was performed. After some trials under TLC plate checking, we observed that when the reaction was performed under high substrate concentration (i.e., 1.0×10^{-2} M in DCM), a large quantity of undesired products (polymers, presumably) was obtained, as revealed by the thickness of the baseline in the TLC plate system. Under high dilution conditions (i.e., 3.0×10^{-4} M), a less complicated TLC pattern was obtained, but the starting material did not completely disappear (except in the case of second-generation Grubbs catalyst at 10 mol%). An intermediate concentration (3.0×10^{-3} M) was afterward chosen, since it allowed the formation of a series of interesting compounds to be isolated and characterized (vide infra). The two catalysts proved to be almost equally effective, but the second left a 10% of starting material at a lower catalyst loading (i.e., 1 mol%). Finally, a combination of temperature (reflux) and reaction time (20 min) was evaluated as the best for the complete disappearance of **1a** on the TLC plate, as compared with room temperature and longer times. On the other hand, as we previously showed, thermal-induced conformational changes from the chair to other stereoisomers do not occur, unless ethereal BF_3 is involved (Botta et al.,1994).

Table 3.1 Summary of results obtained for olefin metathesis reactions of resorc[4]arene 1a.[a]

Substrate conc.	Catalyst (loading)	Yield (%)		
		2a	3a	P1a
3×10^{-3} M	Grubbs 2nd (10%)	46	5	44
	Grubbs-Hoveyda (10%)	30	trace	50
	Grubbs 2nd (1%)	43	trace	n.f.
	Grubbs-Hoveyda (1%)	30[b]	trace	n.f
3×10^{-4} M	Grubbs 2nd (10%)	60	n.f	n.f
	Grubbs-Hoveyda (10%)	40[b]	n.f	n.f
	Grubbs 2nd (1%)	30[b]	n.f	n.f
	Grubbs-Hoveyda (1%)	10[b]	n.f	n.f

[a] Reactions in DCM at reflux temperature and 20 min reaction time. [b] Starting material 1a was present. n.f. = not formed.

The crude reaction mixture obtained under the optimal conditions (see first row of Table 3.1) was treated with a QuadraSil AP metal scavenger (amine-modified silica gel) to remove residual ruthenium by filtration (McEleney et al., 2006). The soluble (DCM) part of the filtrate was purified by silica gel chromatography eluting with DCM/ethyl acetate mixtures of increasing polarity (see A3.2.1 Section). The following

products (Scheme 3.1) were isolated: **2a** (white powder, 46% yield) and **3a** (white powder, 5% yield). The insoluble (in most organic solvents, including DMSO) fraction **P1a** (85 mg, 44%) was obtained in two fractions: the first, as a precipitate (40 mg) and the second, as the material (45 mg) recovered by the top of the chromatographic column. The structure of compounds **2a** and **3a** was assigned by NMR spectroscopy and by electrospray ionization high-resolution mass spectrometry (ESI-HRMS). With regard to **2a**, the comparison of its NMR spectral data with those of the parent resorc[4]arene **1a** evidenced the following points. Proton and carbon signals (AB part of an ABM system) for the terminal methylene group of **1a** are absent, while the signal for an olefinic double bond (M part in **1a**) is still present (slightly shifted upfield) in **2a** and linked with a methylene group of the chain, as shown by TOCSY spectra. These evidences support the formation of a new double bond between two chains with the elimination of one molecule of ethylene, as required by a ring-closing metathesis. As a confirmation, the sodium adduct $[M + Na]^+$ in the ESI mass spectrum of **2a** was found at m/z 1407.84543, that is 56 m/z ($2 \times C_2H_4$) less than the corresponding $[M + Na]^+$ peak of **1a** (m/z 1463.91035). As expected for a long hydrocarbon chain derivative, both the peaks originated a series of ions decreasing in intensity by losses of a methylene unit (14 m/z). Moreover, the resonance at δ 5.34 (*br* t, *J* = 3 Hz) for the =CH methine is flanked by a minor signal (*br* t, *J* =

4 Hz) at δ 5.32. The two peaks, in approximate integrated ratio of 3:1, were correlated (by TOCSY data) to methylene signals at δ 2.01 and 2.03, as well as to the corresponding carbon resonances (by HSQC) at δ 32.0 and 26.8, respectively. The two peaks were thus assigned to *trans* and *cis* olefinic protons, respectively, in agreement with the expected highfield carbon value of the α-CH$_2$ in the *cis* configuration. Furthermore, whereas the signal at δ 5.34 showed a strong spatial correlation (by NOESY data) with the protons of both α- and β-methylene groups, the minor signal at δ 5.32 ppm was NOE-correlated only to the protons of the geminal methylene nucleus, as required for *trans* and *cis* olefinic protons, respectively. Two predictable RCM thus occurred independently between two neighbour chains (e.g. C-2/C-20 or C-8/C-14) on opposite faces of the planar aromatic rings. As a result, two bridges, featuring an inner double bond, were formed, leading to a bicyclic alkene structure for **2a**. The geometrical isomerism of the double bond did not apparently influence the NMR resonances of the remaining methylene groups. Only two small satellite peaks at δ 6.85 and 6.18 appeared in the ^{1}H NMR spectrum of **2a** and were attributed to the H-25/27 and H-26/28 protons of the *cis* form, respectively. Though formally the whole molecule may have a *tt* (55%), *tc* (35%) or *cc* (10%) double bonds distribution pattern, actually the compound can be described as a *E/Z* (3:1) mixture of two independent moieties (for

the sake of clarity, we reported in Scheme 3.1 just the *Z* stereoisomer of **2a**).
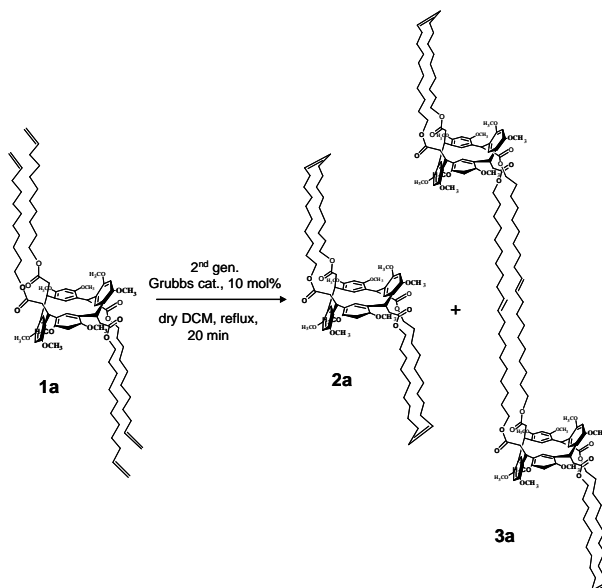
Scheme 3.1 Olefin metathesis reaction on undecenyl resorc[4]arene **1a**.

Catalytic hydrogenation (10% Pd/C) of **2a** led to the unique reduction compound **2ar**, which showed the expected [M + Na]$^+$ peak at 1411.87772 *m/z* and clean signals without satellite peaks in the ^{1}H and ^{13}C NMR spectra.

With regard to the minor product **3a**, the ^{1}H NMR spectral data (see Table 3.3 of Section A3.2) are almost coincident with those of **2a**, except for the signals of a new =CH-CH$_2$-CH$_2$ sequence, belonging to a

second disubstituted *trans* double bond, again with a minor 1:3 *cis* partner. Two diagnostic peaks at 2792.69337 and 1407.84371 *m/z* in the ESI mass spectrum, which were attributed to $[M + Na]^+$ and $[M + 2Na]^{2+}$ sodium adducts, respectively, revealed a molecular weight of 2769.7 Da and a molecular formula $C_{168}H_{240}O_{32}$. The two ions were flanked by the expected peaks corresponding to serial losses of CH_2 (14 and 7 *m/z*, respectively). These findings suggested the presence of two new intermolecular eleven carbon chains, while two intramolecular bridges as in **2a** were still remaining: in summary, the formation of a linear dimer **3a**, as depicted in Scheme 3.1. The novel chain could have been originated by a double cross-metathesis (CM) intermolecular closure of the neighbour chains of two different molecules of **1a**, but, more likely, it derives from the reaction between two molecules of **2a**. The role of bicyclic alkene **2a** as a key intermediate in the pathway leading to the linear dimer **3a** was stressed by submitting an aliquot of pure **2a** to the same olefin metathesis conditions (time, temperature and catalyst) as those used for **1a** (see A3.2.2 Section). As a result, derivative **3a** was obtained in a comparable 10% yield as the main product, among a series of more polar compounds which were not isolated. Around 34% of unreacted starting bicycle **2a** was recovered, but only traces of polymeric products were noticed on the TLC baseline.

69

A.3.1.2 Plausible mechanisms of the olefin metathesis reaction

❖ *Proposed reaction mechanism for the synthesis of* bicyclic alkene **2a** *starting from resorc[4]arene* **1a**

The currently accepted mechanism of olefin metathesis, first proposed by Chauvin in 1971, proceeds via a metallacyclobutene intermediate formed by a [2+2] cycloaddition between the olefin substrate and a transition metal carbine (Grubbs and Burk, 1975). In our case, the synthesis of compound **2a** occurs by two almost contemporary ring-closing metathesis (RCM) reactions, driven by the elimination of two molecules of ethylene, as sketched in Scheme 3.2, plausibly passing through the not isolated intermediate [4a].
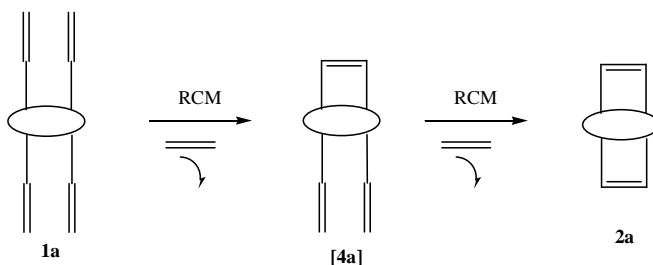
Scheme 3.2 Proposed reaction mechanism for the formation of bicyclic alkene **2a** starting from undecenyl resorc[4]arene **1a**. The asterisk denotes a plausible not isolated intermediate.

A similar intramolecular ring-closing reaction occurred for p-tert-butylcalix[4]arenes **X1** (see Figure 3.2), with two similar but shorter chains ending with a terminal alkene, to give the cyclic alkenes **X2** (Yang and Swager, 2007). The reaction gave almost pure products (*trans* for *n* =1, and *cis* for *n* =2) and the yield increased from 87 to 100% going from **X2a** (*n* =1, six carbons ring) to **X2b** (*n* =2, eight carbons ring).
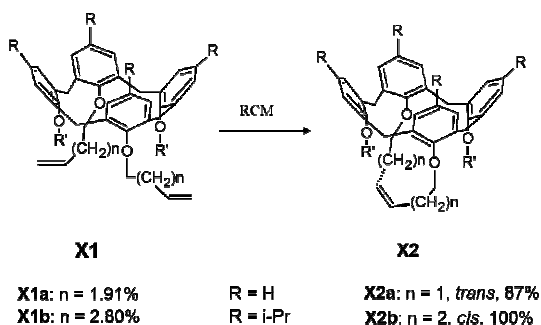
Figure 3.2 Calix[4]arenes **X1** and their metathesis **X2** derivatives (Yang and Swager, 2007).

Moreover, it is generally accepted that macrocyclic ring-closing olefin metathesis using the second-generation Grubbs catalyst provides alkenes with high *E/Z* ratio, regardless of the initial olefin stereochemistry (Lee and Grubbs, 2000). Indeed, the theme of stereoselectivity has been often controversial, in the case of

macrocyclization (Meng et al., 1997; Schinzer et al., 1997; Schinzer et al., 1997; Prunet, 2003). Although the majority of catalysts provide predominantly *E*-alkenes (Fürstner et al., 2001), unprecedented *Z*-selective ruthenium catalysts have been recently developed for a variety of cross-metathesis reactions (Keitz et al., 2012; Meek et al., 2011). In our case, a low *E/Z* selectivity (i.e., 3:1) was obtained, but product **2a** was shown to be the key intermediate in the pathway leading to dimer **3a**, rather than a series of intermolecular CM reactions. Looking at the literature, we found some similarity in the ruthenium-catalyzed ROM-CM reactions of norbornene (Schneider and Blechert, 1996b; Schneider et al., 1997b) and cyclobutene (Randall and Snapper, 1998; Randall et al., 1995; Snapper et al., 1997; Tallarico et al., 1997).

❖ *Proposed mechanistic scenario for the formation of dimer **3a** from bicyclic alkene **2a***

With regard to the mechanistic pathway for the dimerization of **2a** leading to **3a**, we envisaged a series of reversible reactions passing through the not isolated intermediate [**5a**]Ru (Scheme 3.3), which can be considered as the metallated form of a product proposed in the literature for the synthesis of cylindrocyclophanes (Smith et al., 2000; Smith et al., 2001). The linear dimer **3a** has still two reactive alkenes,

which likely could bring to the formation of similar trimers or tetramers, but the presence of such compounds, due to the expected lower yield, was not supported by the isolation.
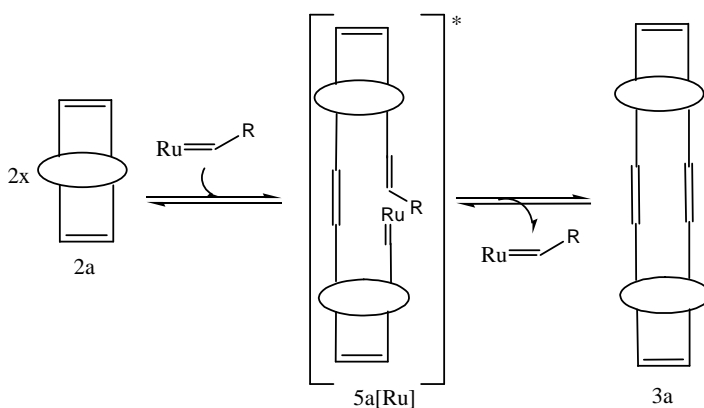
Scheme 3.3 Proposed mechanistic scenario for the formation of dimer **3a** from bicyclic alkene **2a**. The asterisk denotes a plausible not isolated intermediate.

A3.1.3 ADMET-like polymerization

Besides bicycle **2a** and dimer **3a**, olefin metathesis of undecenyl resorc[4]arene **1a** afforded the insoluble (in most organic solvents, including DMSO) fraction **P1a** (85 mg, 44%) as an amorphous solid, which was characterized by solid state ^{13}C CPMAS NMR spectroscopy. Solid state NMR, in fact, is a powerful method to understand

macrostructure and morphology of synthetic polymers (Yu and Guo, 1990). The ^{13}C CPMAS NMR spectrum of **P1a** is shown in Fig. 3.3. The signals obtained, although typically broadened, perfectly match the corresponding signals of **2a** recorded in solution (see Table 3.2 of section A3.2.1), including the disappearance of the terminal methylene signal, which confirmed that a metathesis reaction had occurred. However, the quality of the double bond (whether intra or intermolecular) could not be established.
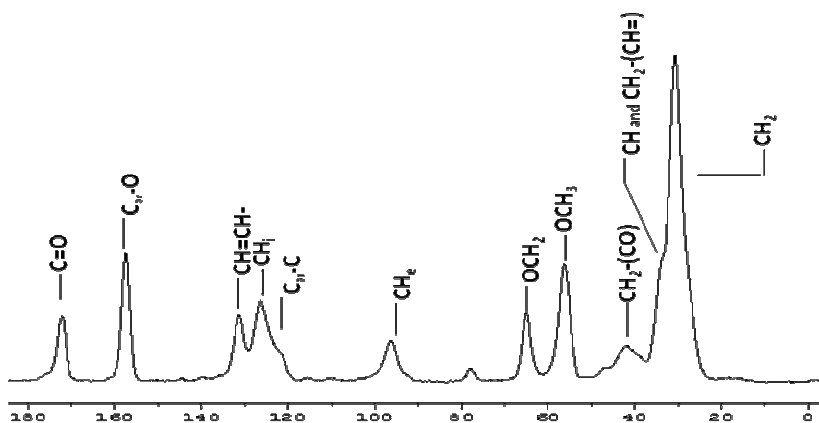
Figure 3.3 Solid state ^{13}C CPMAS NMR spectrum of **P1a** measured at 100.63 MHz with the contact time 6 ms (room temperature).

Fourier-Transform IR spectrum of **P1a** showed a broad absorption band at 3444 cm^{-1} and identical sharp peaks as those obtained for the parent undecenyl resorc[4]arene **1a**, as well as for bicycle **2a** and dimer **3a**. This means that, in the polymer, the typical functional groups are

74

still present. The huge band around 3444 cm^{-1} is indicative of intermolecular hydrogen bonding interactions occurring into the labyrinthic framework of the polymer. Unfortunately, the insolubility of **P1a** in most organic solvents prevented the resort to both gel permeation chromatography (GPC) and MALDI-TOF mass spectrometry to obtain molecular weight distribution; however, elemental analysis of the sample was in satisfactory agreement with the molecular formula $(C_{84}H_{120}O_{16})_n$, where $C_{84}H_{120}O_{16}$ is the monomer (with n =1), if we assume that **P1a** is a homogeneous polymer. We afterwards hypothesized that **P1a** is a cross-linked polymer formed by an ADMET-like reaction, even though in different conditions. The ADMET polymerization is the result of the reversible condensation of highly pure dienes into linear polymers (Wagener et al., 1991a; Wagener et al., 1991b; Tindall et al., 1998). The presence of two isolated undecenoxy groups with active sites quite far from the bulky constituent in the core of the molecule (Allcock et al., 2001) and from any "negative neighboring group" effect (Wagener et al., 1997) makes resorc[4]arene **1a** particularly suitable for such reaction. The ring closure between two vicinal chains is competitive in the CM conditions and, possibly, will complicate the inner structure of the polymer. When the ADMET reaction is carried out under solvent-free conditions with constant (or intermittent) vacuum (Wagener and Smith, 1991; Smith and Wagener, 1993), the competitive intramolecular CM reaction does

not work and the conditions are thus favorable for linear polymers to be formed. Therefore, we submitted resorc[4]arene **1a** to a previously reported ADMET polymerization procedure; again, an insoluble polymer was obtained with a solid state ^{13}C CPMAS NMR spectrum coincident with that of **P1a**, resulting from the olefin metathesis of the same precursor. The insolubility of both the products obtained by classical olefin metathesis and ADMET polymerization of resorc[4]arene **1a** suggests the formation of a complex polymeric architecture with ramifications due to the competitive intramolecular CM reaction and/or the intermolecular link between two distant molecules. We can reasonably expect that a polymeric line will be formed from a chain reaction of two side chains of different molecules A, B, C and so on, but the two free terminal methylene groups of any unit (e.g., A) will react not necessarily with one of the neighbour molecule (e.g., B), rather with any other mobile member of the polymeric line. The structure represented in Fig. 3.4 is only a possible formal representation of the constitutional repeating unit of the polymer, that is $(C_{84}H_{120}O_{16})_n$, and the presence of chains with terminal alkene can be considered negligible. In such a way, bicycle alkene **2a** can be considered as the monomer (n = 1, molecular weight 1385 Da) and compound **3a** the corresponding dimer (n = 2, molecular weight 2770 Da).
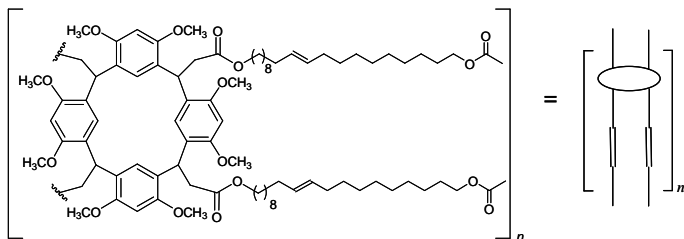
Figure 3.4 Formal representation of the constitutional repeating unit, i.e., $(C_{84}H_{120}O_{16})_n$ of polymer **P1a**.

A3.2 Experimental section

General procedures and materials

All manipulations were performed using a combination of glovebox and high vacuum under a nitrogen atmosphere. HPLC grade solvents were dried and degassed by standard procedures. Second-generation Grubbs and Grubbs-Hoveyda catalysts were purchased from Sigma Aldrich, together with QuadraSil AP silica gel.

NMR measurements

NMR spectra were recorded at 300 K on a Bruker AVANCE AQS600 spectrometer operating at the proton frequency of 600.13 MHz and equipped with Bruker a z-gradient inverse probe head capable of producing gradients in the z-direction with a strength of 55.4 G cm^{-1}. ^{1}H and ^{13}C NMR spectra were always referenced to residual CHCl$_3$ signal (1H, δ = 7.26 ppm; ^{13}C, δ = 77.20 ppm). The ^{1}H NMR spectra were acquired using the following experimental conditions: number of scans 16–32, recycle delay 5 s, π/2 pulse 9.0 μs, and 32K data points. ^{1}H diffusion filter-edited NMR spectra were obtained using a double stimulated echo pulse sequence incorporating a longitudinal eddy current delay with a Δ of 160 ms, a δ of 2.6 ms, and a longitudinal eddy current delay of 25 ms. A gradient pulse recovery time of 0.1 ms, 2%

and 60% of the maximum gradient intensity were used. Sixty-four scans were accumulated in time domain with 32768 points. 2D NMR experiments, namely [1]H–[1]H TOCSY, ^{1}H–^{1}H NOESY, ^{1}H–^{13}C HSQC and ^{1}H–^{13}C HMBC,[35] were performed using the following experimental conditions: [1]H–[1]H TOCSY and [1]H–[1]H NOESY were acquired in phase sensitive mode using TPPI selection, a 6 kHz spectral width in both dimensions, a 1.8 s relaxation delay, a 80 ms contact time for TOCSY and a 400 ms mixing time for NOESY, 2048 data points in f2 and 512 increments in f1. Zero filling in f1 to 1024 real data points and unshifted sinusoidal window functions in both dimensions were applied before Fourier transformation. The ^{1}H–^{13}C gradient-selected HSQC experiment was acquired in phase-selective mode with the following parameters: 13.8 µs π/2 ^{13}C hard pulse and 73 µs for composite pulse GARP ^{13}C decoupling sequence (GARP, Globally optimized Alternating-phase Rectangular Pulses), 6 and 30 kHz spectral widths in the proton and carbon dimensions, respectively, 2.5 s relaxation delay, 1024 data points in f2 and 512 increments in f1. Linear prediction up to 1024 point and unshifted squared cosine window functions were applied in the f1 dimension before Fourier transformation. The ^{1}H–^{13}C HMBC spectrum was obtained with a 2 s relaxation delay, π/2 pulse of 13.8 µs for ^{13}C, 6 and 30 kHz spectral widths in the proton and carbon dimensions, respectively, 1024 data points in f2, 512 increments in f1, linear prediction up to 1024 points in

f1, processed with the use of unshifted sinusoidal window functions in both dimensions.

A3.2.1 Olefin metathesis reaction on undecenyl resorc[4]arene 1a

Resorc[4]arene ω-undecenyl ester **1a** (0.2 g, 0.14 mmol) was dissolved in dry DCM (46 mL) to reach a final substrate concentration of 3.0×10^{-3} M. The solution was heated at reflux temperature and then exposed to a solution of the [(H$_2$IMes)(PCy$_3$)(Cl)$_2$Ru=CHPh)] catalyst (0.012 g, 0.014 mmol, 10 mol%) in dry DCM (4 mL), previously prepared into the glovebox. The reaction mixture was kept at reflux under stirring and nitrogen atmosphere for 20 min and afterwards treated with QuadraSil AP metal scavenger (aminopropyl silica gel, 4 g). After 5 min, the mixture was cooled to room temperature and left under stirring overnight. After filtration and evaporation, the residue was suspended in DCM and the soluble part was applied onto a silica gel column to give compound **2a** (88 mg, 46%, with DCM/ethyl acetate, 97:3) and product **3a** (10 mg, 5%, with DCM/ethyl acetate, 93:7). The yield of the insoluble portion **P1a** (85 mg in total, of which 45 mg recovered from the top of the column) was 44%.

*Bicyclic alkene **2a***

White powder, 46% yield. Mp: 190.9 ± 0.5 °C. ^{1}H and ^{13}C NMR signals are reported in Table 3.2. HRMS (ESI): *m/z* calcd for $C_{84}H_{120}O_{16}+Na^+$: 1407.84686 [M+Na]$^+$ (monoisotopic mass); found: 1407.84543. FT-IR (KBr): 2921, 2850, 1728, 1583, 1506, 1301, 1201 cm^{-1}. In Fig. 3.5 is reported a representative ^{1}H-NMR spectrum of bycyclic alkene **2a**.

Table 3.2 ^{1}H NMR and ^{13}C NMR signals* of bicyclic alkene **2a**

Carbon	^{13}C	^{1}H
C=O	172.5	-
C$_{Ar}$–O	156.5 155.6	-
CH= (*trans*) CH= (*cis*)	130.8 [130.1]	5.34 br t (3) [5.32 br t (4)]
CH$_i$ (26,28) CH$_i$ (25,27)	126.3 125.3	6.17 br s [6.18 br s] 6.84 br s [6.85 br s]
C$_{Ar}$–C	125.3 122.6	-
CH$_e$ (5,17) CH$_e$ (11,23)	97.4 95.5	6.48 s 6.40 s
OCH$_2$	64.3	3.95 dd (11.5, 7) 3.89 m
OMe	56.1 55.9	3.64 s 3.90 s
CH$_2$-(CO)	39.7	2.69 dd (14.5, 7) 2.64 dd (14.5, 7)
CH$_2$-(CH=)	32.0 [26.8]	2.01 m [2.03 m]
CH	32.8	5.05 t (7)
CH$_2$-(CH$_2$-CH=)	28.9	1.35 m
CH$_2$-(CH$_2$O)	28.6	1.50 m
CH$_2$ × 5	29.5 29.3 29.1 28.1 25.9	1.24 br m

* 600 MHz (^{1}H) and 100 MHz (^{13}C), CDCl$_3$, T = 300 K; coupling constants J (Hz) are given in parentheses. Proton and carbon resonances for the *cis* form, not coincident or overlapped by those of the *trans* form, are indicated by square brackets.
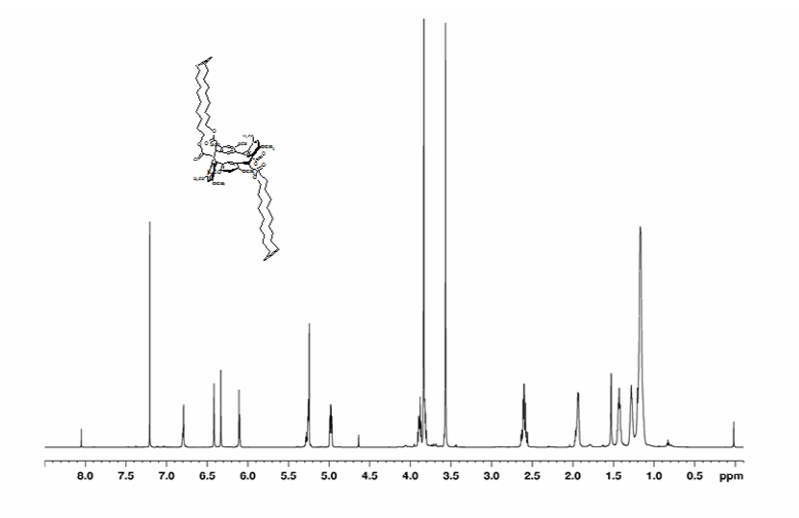
Figure 3.5 ^{1}H NMR spectrum of bicyclic alkene **2a.** 600 MHz, CDCl$_3$, 300 K.

Dimer *3a*

White powder, 5% yield. Mp: 166.9 ± 0.5 °C. ^{1}H and ^{13}C NMR signals are reported in Table 3.3. HRMS (ESI): *m/z* calcd for C$_{168}$H$_{240}$O$_{32}$+Na$^+$: 2792.70450 [*M*+Na]$^+$ (monoisotopic mass) and for C$_{168}$H$_{240}$O$_{32}$+Na^{2+}: 1407.84686 [*M*+2Na]$^{2+}$ (monoisotopic mass); found: 2792.69337 and 1407.84371. FT-IR (KBr): 2923, 2852, 1736, 1508, 1458, 1300, 1203 cm$^-$^{1}. In Fig. 3.6 is reported a representative ^{1}H-NMR spectrum of dimer **3a**.

Table 3.3 ^{1}H NMR and ^{13}C NMR signals* of linear dimer **3a**

Carbon	[13]C	[1]H
C=O	172.5	-
C_{Ar}–O	156.5	-
	155.6	
CH= (*trans*)	130.8	5.33 tt (3,1)
CH= (*cis*)	130.3	5.38 tt (3,1)
	[130.1]	[5.35 m]
	[129.8]	[5.36 m]
CH_i (26,28)	126.3	6.18 br s
CH_i (25,27)	125.3	6.87 br s
C_{Ar}–C	125.3	-
	122.6	
CH_e (5,17)	97.4	6.49 s
CH_e (11,23)	95.5	6.41 s
OCH_2	64.3	3.92 m
		3.87 m
OMe	56.1	3.60 s
	55.9	3.88 s
CH_2-(CO)	39.7	2.67 m
CH_2-(CH=)	32.6	1.96 m
	32.0	2.02 m
	[26.7]	[2.03 m]
	[26.8]	[2.03 m]
CH	32.8	5.04 t (7.5)
CH_2-(CH_2-CH=)	29.4	1.32 m
	28.9	1.35 m
CH_2-(CH_2O)	28.6	1.50 m
$CH_2 \times 5$	29.5; 29.3; 29.1; 28.1; 25.9	1.24 br m

* 600 MHz (^{1}H) and 100 MHz (^{13}C), $CDCl_3$, *T* = 300 K; coupling constants *J* (Hz) are given in parentheses. Proton and carbon resonances for the *cis* form, not coincident or overlapped by those of the *trans* form, are indicated by square brackets.

Figure 3.6 ^{1}H NMR spectrum of linear dimer **3a.** 600 MHz, CDCl$_3$, 300 K.

*Polymer **P1a***

White amorphous solid, 44% yield, which did not melt, nor soften (visually) under 300 °C. Solid state ^{13}C CPMAS NMR: δ 172.4 (C=O), 157.7 (C$_{Ar}$-O), 131.4 (CH=CH-), 126.4 (CH$_i$), 124.3 (C$_{Ar}$-C), 96.4 (CH$_e$), 65.0 (OCH$_2$), 56.3 (OCH$_3$), 41.9 (CH$_2$-C=O), 30.7 (CH and CH$_2$-CH=), 30.6 (CH$_2$). FT-IR (KBr): 3444 (broad), 2925, 2848, 1729, 1614, 1504, 1466, 1301, 1202 cm^{-1}. Elemental analysis (%): found: C 73.9 ± 0.69, H 8.79 ± 0.05. If we assume that **P1a** is a homogeneous polymer and C$_{84}$H$_{120}$O$_{16}$ is the molecular formula of the monomer, it requires C 72.8, H 8.73.

85

A3.2.2 Olefin metathesis reaction on compound 2a

Compound **2a** (0.070 g, 0.05 mmol) was dissolved in dry DCM (17 mL) to reach a final substrate concentration of 3.0×10^{-3} M. The solution was heated at reflux temperature and then exposed to a solution of the [(H$_2$IMes)(PCy$_3$)(Cl)$_2$Ru=CHPh)] catalyst (0.0045 g, 0.005 mmol, 10 mol%) in dry DCM (3 mL), previously prepared into the glovebox. The reaction mixture was kept at reflux under stirring and nitrogen atmosphere for 60 min and afterwards treated with QuadraSil AP metal scavenger (aminopropyl silica gel, 1.5 g). After 5 min, the mixture was cooled to room temperature and left under stirring overnight. After filtration and evaporation, the residue was purified by silica gel chromatography with DCM/ethyl acetate, 93:7 (v/v) as eluent, to give compound **3a** (7 mg, 10%) and more polar compounds which were not isolated. The starting bicyclic alkene **2a** was recovered unreacted from the column eluting with DCM/ethyl acetate, 97:3 (46 mg, 34% by weight).

A3.2.3 Catalytic hydrogenation of 2a

After two vacuum/nitrogen cycles to replace the air inside the reaction tube, compound **2a** (42 mg, 0.030 mmol) and 10% Pd/ C (10 mg) in dry THF (5 mL) were vigorously stirred at room temperature under 1 atm of hydrogen for 24 h. The reaction mixture was filtered through a membrane filter (Millipore, Millex-LH, 0.45 mm) and the filtrate was

concentrated. Purification of the residue by silica gel chromatography (DCM : ethyl acetate = 99 : 1 → 97 : 3) gave compound **2ar** (white solid, 42 mg, 0.030 mmol, quantitative yield). Mp: 184.3 ± 0.5 °C. ^{1}H NMR (400 MHz, CDCl$_3$, 300 K): δ (ppm) 6.81 (br s, CH$_i$-25,27), 6.45 (s, CH$_e$-5,17), 6.39 (s, CH$_e$-11,23), 6.21 (br s, CH$_i$-26,28), 5.03 (t, J = 7 Hz, 4H, CH), 3.92 (dd, J = 11.5 Hz, J = 7 Hz, 4H, OCH2), 3.87 (s, 12H, OMe), 3.91 (m, 4H, OCH$_2$), 3.64 (s, 12H, OMe), 2.69 (dd, J = 14.5 Hz, J = 7 Hz, 4H, CH$_2$–CO), 2.66 (dd, J = 14.5 Hz, J = 7 Hz, 4H, CH$_2$–CO), 1.49 (m, 8H, CH$_2$–CH$_2$O), 1.26 (br m, 16H, 8 6 CH$_2$); 13C NMR (100 MHz, CDCl$_3$, 300 K): δ (ppm) 172.4 (s, C=O), 156.5, 155.8 (s each, C$_{Ar}$–O), 126.6 (d, CH$_i$ 26,28), 125.8 (d, CH$_i$ 25,27), 125.1, 122.8 (s each, C$_{Ar}$–C), 97.3 (d, CH$_e$ 5,17), 95.6 (d, CH$_e$ 11,23), 64.2 (t, OCH$_2$), 56.1, 55.9 (q each, OMe), 39.6 (t, CH$_2$–CO), 32.8 (d, CH), 29.7, 29.3, 29.0, 28.9, 28.8, 28.5, 28.3, 28.2, 25.7 (t each, 9 x CH$_2$). HRMS (ESI): *m/z* calcd for $C_{84}H_{124}O_{16}{}^+$ Na$^+$: 1411.87816 [M + Na]$^+$ (monoisotopic mass); found: 1411.87772.

A3.2.4 ADMET reaction on undecenyl resorc[4]arene 1a

According to a literature method (Allcock et al., 2001), resorc[4]arene ω-undecenyl ester **1a** (0.5 g, 0.35 mmol) was added under a dry, nitrogen atmosphere to a previously evacuated and flame dried, high-vacuum valve equipped flask. The [(H$_2$IMes)(PCy$_3$)(Cl)$_2$Ru=CHPh)] catalyst (7.5 mg, 8.8×10^{-3} mmol, 2.5 mol%) was dissolved in dry DCM

(0.5 mL) into the glovebox under a nitrogen atmosphere. Such solution was *vacuum* transferred to the flask and the resulting mixture heated at 60 ºC under full vacuum and magnetic stirring. After 1 h and evaporation of all the solvent, the temperature was gradually increased to 80 °C to maintain fluidity and facilitate stirring. Immobilization of the stirrer bar and discoloration of the catalyst occurred within an additional half an hour. The reaction mixture was filtered on paper and washed with DCM to give AD-1 fraction (223 mg). The washings were concentrated and the residue was suspended in a small volume of DCM. The insoluble gelly fraction was separated, washed with *n*-hexane/DCM mixtures to give a second AD-2 fraction (12 mg) for an overall 49% yield. Both AD-1 and AD-2 fractions were insoluble in most organic solvents (including DMSO), as well as in 1 N or 12 N HCl. Solid state ^{13}C CPMAS NMR of fraction AD-1: δ 172.8 (C=O), 157.9 (C_{Ar}-O), 131.8 (CH=CH-), 126.7 (CH_i), 124.5 (C_{Ar}-C), 96.6 (CH_e), 65.4 (OCH_2), 56.6 (OCH_3), 42.2 (CH_2-C=O), 31.1 (CH and CH_2-CH30.8 (CH_2). Solid state ^{13}C CPMAS NMR of fraction AD-2: δ 172.2 (C=O), 157.4 (C_{Ar}-O), 131.2 (CH=CH-), 126.3 (CH_i), 124.0 (C_{Ar}-C), 96.1 (CH_e), 64.9 (OCH_2), 56.1 (OCH_3), 41.7 (CH_2-C=O), 31.5 (CH and CH_2-CH=), 30.5 (CH_2). Elemental analysis of AD-1 fraction: calcd (%) for $(C_{84}H_{120}O_{16})_n$: C 72.8, H 8.73; found: C 73.5 $\pm$ 0.69, H 8.94 $\pm$ 0.16

Chapter A4

Metathesis Reaction of Resorc[4]arene ω-undecenyl esters:
the *cone* form

A4.1 Results and discussion

Chapter A3 reported that four eleven-chain terminal alkenes linked by different arrangements to conformationally flexible resorc[4]arenes proved intriguing substrates of olefin metathesis reactions with second-generation ruthenium catalysts. This chapter report the results obtained with the *cone* stereoisomer of undecenyl resorc[4]arenes **1b**, (Fig. 4.1) in which the four side chains are all-*cis* (rccc) in the lower part of the macrocycle. Whilst in the *chair* conformer **1a** the side chains were isolated two by two in opposite sides of the molecule and could react independently, in the case of the *cone* conformer **1b**, the proximity of the four neighbour chains induced by the conformation may provide new findings or confirm the previous results.

A4.1.1 Olefin metathesis reaction on resorc[4]arene 1b

For the sake of comparison, the reaction parameters applied to resorc[4]arene **1b** (i.e., substrate concentration 3×10^{-3} M in DCM, second-generation Grubbs catalyst at 10 mol%, reflux temperature, and 20 min reaction time) were the same as used for the *chair* stereoisomer **1a** and previously optimized. (see Section A3.1.1)
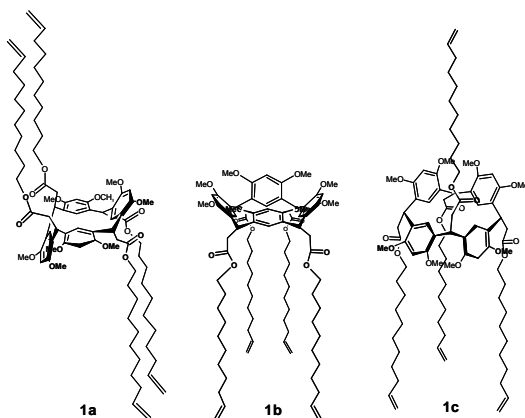
Figure 4.1 Chemical structures of resorc[4]arene ω-undecenyl esters **1a** (*chair*), **1b** (*cone*), and **1c** (*1,2-alternate*) synthesized as described in Chapter A3.

The crude reaction mixture obtained under these conditions was treated with a metal scavenger (QuadraSil AP) to remove residual ruthenium by filtration, and purified by silica gel chromatography with eluting mixture of increasing polarity (see Section A4.3.1). The following products (Scheme 4.1) were isolated in the order: **2b** (yellow solid, 15% yield), **3b** (white solid, 50% yield), **4b** (white solid, 9% yield), and **5b** (white solid, 5% yield). The structures of compounds **2b–5b** were unambiguously confirmed through NMR spectroscopy and electrospray ionization high-resolution mass spectrometry (ESI-HRMS).
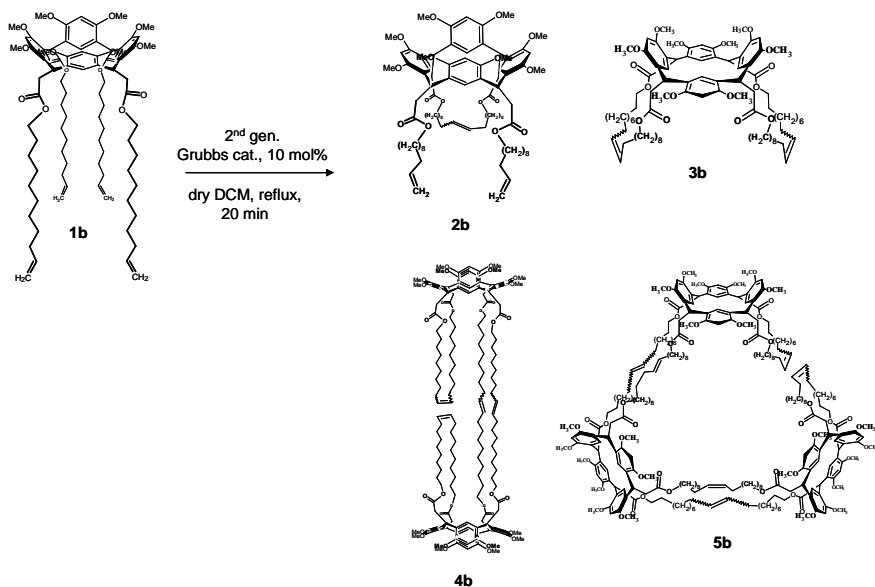
Scheme 4.1 Olefin metathesis reaction of resorc[4]arene **1b**.

A4.1.1.1 Structures of the products obtained by olefin metathesis

The ^{1}H and ^{13}C NMR spectral data of undecenyl resorc[4]arene **1b** were previously reported (see Section A.3.1.1). The presence of single signals for equivalent aromatic and methoxyl protons and carbons suggested that the molecule assumes in solution the *cone* conformation with a C_4 symmetry. All NOESY cross peaks have a negative NOE, pointing out that the system is in a fast tumbling motion regime, as expected for a conformation created by the

equilibrium between two *flattened-cone* forms (Högberg, 1980a; Högberg, 1980a; Botta et al., 2005).

Basket 3b

Comparison of the NMR spectral data of **3b**, the most abundant product (i.e., 50% yield), with those of the starting resorc[4]arene **1b** evidenced the following points. Proton and carbon signals for the terminal methylene of **1b** are no more present in the NMR spectra of **3b**, while the signal for an olefin methine is still linked (as shown by TOCSY spectra) with the methylene groups of the chain, but shifted highfield. These findings confirm the occurrence of an RCM reaction, i.e., the formation of a double bond between two chains with the elimination of one molecule of ethylene. Accordingly, the sodium adduct $[M + Na]^+$ in the ESI mass spectrum of **3b** was found at m/z 1407.84756, which is 56 m/z (2 × C_2H_4) less than the corresponding $[M + Na]^+$ peak of **1b** (m/z 1463.91035). These findings fix at about 1385 the molecular weight of **3b**, with a molecular formula of $C_{84}H_{120}O_{16}$, requiring two intramolecular bridges by two almost contemporary RCM reactions. A second issue which emerged by comparison of the NMR spectra of compounds **3b** and **1b** is the number of signals for the aromatic and methoxyl protons basically doubled (*vide infra*) in the case of **3b**, revealing a loss of symmetry of the upper rim. The distribution pattern of the

signals, particularly the highfield resonances for the equivalent H-25/H-27 aromatic protons (A/C rings) and for the methoxyl groups (B/D-rings) requires that the aromatic rings are alternatively quasi perpendicular: the B/D rings are face to face and the A/C rings lie almost in the plane identified by the four bridge methines. NOESY spectra confirmed the spatial correlations between these protons and both the internal aromatic protons (namely, H-26/H-28 and H-25/H-27), while strong positive cross peaks between H-26/H-28 and H-25/H-27 signals, together with the absence of interaction peaks between external H-5/H-17 and H-11/H-23 aromatic protons, supported a rigidified *boat* conformation with the all-*cis* configuration of the bridge chains (Högberg, 1980a; Högberg, 1980a; Botta et al., 2005).

We previously attributed such a conformation, named also *flattened cone*, to a double-spanned resorcarene, in which the insertion of two polymethyene bridges led to the formation of a cavity-shaped architecture resembling a basket (Botta et al., 1997). The ^{1}H and ^{13}C NMR spectra of **3b**, however, are complicated by the presence of satellite signals: the resonance at δ = 5.24 (br t, *J* = 4 Hz) for the disubstituted =CH methine is flanked by a minor signal of the same nature (br t, *J* = 5 Hz) at δ = 5.27. The two peaks, in an approximate integrated ratio of 3 : 1, were correlated (by TOCSY data) to methylene signals at δ = 1.95 and δ = 1.92, whose corresponding

carbon resonances (by HSBQ) appear at quite different values (δ = 2.65 vs 28.91). The two peaks were thus assigned to *trans* and *cis* olefinic protons, respectively, in agreement with the major shielding of the α-CH$_2$ in the *cis* configuration. Moreover, the highfield signal (δ = 5.24 ppm) showed a strong spatial correlation (by NOESY) with the protons of both α- and β-methylene groups, whereas the minor signal (at δ = 5.27 ppm) was NOE-correlated only to the protons of the geminal methylene nucleus, as expected for *trans* and *cis* olefinic protons, respectively. With regard to the two different geometries of the double bond, three possible arrangements of the whole molecule can be envisaged, i.e., *trans*/*trans*, *trans*/*cis*, and *cis*/*cis*. The overall 3 : 1 ratio between the *trans* and *cis* signals requires that *tt*-, *tc*- and *cc*-forms are in a relationship 9: 6: 1. As a consequence, not only the signals for the α-CH$_2$ are affected, but the entire ^{1}H NMR spectrum. While the signals of the remaining methylene groups of the aliphatic chains cannot be distinguished, the chemical shifts of the singlets corresponding to the aromatic and methoxyl protons depend on the three possible arrangements of the whole molecule. As a result, satellite minor peaks flank the major signals, attributed to the *tt*- form. A tentative assignment of all proton resonances of **3b**, taking into consideration the superimposition of some signals, is summarized in Table 4.1. The comparison is somehow consistent with this picture.

Catalytic hydrogenation (10% Pd/C) of **3b** led to the unique reduction compound **3br** (Fig. 4.2), which showed the expected [*M* + Na]⁺ peak at *m/z* 1411.87772 and clean signals without satellite peaks in the ¹H and ¹³C NMR spectra (see Section A4.2.3).
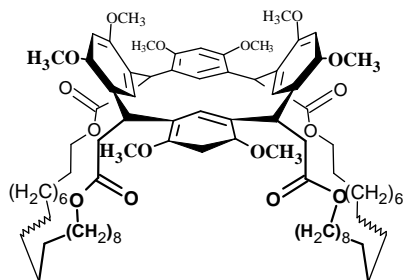
Figure 4.2 Catalytic hydrogenation of **3b** led to the unique reduction compound **3br**.

The reduction influenced the chemical shifts of the aromatic protons, which however maintained the typical distribution pattern (H-25/H-27, H-11/H-23, H-5/H-17, H-26/H-28) of a *flattened cone* form.

Hemi-basket 2b

In the ¹H and ¹³C NMR spectra of the second product **2b** (15% yield) both the signal (at δ = 5.34 ppm) for a disubstituted double bond (as

in **3b**) and the AMN system (at δ = 5.82, 4.99 and 4.93 ppm, respectively) of the vinylidene group (as in the parent resorc[4]arene **1b**) were found. These findings and the sodium adduct [*M* + Na]⁺ in the ESI mass spectrum at *m/z* 1435.87745 suggest that only one ring closure occurred between two side chains, the remaining two being still free. The complicate distribution pattern of the signals – mainly doubled – for aromatic protons and methoxyl groups in the ^{1}H NMR spectrum of **2b** was attributed to the presence of two forms in equilibrium, originated by the loss of freedom of the aromatic B ring (see Figure 4.3) connected to the new bridge-chain. The two forms are depending on the free oscillation of D ring, which will be approximately parallel (α) or perpendicular (β) to the opposite B ring. The α-form maintains the arrangement of a *flattened cone* of the original *cone* conformation (that of the starting **1b**), while the β-form assumes the conformation of a *chair*-like partial *flattened cone*. The ^{1}H NMR spectral data of the two conformers are expected quite similar, and a non-tentative assignment is possible only for H-26 proton, which undergo different shielding effects of the aromatic ring B in the two α and β forms. The presence in the proton spectrum of minor signals in the regions of the aromatic rim was again attributed to the α and β forms of the *cis* isomer, in a ratio 1 : 3 with the *trans* isomer, as confirmed by integration of the signals at δ = 5.36 (br t, *J*

= 4 Hz) and δ = 5.34 (br t, *J* = 3 Hz), respectively. Compound **2b** is obviously the intermediate precursor of basket **3b** and, in this sight, it can be designated as a hemi-basket.
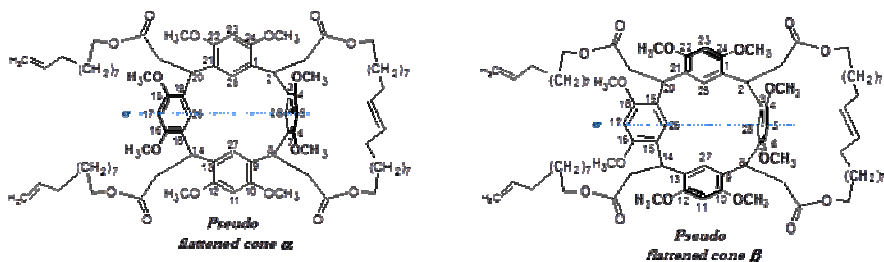
Figure 4.3 Conformers in equilibrium for the hemi-basket **2b** in solution.

Dimer 4b

With regard to compound **4b**, the first of two minority and more polar products (9% yield), the ^{1}H and ^{13}C NMR spectral data were very similar to those of the basket derivative **3b**. Again, the signals for the terminal methylene in the starting **1b** disappeared, but to be substituted by those for two disubstituted *trans*-double bonds. Actually, the two =CH resonances were linked to methylene signals with δ values 32.15 and 32.50, that require both to be in α position to a *trans*-double bond. Although in the ^{1}H NMR spectrum the signals for a *cis*-olefin could not be distinguished by the two main values (δ = 5.36 and 5.32), in the ^{13}C NMR spectrum the resonances

at δ = 130.7 and 130.2 were flanked by two smaller (visually 30%) partners at δ = 129.69 and 129.65. Therefore, we hypothesized the presence of two different types of chain, the first involving a sequence of signals for =CH, α-CH$_2$ and β-CH$_2$ comparable to those of **3b**, and the second with slightly different values for the above groups, both ending in a series of methylenes (from γ to ω) giving undistinguishable signals. The changes in the second chain were attributed to the formation of two intermolecular double bonds from two side chains of two molecules, while the other two original intramolecular double bonds remained unchanged, in conclusion to the obtainment of a dimer with structure **4b** (Scheme 4.1). Two diagnostic peaks at *m*/*z* 2792.69337 and 1407.84371 in the ESI mass spectrum, which were attributed to [*M* + Na]+ and [*M* + 2Na]$^{2+}$ sodium adducts, respectively, revealed for dimer **4b** a molecular weight of 2769.7 Da (2 times that of **3b**) and a molecular formula of $C_{168}H_{240}O_{32}$. Both the diagnostic peaks originated serial losses of CH$_2$ (14 and 7 m/z, respectively), as expected for compounds endowed with a long hydrocarbon chain. The distribution pattern of the signals for aromatic and methoxyl protons was again in agreement with a *flattened cone* arrangement of the two aromatic rims. However, weak negative NOESY peaks between H-25/H-27 and H-26/H-28 suggested the interconversion between two *flattened cone* α and β forms, where two opposite, e.g., A/C, aromatic rings are

alternatively vertical or planar, respectively. (Högberg, 1980a; Högberg, 1980a; Botta et al., 2005) Moreover, negative NOE peaks between H-5/H-17 and the corresponding methoxyl protons, as well as positive NOE peaks between H-11/H-23 and the corresponding methoxyl protons, require that planar and vertical aromatic rings have different mobility. On the other hand, the α-CH$_2$ signal shows a cross peak with the H-25/H-27 resonance in both NOESY and ROESY spectra, but it could be correlated to H-26/H-28 proton only in the ROESY experiment. These findings suggest that the oscillations of the two *flattened cone* α and β forms, as a consequence of the presence of two different side chains, undergo a slow down and will have longer lifetimes than the NMR acquisition time. Consequently, the signals from both conformers will be registered, as in the somehow similar hemi-basket compound **2b**. Indeed, the ^{1}H NMR spectrum of **4b** is characterized by the presence of multiple or broadened (br) signals for aromatic protons and methoxyl groups, whereas the appearance of the aliphatic methine as a triplet (with *J* = 7.5 Hz) instead of a double doublet (with *J* = 7 and 8 Hz) testify the relative freedom of **4b** with respect to **3b** due to the formation of a greater macrocycle.

Trimer 5b

The NMR spectral data of the second polar product **5b** (5% yield) are almost coincident with those of **4b**. Two different *trans*-CH= are still present, suggesting the presence of both inter and intramolecular double bonds, while the multiplicity (t, *J* = 7 Hz) of the aliphatic methine accounts for a comparable mobility of **4b** and **5b**. Conversely, the signals for the aromatic rim appear to be multiplied and, in some case, coalesce. The ESI mass spectrum of **5b** showed two diagnostic peaks at *m/z* 1407.85164 and 2101.76775, which were assigned to triply charged $[M + 3Na]^{3+}$ and doubly charged $[M + 2Na]^{2+}$ sodium adducts, respectively. A trimeric structure, as compared with the monomer **3b**, with a molecular weight of about 4154 Da and corresponding to a molecular formula of $C_{252}H_{360}O_{48}$ was thus assigned to compound **5b**. It is worthy of note that the *cone* undecenyl resorc[4]arene **1b** did not give any detectable polymer by olefin metathesis, while, at the same substrate concentration, the *chair* stereoisomer **1a** underwent an ADMET-like polymerization to furnish, although in unfavourable conditions, an insoluble polymer product. Evidently, the crowded arrangement of the *cone* conformer with respect to the other prevents the occurrence of such reaction.

A4.1.2 Reactivity of basket 3b

The synthesis of basket **3b** from undecenyl resorc[4]arene **1b** passes through the formation of hemi-basket **2b**, and occurs by two almost contemporary RCM reactions, driven by the loss of two molecules of ethylene, as we have already proposed (see Section A3.1.2). Notably, whereas in the case of the *chair* stereoisomer **1a** we did not isolate the hemi-functionalized intermediate, now we can confirm the proposed reaction mechanism.

The attribution of structures **4b** and **5b** as the homo-dimer and homo-trimer, respectively, of **3b** and the central position of the basket derivative **3b** in the overall metathesis reaction was stressed by submitting an aliquot of pure **3b** to olefin metathesis conditions (see Section A4.2.2). As a result, compounds **4b** and **5b** were again obtained in 9.5 and 14% yields, respectively, and around 64% of the unreacted starting **3b** was recovered. These results exclude that the central ring of the two **4b** and **5b** compounds could have been originated by two intermolecular cross-metathesis (CM) reactions, because the formation of the macro ring requires the opening of two smaller rings and a novel closure to the big one. On the other hand, we have already showed that the intermolecular closure between chains of different molecules would start more likely an ADMET-like polymerization.

A4.2 Experimental section

General procedures and materials

All manipulations were performed using a combination of glovebox and high vacuum under a nitrogen atmosphere. HPLC grade solvents were dried and degassed by standard procedures. Second-generation Grubbs catalyst and QuadraSil AP silica gel were purchased from Sigma Aldrich.

A4.2.1 Olefin metathesis reaction of resorc[4]arene 1b

Resorc[4]arene ω-undecenyl ester **1b** (0.25 g, 0.17 mmol), obtained as previously described (see Section A2.2.2), was dissolved in dry DCM (57 mL) to reach a final substrate concentration of 3.0×10^{-3} M. The solution was heated at reflux temperature and then exposed to a solution of the [(H$_2$IMes)(PCy$_3$)(Cl)$_2$Ru=CHPh)] catalyst (0.015 g, 0.017 mmol, 10 mol%) in dry DCM (3 mL), previously prepared in the glovebox. The reaction mixture was kept at reflux under stirring and nitrogen atmosphere for 40 min, and then treated with QuadraSil AP metal scavenger (aminopropyl silica gel, 4 g). After 5 min, the mixture was cooled to room temperature and left under stirring overnight. After filtration and evaporation, the residue was suspended in DCM and applied onto a silica gel column to give compounds **2b** (36 mg; 15%) and **3b** (120 mg; 50%) with DCM: ethyl

acetate 91:9); compounds **4b** (21.5 mg; 9%) and **5b** (12 mg; 5%) with chloroform: methanol, 99:1.

Compound 3b. White solid, mp 175–176 °C, 120 mg, 0.087 mmol (50% yield). ^{1}H and ^{13}C NMR signals are given in Table 4.1. ESI-HRMS (positive): $C_{84}H_{120}O_{16}Na$ requires 1407.84741 (monoisotopic mass), *m/z* found 1407.84756 ([M + Na]$^+$). FT-IR (KBr): 2921, 2850, 1728, 1583, 1506, 1301, 1201 cm^{-1}. In Fig. 4.4 is reported a representative ^{1}H-NMR spectrum of basket **3b**.

Figure 4.4 ^{1}H NMR spectrum of basket **3b .** 600 MHz, CDCl$_3$, 300 K.

Table 4.1 ^{1}H NMR and ^{13}C NMR Signals* of basket Resorc[4]arene **3b**.

Carbon	^{1}H	^{13}C
C=O	-	172.5
C$_{Ar}$–O	-	156.4
		155.7
CH= **	5.31 t (4)	130.7
CH$_i$ (25,27)	6.12 s	126.2
CH$_i$ (26,28)	6.88 s	125.3
C$_{Ar}$–C	-	125.0
		123.2
CH$_e$ (5,17)	6.16 br s	97.3
CH$_e$ (11,23)	6.42 br s	95.2
OCH$_2$	3.99 dt (10.7, 6.8)	64.3
	3.90 dt (10.7, 6.8)	
OMe	3.82 s	55.9
	3.42 s	55.8
CH$_2$-(CO)	2.78 dd (15.5, 8)	39.1
CH	4.94 dd (8, 7)	33.0
CH$_2$-(CH=)**	2.02 m	32.0
CH$_2$-(CH$_2$-CH=)	1.33 m	29.3
CH$_2$-(CH$_2$O)	1.53 br m	28.7
CH$_2 \times 5$	1.23 br m	29.5
		29.1
		29.0
		28.1
		26.0

* 600 MHz (^{1}H) and 100 MHz (^{13}C), CDCl$_3$, T = 300 K; coupling constants J (Hz) are given in parentheses. **Only the signals assigned to the predominant isomer are reported.

Compound 2b. Yellow solid, mp 123–124 °C, 36 mg, 0.025 mmol (15% yield). ^{1}H and ^{13}C NMR signals are given in Table 4.2 ESI-HRMS (positive): $C_{86}H_{124}O_{16}Na$ requires 1435.87816 (monoisotopic mass), *m/z* found 1435.87745 ([M + Na][+]). FT-IR (KBr): 2921, 2850, 1728, 1583, 1506, 1301, 1201 cm^{−1}. In Fig. 4.5 is reported a representative ^{1}H-NMR spectrum of hemi-basket **2b**.
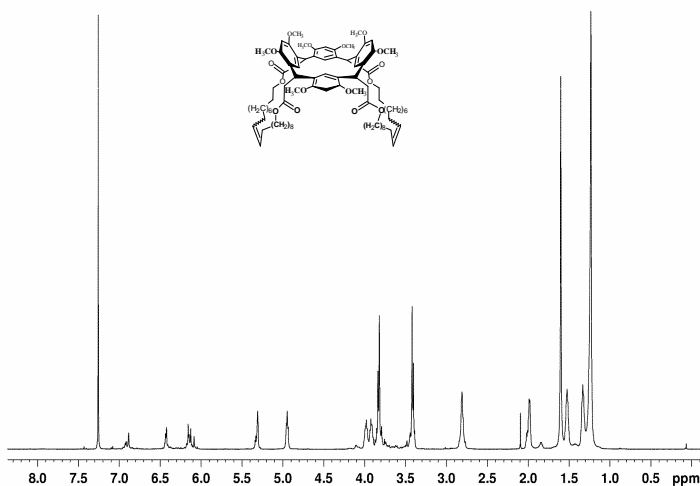

Figure 4.5 ^{1}H NMR spectrum of hemi-basket **2b.** 600 MHz, CDCl$_3$, 300 K.

Table 4.2 ^{1}H NMR and ^{13}C NMR Signals* of hemi-basket Resorc[4]arene **2b**.

Carbon	[1]H	[13]C
C=O	-	172.5
		172.4
C_{Ar}–O	-	156.1, 156.0
		155.7, 155.5
CH=(CH_2)	5.82 ddt (17, 10, 6.5)	132.7
CH=(CH)	5.34 br t (3)	130.7
CH_i (25,27)	6.24, 6.23 × 2 s	126.4, 126.2
CH_i (26)	6.78 (α), 6.53 (β) s	125.7, 125.5
CH_i (28)	6.73, 6.72 s	
C_{Ar}–C	-	Not detected
=CH_2	4.99 br d (17)	114.1
	4.93 br d (10)	
CH_e (5,17)	6.31, 6.30 s	97.1, 97.0
CH_e (11,23)	6.38, 6.37 s	95.9, 95.8
OCH_2	4.00 dt (10.8, 6.5)	64.3
	3.90 m	64.3
	3.95 × 2 t (7)	
OMe	3.52 × 2 s	55.9
	3.75, 3.73 s	
	3.65, 3.63 × 2 s	
CH_2-(CO)	2.85, 2.81 m	39.1
	2.83 d (7) × 2	
CH	4.96, 4.94** m	33.1, 32.9
CH_2-(CH=)	2.03 br q (6.5)	33.8, 32.14
CH_2-(CH_2-CH=)	1.35 m	28.6, 28.6
CH_2-(CH_2O)	1.52, 1.47 m	28.9
CH_2 × 5	1.24 br m	29.6
		29.3
		29.2
		29.0
		26.0

* 600 MHz (^{1}H) and 100 MHz (^{13}C), CDCl$_3$, *T* = 300 K; coupling constants *J* (Hz) are given in parentheses. ** Tentative assignment due to superimposition of =CH_2 signals.

Compound 4b. White solid, mp 144–145 °C, 21.5 mg, 0.008 mmol (9% yield). ^{1}H and ^{13}C NMR signals are given in Table 4.3. ESI-HRMS (positive): $C_{168}H_{240}O_{32}Na$ requires 2792.70450 (monoisotopic mass), *m/z* found 2792.69337 ([M + Na][+]); $C_{168}H_{240}O_{32}Na_2$ requires 1407.84686 (monoisotopic mass), *m/z* found 1407.84371 ([M + 2Na][2+]). FT-IR (KBr): 2923, 2852, 1736, 1508, 1458, 1300, 1203 cm^{-1}. In Fig. 4.6 is reported a representative ^{1}H-NMR spectrum of dimer **4b**.
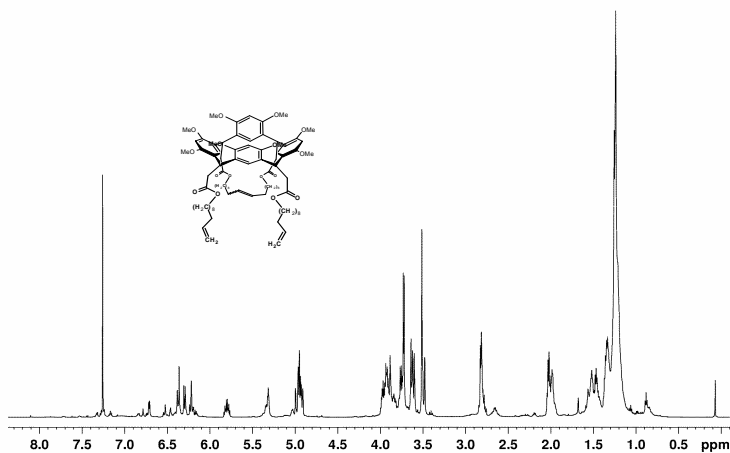

Figure 4.6 ^{1}H NMR spectrum of dimer **4b.** 600 MHz, CDCl$_3$, 300 K.

Table 4.3 ^{1}H NMR and ^{13}C NMR Signals* of dimer **4b**.

Carbon	[1]H	[13]C
C=O	-	172.5
C_{Ar}–O	-	156.4
		155.7
CH= (t)	5.32 m	130.8
	5.36 m	130.1
CH_i (25,27)	6.16 × 2, 6.14, 6.11 br s	126.2
CH_i (26,28)	6.94, 6.91, 6.90, 6.89 br s	125.4
C_{Ar}–C	-	125.1
		123.3
CH_e (5,17)	6.19 × 3, 6.18 br s	97.6
CH_e (11,23)	6.46, 6.41 × 3 br s	95.6
OCH_2	3.99 dd (11.5, 7)	64.5
	3.93 dd (11.5, 7)	
OMe	3.85, 3.83 × 3 br s	56.2
	3.45 × 3, 3.43 br s	55.9
CH_2-(CO)	2.83 br d (7)	39.2
CH	4.94 t (7.5)	33.1
CH_2-(CH=)	1.98 m	32.7
	2.02 m	32.2
CH_2-(CH_2-CH=)	1.33 m	29.4
	1.31 m	Not detected
CH_2-(CH_2O)	1.53 br m	28.7
CH_2 × 5	1.24 br m	29.5
		29.2
		29.0
		28.2
		26.0

* 600 MHz (^{1}H) and 100 MHz (^{13}C), $CDCl_3$, T = 300 K; coupling constants J (Hz) are given in parentheses.

Compound 5b. White solid, mp 150–151 °C, 12 mg, 0.0029 mmol (5% yield). ^{1}H and ^{13}C NMR signals are given in Table 4.4. ESI-HRMS (positive): $C_{252}H_{360}O_{48}Na_2$ requires 2100.27623 (monoisotopic mass), *m/z* found 2101.76775 ([M + 2Na]$^{2+}$). $C_{252}H_{360}O_{48}Na_3$ requires 1407.84741 (monoisotopic mass), *m/z* found 1407.85164 ([M + 3Na]$^{3+}$). FT-IR (KBr): 2923, 2852, 1736, 1508, 1458, 1300, 1203 cm^{-1}. In Fig. 4.7 is reported a representative ^{1}H-NMR spectrum of trimer **5b**.
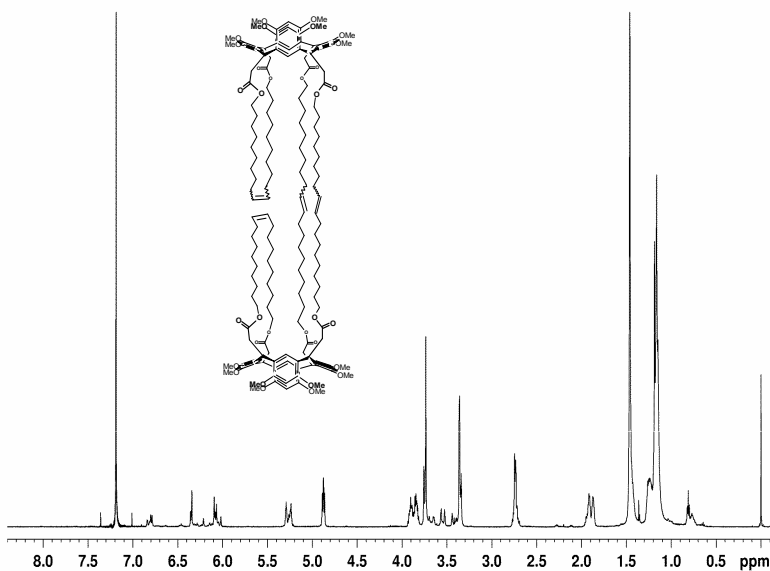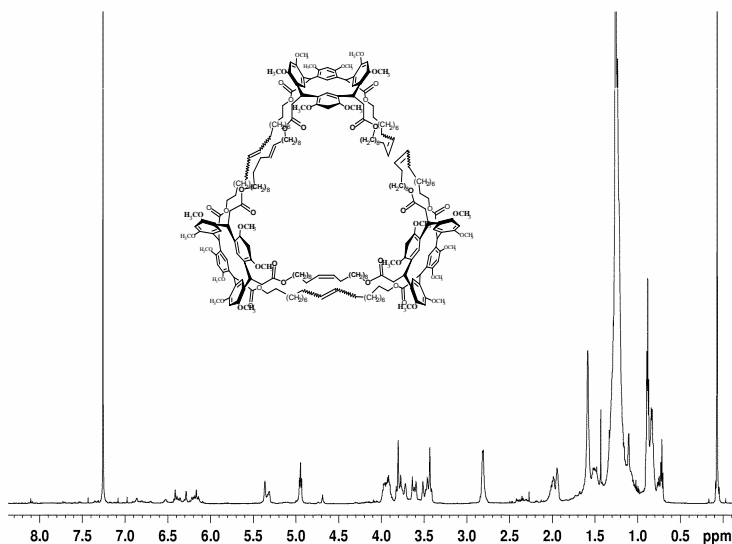

Figure 4.7 ^{1}H NMR spectrum of trimer **5b**. 600 MHz, CDCl$_3$, 300 K.

Table 4.4 ^{1}H NMR and ^{13}C NMR Signals* of trimer **5b**.

Carbon	[1]H	[13]C
C=O	-	172.4
C_{Ar}–O	-	156.3
		155.5
CH= (t)	5.32 m	130.7
	5.36 m	130.2
CH_i (25,27)	6.14 br s	126.2
CH_i (26,28)	6.87 br s	126.0
C_{Ar}–C	-	124.9
		123.2
CH_e (5,17)	6.17 br s	97.4
CH_e (11,23)	6.41 br s	95.3
OCH_2	3.96 m	64.5
	3.92 m	
OMe	3.82 br s	56.2
	3.41 br s	55.9
CH_2-(CO)	2.81 m	39.0
CH	4.95 t (7.5)	32.9
CH_2-(CH=)	1.94 m	32.5
	1.98 q (6.5)	32.2
CH_2-(CH_2-CH=)	1.32 m	29.5
	1.30 m	Not detected
CH_2-(CH_2O)	1.50 m (6.5)	28.6
$CH_2 \times 5$	1.23 br m	29.6
		29.3
		29.0
		28.6
		26.7

* 600 MHz (1H) and 100 MHz (13C), CDCl3, T = 300 K; coupling constants J (Hz) are given in parentheses.

ì

A4.2.2 Olefin metathesis reaction on compound 3b

Compound **2a** (0.14 g, 0.1 mmol) was dissolved in dry DCM (4 mL) to reach a final substrate concentration of 1.65×10^{-2} M. The solution was heated at reflux temperature and then exposed to a solution of the $[(H_2IMes)(PCy_3)(Cl)_2Ru=CHPh)]$ catalyst (0.008 g, 0.01 mmol, 10 mol%) in dry DCM (2 mL), previously prepared into the glovebox. The reaction mixture was kept at reflux under stirring and nitrogen atmosphere for 40 min and afterwards treated with QuadraSil AP metal scavenger (aminopropyl silica gel, 2.27 g). After 5 min, the mixture was cooled to room temperature and left under stirring overnight. After filtration and evaporation, the residue was purified by silica gel chromatography with chloroform: methanol, 99:1 (v/v) as eluent, to give compound **4b** (21.5 mg; 9%) and compound **5b** (12 mg; 5%). The starting basket **3b** was recovered unreacted from the column eluting with DCM/ethyl acetate, 97:3 (30 mg, 22% by weight).

A4.2.3 Catalytic hydrogenation of 3b

After two vacuum/nitrogen cycles to replace the air inside the reaction tube, compound **3b** (42 mg, 0.030 mmol) and 10% Pd/ C (10 mg) in dry THF (5 mL) were vigorously stirred at room temperature under 1 atm of hydrogen for 24 h. The reaction mixture was filtered through a membrane filter (Millipore, Millex-

LH, 0.45 mm) and the filtrate was concentrated. Purification of the residue by silica gel chromatography (DCM : ethyl acetate = 99 : 1 → 97 : 3) gave compound **3br** (white solid, 42 mg, 0.030 mmol, quantitative yield). Mp: 171,8 ± 0.3 ºC. ^{1}H NMR (400 MHz, CDCl$_3$, 300 K): δ (ppm) 6.70 (br s, CH$_i$-26,28), 6.35 (br s, CH$_i$-25,27), 6.35 (s, CH$_e$-11,23), 6.23 (s, CH$_e$-5,17), 4.96 (t, J = 7 Hz, 4H, CH), 3.96 (8H, m; OCH$_2$), 3.71 (s, 12H, OMe), 3.53 (s, 12H, OMe), 2.81 (8H, d, J = 7Hz; CH$_2$CO), 1.53 (m, 8H, CH$_2$– CH$_2$O), 1.26 (14 H, br m; 7 x CH$_2$); ^{13}C NMR (100 MHz, CDCl$_3$, 300 K): δ (ppm) 172.53 (s, C=O), 156.20, 155.91 (s each, C$_{Ar}$–O), 125.60 (d, CH$_i$ 26,28), 125.93 (d, CH$_i$ 25,27), 124.64, 123.89 (s each, C$_{Ar}$–C), 95.97 (d, CH$_e$ 11,23), 96.93 (d, CH$_e$ 5,17), 64.35 (t, OCH$_2$), 56.0, 55.93 (q each, OMe), 39.26 (t, CH$_2$–CO), 32.98 (d, CH), 29.70, 29.13, 28.70, 28.60, 28.35, 28.29, 28.08, 25.88 (t each, 9 x CH$_2$). HRMS (ESI): m/z calcd for C$_{84}$H$_{124}$O$_{16}^+$ Na$^+$: 1411.87816 [M + Na]$^+$ (monoisotopic mass); found: 1411.87772.

Chapter A5

Metathesis Reaction of Resorc[4]arene ω-undecenyl esters: the *1,2-Alternate* form

A5.1 Results and discussion

This chapter report the results obtained with the *1,2-alternate* stereoisomer of undecenyl resorc[4]arenes **1c** (Fig. 5.1). In ^{1}H- and ^{13}C-NMR spectra of the stereoisomer **1c** the signals belonging to the aliphatic moiety exhibit a distribution pattern of the areas essentially 1: 2: 1, whereas the aromatic or methoxyl-group protons gave 4 singlets. The molecule has thus a Cs symmetry due to a plane passing trough C-2 and C-14 methines and perpendicular to the macrocyclic ring. After a comparison with the literature data [A,B] the compound was assigned a *1,2-alternate* conformation with a *cis-trans-cis* arrangement (relative to C-2) of the pseudoaxial substituents.

A5.1.1 Olefin metathesis reaction on resorc[4]arene 1b

For the sake of comparison, the reaction parameters applied to resorc[4]arene **1c** (i.e., substrate concentration 3×10^{-3} M in DCM, second-generation Grubbs catalyst at 10 mol%, reflux temperature, and 20 min reaction time) were the same as used for the *chair* stereoisomer **1a** and previously optimized. (see Section A3.1.1)
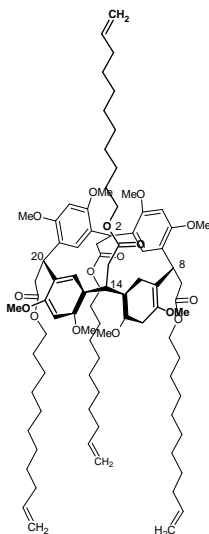
Figure 5.1 Chemical structures of resorc[4]arene ω-undecenyl esters **1c** (*1,2-alternate*) synthesized as described in Chapter A3.

The crude reaction mixture obtained under these conditions was treated with a metal scavenger (QuadraSil AP) to remove residual ruthenium by filtration, and purified by silica gel chromatography with eluting mixture of increasing polarity (see Section A5.2.1). The following products were isolated in the order: **2c** (yellow solid, 15% yield), **3c** (white solid, 26% yield). The structures of compounds **2c** and **3c** were confirmed through NMR spectroscopy and electrospray ionization high-resolution mass spectrometry (ESI-HRMS).

A5.1.2 Structures of the products obtained by olefin metathesis

Proton and carbon spectra of **1c** (see Section A2.2.2) are compared with those of the reaction products **2c** and **3c** reported in Tables 5.1 and 5.2. The distribution pattern of the signals of **2c** suggest that once again the metathesis reaction occurred for the disappearance of the resonances relative to the terminal methylene and the presence of those relative to two new inner double bonds, which by the chemical shifts can be defined as intramolecular (δ 5.3) and intermolecular (δ 5.5), respectively. Both ^{1}H- and ^{13}C-NMR spectra of **2c** are polluted by minor signals due to cis/trans isomerism of the new double bonds: the cis/trans ratio could not be measured because of the superimposition of the signals, but should not be different from that (1/3) obtained in previous experiments. The effects of the phenomenon were however deleted by the catalytic hydrogenation (10% H_2/Pd) of **2c** that gave a unique reduction product with clean signal in ^{1}H and ^{13}C NMR spectra. The NMR findings support the hypothesis of an intramolecular ring closure between the C-8 and C-20 side chains, neighbor with the same orientation. The second intermolecular closure between the remaining active C-2 and C-14 substituents, pointing out to opposite directions is no more possible. Analogously, the formation of a closed dimer can be excluded.

If the C-2a substituent of molecule A is linked e.g. to the C-14b of a second molecule B, the remaining terminal methylenes on the C-14a and C-2b chains will be farther away. We can thus foresee the growth of an open linear polymer of *n* units, where *n* (also the number of inner double bonds) is so high that the signal of terminal =CH$_2$ becomes insignificant or a cyclic oligomer of *m* units where finally C-14a and C-2*m* could achieve the intermolecular connection. Accordingly the mass spectrum (EIMS) of **2c** showed two main mono-isotopic peaks at 2792.7 and 1407.8 *m/z*, both with the typical losses of 14 *m/z* (CH$_2$), which correspond numerically to [2M + Na]$^+$ and [M + Na] with M = 1384 D. The reaction product **3br**, obtained from the starting isomer compound **1b,** (cone conformation), by double intra-molecular ring closure has a molecular weight 1384 D, a base peak at 1407.8 *m/z*, but no [2M + Na] ion is formed at 2792.7. Conversely, the open dimer **4b**, produced by the same metathesis reaction, has a molecular weight 2768 D and exhibit a peak corresponding to [2M + Na] at 2792.7. *m/z*. In the mass spectrum of **4b** a base peak at 1407.8 is also present, but it corresponds to a double charged ion [2M + 2Na]$^{+2}$ with a typical cluster (isotopic peaks separated by 0.5 *m/z*). Finally the possibility that one of the two main peaks could belong to an impurity was excluded, because in the mass spectrum of the

reduction product **2cr**, both the candidates are shifted to 1411.7 and 2800.8, respectively.

The two peaks were thus thaught to come from an oligomer of n units with mass M, but nor a metastable peak m* was detected for the passages nMNa → MNa or nMNa → 2MNa, neither a pluri-charged ion $[nM + xNa]^{+x}$ was found, also because the EIMS spectrum covers a limited range of *m/z* (0 – 4000). In conclusion, at the moment we may attribute to 2c the structure of a cyclic oligomer of n units, where n is at least > 3 (Fig. 5.2).

n>3
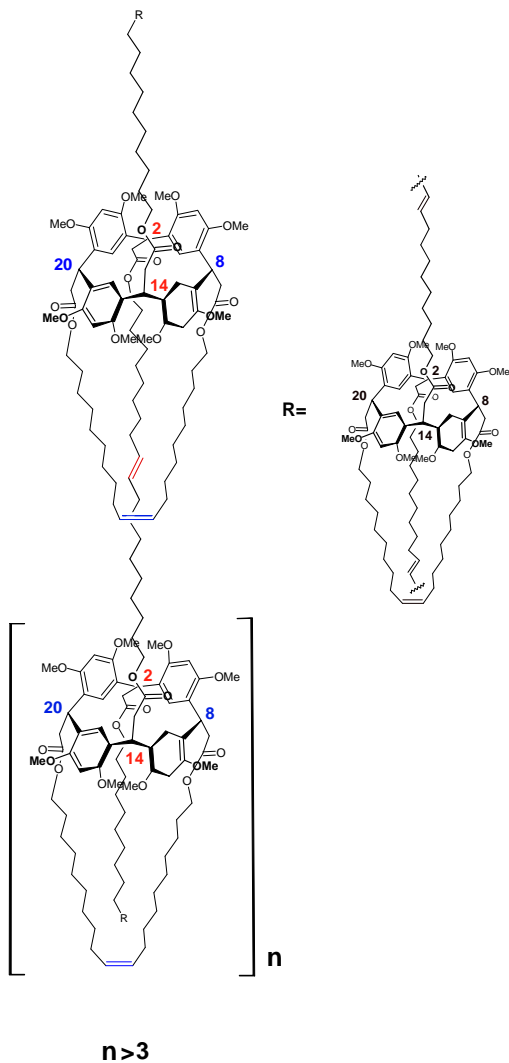
Figure 5.2 Structure of the hypothetical cyclic oligomer **2c** of n units, where n is at least > 3.

120

The second reaction product **3c** showed more complex ^{1}H- and ^{13}C-NMR spectra than **2c**. However, if we do not consider the satellite signals, due to the cis/trans isomeris, which were indeed eliminated in the spectra of the reduction derivative **3cr**, we obtain a survey (Tables 5.2) with readable features: i) The olefin signals are coincident with those of **2c**, that is the molecule has the same number of intra- and intermolecular double bonds; b) the resonances of aromatic and methoxyl group protons; c) the equivalent methine protons CH-8 and CH-20 give now separate signals. These findings reveal that the first ring closure occurs between C-2 and C-8 or C-2 and C-20: in any case the symmetry plane is lost and the elements of the pairs H-25/H-26, H-6/H-23, H-8/H-20, 4.=Me/24-OMe etc are no more equivalent. As a result the NMR spectra display one signal for each proton or carbon. A closure including C-2 side chain involves two substituents (C-2/C-8, C-2/C-20) more distant than the pair C-8/C-20 but has a double possibility to occur. We can thus forecast that the compound **3c** is going to be formed in higher yield and take the experimental result as a confirm of our hypothesis. The two postulated asymmetric intermediates will have however no overall effect on the chirality, being enantiomeric each other.

The two free substituents (C-14 and C-8 or C-20 side chains) are not in the same plane as for **2c**, but in both cases in two perpendicular planes (C-2÷C-14 *vs* C-8÷C-20). We can foresee a different following polymerization for the **3c** intermediate, even taking in account the mobility of the two remaining active side chains (Fig. 5.3).
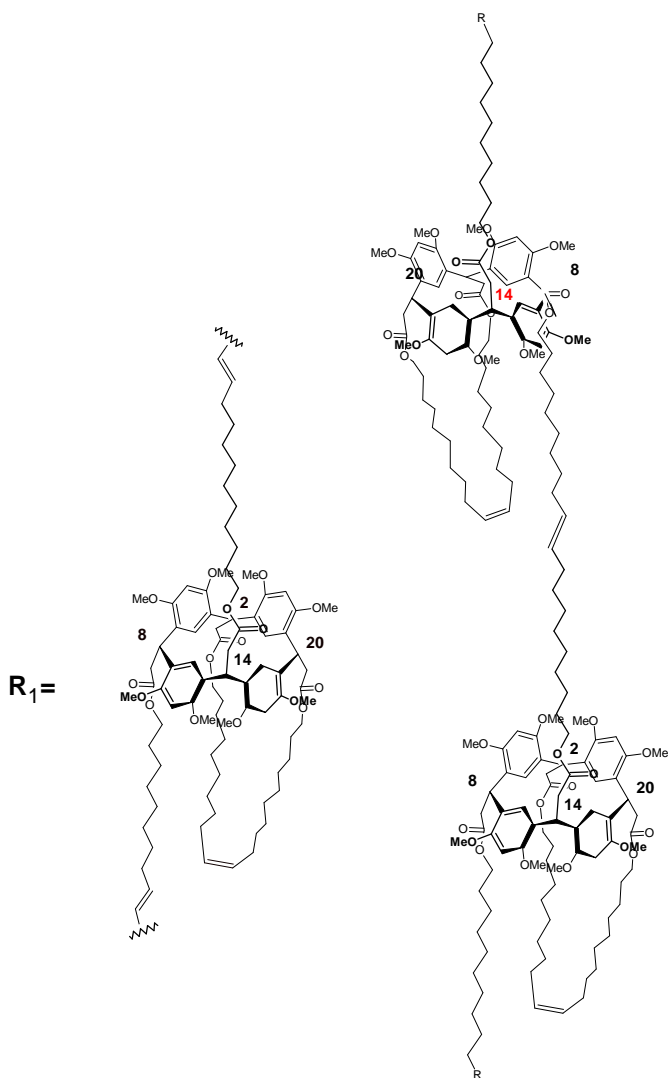
Figure 5.3 A different following polymerization for the **3c** intermediate.

The mass spectrum of **3c** steps on the foot of that one from **2c** with the same two important peaks at 1407.7 (100%) and 2792.8 (23%) *m/z*, corresponding to [M + Na]$^+$ and [2M + Na]$^+$ ions, but with a significant difference: a small (2-3%) cluster of peaks at 2100 *m/z* corresponding to a double charged ion [3M + 2Na]$^{+2}$. Regularly, the cluster is composed by isotopic peaks differing 0.5 *m/z* and flanked by a minor similar cluster at a distance of 7 *m/z*, related to the loss of CH_2, *i.e*. [3MNa – CH_2]$^{+2}$. In the mass spectrum of the above cited compound **5b**, another reaction product of resorcarene **1b**, an identical distribution pattern has been found and correlated to a molecular weight 3M = 4154 D, *i.e*. a trimer of the starting macrocycle. Notably, in the mass spectrum of the reduction product **3cr** the three peaks undergo different shifts of 4 *m/z* (1408 → 1412), 8 *m/z* (2793 → 2801) and 12 *m/z* (the double charged ion 2100 → 2106), respectively. These findings suggest that the former two represent the monomer and dimer unit of a trimer molecule. In the mass spectrum of **5b** the base peak is also at 1407.8 *m/z*, but corresponds to a triple charged ion [3M + 3Na]$^{+3}$, while no peak is registered at 2792.7 *m/z*. Resorcarene **5b** was thus assigned the structure of a linear trimer, where the central unit formed four intermolecular linkages with the external units, which in turn contain an intramolecular ring. The molecule accounts for two intra-molecular double bonds and four intermolecular alkene linkages.

124

Conversely, the **3c** trimer can be built logically from the postulated intermediate unit, with two free substituents almost perpendicular, by forming a triangle, where the sides are represented by the intermolecular alkene chains (Fig. 5.4). If we suppose to link two intermediates A and B, *e.g.* by C-8a and C-14b, in the formed linear dimer the remaining active chains C-14a and C-8b are now (compare with the case of **2c**) brought closer and the reaction with the terminal chains of a third molecule C (C-8c and C-14c) is quite likely. The diverse arrangements of **5b** and **3c** can explain the diverse mass fragmentation. The elements of **5b** are put strongly together by a double alkene chain, while the units of **3c** are linked by only one. The latter may give one unit or two units fragments by rupture of two linkages, whereas **5b** should need the rupture of four double bonds and the molecules is represented only by pluri-charged ions of the trimer.
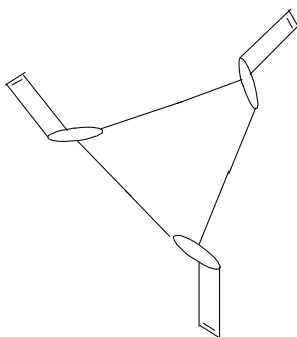
Figure 5.4 Schematic rappresentation of the **3c** trimer as a triangle, where the sides are represented by the intermolecular alkene chains.

A5.2 Experimental section

General procedures and materials

All manipulations were performed using a combination of glovebox and high vacuum under a nitrogen atmosphere. HPLC grade solvents were dried and degassed by standard procedures. Second-generation Grubbs catalyst and QuadraSil AP silica gel were purchased from Sigma Aldrich.

A5.2.1 Olefin metathesis reaction of resorc[4]arene 1c

Resorc[4]arene ω-undecenyl ester **1c** (0.25 g, 0.17 mmol), obtained as previously described (see Section A2.2.2), was dissolved in dry DCM (57 mL) to reach a final substrate concentration of 3.0×10^{-3} M. The solution was heated at reflux temperature and then exposed to a solution of the $[(H_2IMes)(PCy_3)(Cl)_2Ru=CHPh)]$ catalyst (0.015 g, 0.017 mmol, 10 mol%) in dry DCM (3 mL), previously prepared in the glovebox. The reaction mixture was kept at reflux under stirring and nitrogen atmosphere for 40 min, and then treated with QuadraSil AP metal scavenger (aminopropyl silica gel, 4 g). After 5 min, the mixture was cooled to room temperature and left under stirring overnight. After filtration and evaporation, the residue was suspended in DCM and applied onto a silica gel column to give compounds **2c** (36 mg; 15%) and **3c** (62 mg; 26%) with DCM: ethyl acetate 96:4).

Compound 2c. Yellow oil, 62 mg, 26% yield. ^{1}H and ^{13}C NMR signals are given in Table 5.1. ESI-HRMS spectrum (100 µg/mL, MeOH), *m/z* (%): 2794.7 (30), 2793.7 (32), 2792.7 (15) [2M + Na]$^+$, 2780,7 (11), 2779.7 (12), 2778.69 (6) [2MNa − CH$_2$]$^+$, 1409.8 (36), 1408.8 (90), 1407.8 (100) [M + Na]$^+$, 1402.9 (22) [M + H$_2$O]$^+$, 1394.8 (20), 1393.8 (18) [MNa − CH$_2$]$^+$. MW = nM (n·1384 D) n·C$_{84}$H$_{120}$O$_{16}$.

Table 5.1 ^{1}H NMR and ^{13}C NMR Signals* of **2c**.

Carbon	^{1}H	^{13}C
C=O	-	172.4, 172.8
C_{Ar}–O	-	156.6, 156.2, 155.7
CH= (t)	5.39 q	130.8, 130.6, 130.2
	5.31 q	
CH_i (25,27)	7.45 br s	127.1
CH_i (26,28)	6.28 br s	126.1
C_{Ar}–C	-	125.2, 124.8, 123.8, 123.6
CH_e (5,17)	6.32 br s	96.7
CH_e (11,23)	6.35 br s	95.7
OCH_2	3.91 t	64.5
	4.04 t	64.1
	4.02 t	63.9
OMe	3.85, 3.84	56.3, 56.27
	3.70, 3.63	56.1, 55.5
CH_2-(CO)	2.17 d	42.3, 40.8, 39.8
	2.83 d	
	2.92 d	
CH	5.48 t	32.5
	5.08 t	32.4
	5.07 m	32.1
CH_2-(CH=)	2.01 t	33.9
	2.02 t	
	2.00 m	
CH_2-(CH_2-CH=)	1.34 m	29.3
CH_2-(CH_2O)	1.61 m	28.4
	1.53 m	
$CH_2 \times 5$	1.24 br m	29.7
		29.4
		28.9
		28.1
		25.6

* 600 MHz (^{1}H) and 100 MHz (^{13}C), CDCl3, T = 300 K; coupling constants J (Hz) are given in parentheses.

Compound 3c. White solid, mp 151.6 ± 0.1 °C, 120 mg, 15% yield. ^{1}H and ^{13}C NMR signals are given in Table 5.2. ESI-HRMS spectrum (50 µg/mL, MeOH), *m/z* (%): 2794.7 (40), 2793.7 (43), 2792.7 (23) [2M + Na]$^+$, 2788.7 (3), 2787.7 (3) [2M + H_2O] 2780,7 (12), 2779.7 (13), 2778.7 (6) [2MNa − CH_2]$^+$, 2101.7 (3), 2101.3 (3), 2100. 7 (2) [3M + 2Na]$^{+2}$, 2093.7 (2), 2093.3 (2), 2092.7 (2) [3M·2Na− CH_2]$^{+2}$, 1409.8 (46), 1408.8 (90), 1407.8 (100) [M + Na]$^+$, 1402.9 (15) [M + H_2O]$^+$, 1394.8 (12), 1393.8 (14) [MNa − CH_2]$^+$, 1388.8 (3) [M·H_2O − CH_2]. MW = 3M (4154 D) $C_{252}H_{360}O_{48}$.

Table 5.2 ^{1}H NMR and ^{13}C NMR Signals* of trimer **3c.**

Carbon	[1]H	[13]C
C=O	-	172.6, 172.3
C_{Ar}–O	-	156.5, 156.4, 156.0, 155.8, 155.7, 155.60
CH= (t)	5.37 m 5.31 t	130.7 130.6
CH_i (25,27) CH_i (26,28)	7.20, 7.05 6.34, 6.28	127.7, 127.6 127.5, 127.1
C_{Ar}–C	-	126.0, 124.7, 124.5, 124.3, 124.2, 124.1, 123.4, 123.3
CH_e (5,17) CH_e (11,23)	6.42, 6.35 6.53, 6.39	96.8, 96.2 95.7
OCH_2	3.92 t 3.99 m	64.3 64.1 64.0
OMe	3.87, 3.85, 3.80, 3.77, 3.76, 3.70, 3.69, 3.63	56.3, 56.2, 56.0, 55.9, 55.7, 55.5
CH_2-(CO)	2.38 2.49 dd 2.87 t 2.98 dd 2.80 dd	40.6, 39.9, 39.7, 40.5
CH	4.91 t 5.10 dd 5.01 dd 5.36 t	32.6, 32.4, 32.1, 31.6
CH_2-(CH=)	1.99 m	35.1, 35.0
CH_2-(CH_2-CH=)	1.35 m	29.3
CH_2-(CH_2O)	1.62 m 1.51 m	28.7
$CH_2 \times 5$	1.26 br m	29.4, 29.3, 29.2, 29.0 28.9, 28.7, 25.9

* 600 MHz (^{1}H) and 100 MHz (^{13}C), CDCl3, T = 300 K; coupling constants J (Hz) are given in parentheses.

131

A5.2.2 Catalytic hydrogenation of 2c

After two vacuum/nitrogen cycles to replace the air inside the reaction tube, compound **2c** (42 mg, 0.030 mmol) and 10% Pd/ C (10 mg) in dry THF (5 mL) were vigorously stirred at room temperature under 1 atm of hydrogen for 24 h. The reaction mixture was filtered through a membrane filter (Millipore, Millex-LH, 0.45 mm) and the filtrate was concentrated. Purification of the residue by silica gel chromatography (DCM : ethyl acetate = 99 : 1 → 97 : 3) gave compound **2cr** (white solid, 42 mg, 0.030 mmol, quantitative yield). Yellow oil. ^{1}H and ^{13}C NMR signals are given in Table 5.3. HRMS (ESI spectrum (80 µg/mL, MeOH), *m/z* (%): 2802.7 (20), 2801.7 (16), 2800.7 (10) $[2M + Na]^+$, 2788,7 (8), 2787.7 (8), 2786.7 (4) $[2MNa - CH_2]^+$, 1413.8 (32), 1412.8 (80), 1411.8 (100) $[M + Na]^+$, 1398.8 (15), 1397.8 (12) $[MNa - CH_2]^+$. MW = nM (n·1388 D) n·$C_{84}H_{124}O_{16}$.

Table 5.3 ^{1}H NMR and ^{13}C NMR Signals* of **2cr**.

Carbon	[1]H	[13]C
C=O	-	172.5, 171.4
C_{Ar}–O	-	156.4, 156.0, 155.7, 155.5
CH_i (25,27)	7.45 br s	127.2
CH_i (26,28)	6.28 br s	126.1
C_{Ar}–C	-	125.2, 124.9, 124.1, 123.7
CH_e (5,17)	6.35 br s	96.7
CH_e (11,23)	6.32 br s	95.7
OCH_2	3.91 t	64.5
	4.04 t	64.1
	4.02 t	63.8
OMe	3.86, 3.75, 3.70	56.3, 56.27, 55.4
CH_2-(CO)	2.17 d	41.3, 40.8, 39.8
	2.83 d	
	2.92 d	
CH	5.48 t	32.5
	5.08 t	32.4
	5.07 m	32.0
CH_2-(CH_2O)	1.45 m	28.5
$CH_2 \times 5$	1.24 m	29.7
		29.4
		29.3
		28.9
		27.9
		25.6

* 600 MHz (^{1}H) and 100 MHz (^{13}C), CDCl3, T = 300 K; coupling constants J (Hz) are given in parentheses.

A5.2.3 Catalytic hydrogenation of 3c

After two vacuum/nitrogen cycles to replace the air inside the reaction tube, compound **3c** (42 mg, 0.030 mmol) and 10% Pd/ C (10 mg) in dry THF (5 mL) were vigorously stirred at room temperature under 1 atm of hydrogen for 24 h. The reaction mixture was filtered through a membrane filter (Millipore, Millex-LH, 0.45 mm) and the filtrate was concentrated. Purification of the residue by silica gel chromatography (DCM : ethyl acetate = 99 : 1 → 97 : 3) gave compound **3cr** (white solid, 42 mg, 0.030 mmol, quantitative yield). Yellow oil. ^{1}H and ^{13}C NMR signals are given in Table 5.4. HRMS (ESI spectrum (40 µg/mL, MeOH), *m/z* (%): 2802.7 (17), 2801.7 (16), 2800.7 (8) $[2M + Na]^+$, 2788,7 (7), 2787.7 (5), 2786.69 (6) $[2MNa - CH_2]^+$, 2107.8 (4), 2101.3 (3), 2106.7 (2) $[3M + 2Na]^{+2}$, 2100.7 (3), 2100.3 (2), 2099.7 (2) $[3M \cdot 2Na - CH_2]^{+2}$, 1413.8 (45), 1412.8 (90), 1411.8 (100) $[M + Na]^+$, 1398.8 (12), 1397.8 (14) $[MNa - CH_2]^+$. MW = 3M (4166.5 D) $C_{252}H_{372}O_{48}$.

Table 5.4 ^{1}H NMR and ^{13}C NMR Signals* of trimer **3cr.**

Carbon	[1]H	[13]C
C=O	-	172.7, 172.5
C_{Ar}–O	-	156.3, 156.1, 155.1
CH_i (25,27) CH_i (26,28)	7.22, 6.98, 6.36,	127.6, 127.3
C_{Ar}–C	-	126.7, 126.5 126.2, 124.8, 124.1, 124.0, 123.4
CH_e (5,17) CH_e (11,23)	6.44, 6.41 6.37	96.8, 96.5, 96.2, 95.9
OCH_2	3.93 t 3.98 m	64.3, 64.2, 64.0, 63.9
OMe	3.85, 3.84, 3.81, 3.77, 3.73, 3.66, 3.65	56.4, 56.2, 55.8, 55.7, 55.6, 55.5, 55.4
CH_2-(CO)	3.04 2.90 dd 2.88, 2.32 dd	39.0, 37.3, 37.0
CH	5.43 t 5.10, 5.05 dd 4.98 t	32.5, 31.8
CH_2-(CH_2O)	1.55 m	28.4
$CH_2 \times 5$	1.26 br m	29.7, 29.5, 29.3, 28.8 27.7, 26.1

* 600 MHz (^{1}H) and 100 MHz (^{13}C), CDCl3, T = 300 K; coupling constants J (Hz) are given in parentheses.

Chapter A6

References

Abis L., Dalcanale E., Du Vosel A., Spera S., *J. Org. Chem.*, **1988**, *53*, 5475.

Ackermann L., Fürstner A., Weskamp T., Kohl F. J. and Herrmann W. A., *Tetrahedron Lett.*, **1999**, 40, 4787.

Aeilts S. L., Cefalo D.R., Bonitatebus P. J., Houser J. H., Hoveyda, R. R. Schrock, *Angew. Chem.*, Int. Ed., **2001**, 40, 1452.

Allcock H.R., Kellam E.C., III, Hofmann M.A., *Macromolecules*, **2001**, 34, 5140.

Arduengo A.J., *Acc. Chem. Res.*, **1999**, 32, 913.

Arduini A., Pochini A., Secchi A., Ugozzoli F., "Recognition of Neutral Molecules", In *Calixarenes* 2001, Asfari Z., Böhmer V., Harrowfield J., Vicens J. (Eds.), Kluwer Academic Publishers: Dordrecht, The Netherlands, **2001**, Chapter 25.

Asfari Z., Böhmer V., Harrowfield J., Vicens J., Eds. *Calixarenes 2001*, Kluwer Academic Publisher: Dordrecht, **2001**.

Astruc D., *New J. Chem*., **2005**,29, 42.

Atiqullah M., Hammawa H., Hamid H., *Eur. Polym. J.* **1998**, 34, 1511.

Baeyer A., *Ber. Dtsch. Chem. Ges.*, **1872a**, *5*, 25;

Baeyer A., *ibid.*, **1872b**, *5*, 280.

Banks R.L., Bailey G. C., *Int. Eng. Prod. Dev.*, **1964**, 3, 170.

Bazan G.C., Khosravi E., Scrock R.R., Feast W. J., Gibson V.C., O'Regan M.B., Thomas J.K. and Davis W.M., *J. Am. Chem. Soc.*, **1990**, 112, 8378.

Bazan G. C., Oskam J. H., Cho H. N., Park L. Y., Schrock R. R., *J. Am. Chem. Soc.*, **1991**,113, 6899.

Blanchard M., Mortreux A., *Bull. Soc. Chim.*, **1972**, 4, 1641.

Blanchard M., Mortreux A., *J. Mol. Catal.*, **1975**, 1, 101.

Böhmer V., *Angew. Chem. Int. Ed. Engl.*, **1995**, 34, 713.

Bourissou D., Guerret O., Gabbaï F. P., Bertrand G., *Chem. Rev.*, **2000**, 100, 39.

Botta B., Iacomacci P., Di Giovanni M.C., Delle Monache G. Gacs-Baitz E., Botta M., Tafi A., Corelli F., Misiti D., *J. Org. Chem.*, **1992**, 57, 3259.

Botta B., Delle Monache G., De Rosa M. C., Seri C., Benedetti E., Iacovino R., Botta M., Corelli F., Masignani V., Tafi A., Gács-Baitz E., Santini A., Misiti D., *J. Org. Chem.*, **1997**, *62*, 1788.

Botta B., Cassani M., D'Acquarica I., Misiti D., Subissati D., Delle Monache G., *Curr. Org. Chem.*, **2005**, 9, 337.

Botta B., D'Acquarica I., Delle Monache G., Nevola L., Tullo D., Ugozzoli F., Pierini M., *J.Am. Chem. Soc.*, **2007**, 129, 11202.

Bunz U.H.F., in Modern Arene Chemistry, ed. Astruc D., Wiley-VCH, *Weinheim*, **2002**, 217.

Bunz H.H.F., in Handbook of Metathesis, ed. Grubbs R. H., Wiley-VCH, *Weinheim*, **2003**, 3, 3, 10.

Calderon N., *Tetrahedron Lett.*, **1967**, 34, 3327.

Calderon N., *Acc. Chem. Res.*, **1972**, 5, 127.

Cao Y., Wang L., Bolte M., Vysotsky M. O., Böhmer V., *Chem. Commun.*, **2005**, 3132.

Casnati A., Sansone F., Ungaro R., *Acc. Chem. Res.*, **2003**, *36*, 246.

Chatterjee A. K., Choi T.-L., Sanders D. P. and Grubbs R. H., *J. Am. Chem. Soc.*, **2003**, 125, 11360.

HérissonJ.-L., Chauvin Y., Makromol. Chem., **1971**, 141,161.

Choi T.-L., Grubbs R. H.; *Angew. Chem. Int. Ed.* **2003**, 42, 1743.

Connon S. J., Dunne A. and Blechert S., *Angew. Chem. Int. Ed.*, **2002**, 41, 3835.

Conrad J. C., Fogg D. E., *Curr. Org. Chem.*, **2006**, 10, 185.

Cometti G., Dalcanale E., Du Vosel A., Levelut A.-M., *Liquid Crystals*, **1992**, 11, 93.

Dalla Cort A., Mandolini L., "Calixarenes As Hosts for Quats", in *Calixarenes in Action*, Mandolini L., Ungaro R. (Eds.), Imperial College Press, London, **2000**, Chapter 5.

Dunne A.M., Mix S., Blechert S., *Tetrahedron Lett.*, **2003**, 44, 2733.

Egberink R.J.M. , Cobben P.L.H.M. , Verboom W. , Harkema S. , Reinhoudt D.N. J., *Inclusion Phenom.*, **1992**, 12, 151.

Eleuterio H.S., *J. Mol. Catal.*, **1991**, 65, 55.

Eleuterio H.S., German Pat. 1072811, **1960**.

Erdtman H., Högberg S., Abrahamsson S., Nilsson B., *Tetrahedron Lett.*, **1968**, *9*, 1679;

Falana O.M., Al-Farhan E., Keehn P.M., Stevenson R., *Tetrahedron Lett.*, **1994**, 35, 65.

Fischer E.O., *Angew. Chem.*, Int. Ed. Engl., **1964**, 580.

France M.B., Grubbs R.H., McGrath V., Paciello R.A., *Macromolecules*, **1993**, 26, 4742.

Fürstner A., Dierkes T., Thiel O.R., Blanda G., *Chem. Eur. J.*, **2001**, 7, 5286.

Ghosh S., Ghosh S., Sarkar N., *J. Chem. Sci.*, **2006**, 118, 3, 223.

Grela K., Ignatowska J., *Org. Lett.*, **2002**, 4, 3747.

Grela K., Harutyunyan S., Michrowska A., *Angew. Chem. Int. Ed.*, **2002**, 41, 4038.

Grela K., Harutyunyan S., Michrowska A., *Angew. Chem. Int. Ed.*, **2002**, 41, 4038.

Guerchais V., Astruc D. J., *Chem. Soc.*, *Chem. Commun.*, **1985**, 835.

Gutsche C.D., *Acc. Chem. Res.*, **1983**, 16, 161.

Gutsche C.D., Calixarenes, Monographs in Supramolecolar Chemistry, Stoddart, J.F., Ed.; Royal Society of Chemistry: Cambridge, **1989**; 1.

Gutsche, C.D. *Aldrichimica Acta*, **1995**, 28, 3.

Gutsche C.D., in *Calixarenes Revisited*, J. F. Stoddart (Ed.); The Royal Society of Chemistry, Cambridge, **1998**.

Green M.L.H., Mitchard L.C., Swanwick M.G., *J. Chem. Soc. A*, **1971**, 794.

Grubbs R.H., *J. Am. Chem. Soc.*, **1972**, 94, 2538.

Grubbs R.H., Burk P.L., Carr D.D., *J. Am. Chem. Soc.*, **1975**, 97, 3265.

Grubbs R.H., Tumas W.J., *Science*, **1989**, 243, 907.

Grubbs R.H., Chang S., *Tetrahedron*, **1998**, 54, 4413.

Grubbs R.H., Handbook of Metathesis; Ed.; Wiley-VCH: Weinheim, Germany, **2003**.

Hansen S.M., Rominger F., Metz M. and Hofmann P., *Chem.-Eur. J.*, **1999**, 5, 557.

Hérisson J.-L., Chauvin Y. *Makromol. Chem.* **1971**, 141, 161.

Herrmann W.A., Köcher C., *Angew. Chem. Int. Ed. Engl.*, **1997**, 109, 2256.

Högberg A. G. S., *J. Am. Chem. Soc.*, **1980a**, 102, 6046.

Högberg A. G. S., *J. Org. Chem.*, **1980b**, 45, 4498.

Honda T., Namiki H., Kaneda K. and Misutani H., *Org. Lett.*, **2004**, 6, 87.

Hoveyda A.H., Schrock R.R., *Angew. Chem. Int. Ed.*, **2001**, 40, 1452.

Huc V., Weihofen R., Martin- Jimenez I., Oulie´ P., Lepetit C., Lavigne G., Chauvin R., *New J. Chem.*, **2003**, 27, 1412.

Jerschow A., Mueller N., *J. Magn. Reson. A*, **1997**, 125, 372.

Katsuhiko A., Toyoki K., *Supramolecular Chemistry-Fundamentals and Application*, Iwanami Shoten Publishers , Tokyo, Springer, **2006**.

Keitz B. K., Endo K., Patel P.R., Herbert M.B., Grubbs R.H., *J. Am. Chem. Soc.* **2012**, 134, 693.

Kingsbury J. S., Harrity J. P. A., Bonitatebus P. J., Hoveyda A. H., *J. Am. Chem. Soc.*, **1999**, 121, 791;

Konishi H., Iwasaki Y., Morikawa O., Okano T., Kiji J., *Chem. Express*, **1990**, 5, 869.

Lee C.W., Grubbs R.H., *Org. Lett.*, **2000**, 2, 2145.

Loupy A., Tchoubar B. and Astruc D., *Chem. Rev.*, **1992**, 92, 1141.

Love J.A., Sanford M.S., Day M.W. and Grubbs R.H., *J. Am. Chem. Soc.*, **2003**, 125, 10103.

Ludwig R., *Microchim. Acta*, **2005**, *152*, 1.

Mandolini, L., Ungaro, R. Eds., *Calixarenes in Action*, Imperial College Press, **2000**.

McEleney K., Allen D.P., Holliday A.E.,. Crudden C. M, *Org. Lett.*, **2006**, 8, 2663.

Meek S.J., O'Brien R.V., Llaveria J., Schrock R.R., Hoveyda A.H., *Nature* **2011**, 471, 461.

Meng, D., Bertinato P., Balog A., Su D.-S., Kamenecka T., Sorensen E.J., Danishefsky S. J., *J. Am. Chem. Soc.*, **1997**, 119, 10073.

Morril C. , Grubbs R.H., *J. Org. Chem.*, **2003**, 68, 603.

Mortreux A., Delgrange J.C., Blanchard M., Lubochinsky B., *J. Mol. Catal.*, **1977**, 2, 73.

Mortreux A., Petit F., Blanchard M., *Tetrahedron Lett.*, **1978**, 49, 4967.

Mortreux A., Petit F., Petit M., Szymanska-Buzar T., *J. Mol. Catal. A: Chem.*, **1995**, 96, 95.

Michrowska A., Bujok R., Harutyunyan S., Sashuk V., Dolgonos G. and Grela K., *J. Am. Chem. Soc.*, **2004**, 126, 9318.

Natta G., *Angew. Chem. Int. Ed. Engl.*, **1964**, 3, 723.

Natta G., Dall'Asta G., Porri L., *Makromol. Chem.*, **1965**, 81, 253.

Nguyen S.T., Johson L. K., Grubbs R.H., Ziller J. W., *J. Am. Chem. Soc.*, **1992**, 114, 3974.

Novak B.M., Grubbs R.H., *J. Am. Chem. Soc.*, **1988**, 110, 7542.

Perrin M., Oehler D., in Calixarenes. A Versatile Class of Macrocyclic Compounds (Eds: J. Vicens, V. Böhmer), KLUWER Academic Publishers, Dordrecht, The Netherlands, **1991**, 65.

Pitarch M., McKee V., Nieuwenhuyzen M., McKervey M. A., J. Org. Chem., **1998**, 63, 946.

Prunet J., *Angew. Chem. Int. Ed.*, **2003**, 42, 2826.

Pusztay S.V., Wei A., Stavens K.B., Andres R.P., *Supramol. Chem.*, **2002**, 14, 291.

Randall M.L., Tallarico J.A., Snapper M.L., *J. Am. Chem. Soc.*, **1995**, 117, 9610.

Randall M.L., Snapper M.L., *J.Mol. Catal. A*, **1998**, 133, 29.

Rouhi M.R., *Chem. Eng. News*, **2002**, 29.

Schinzer D., Limberg A., Bauer A., Bohm O.M., Cordes M., *Angew. Chem. Int. Ed.*, **1997**, 36, 523.

Schinzer D., Bauer S., Bohm L., Limberg A., Cordes M., *Chem. Eur. J.*, **1999**, 5, 2483.

Schneider M.F., Blechert S., *Angew. Chem.*, **1996a**, 108, 479.

Schneider M.F., Blechert S., *Angew. Chem. Int. Ed. Engl.*, **1996b**, 35, 411.

Schneider M.F., Lucas N., Velder J., Blechert S., *Angew. Chem.* **1997a**, 109, 257.

Schneider M.F., Lucas N., Velder J., Blechert S., *Angew. Chem. Int. Ed. Engl.*, **1997b**, 36, 257.

Scholl M., Trnka T.M., Morgan J.P. and Grubbs R.H., *Tetrahedron Lett.*, **1999a**, 40, 2247.

Scholl M., Ding S., Lee C. W. and Grubbs R. H., *Org. Lett.*, **1999b**, 1, 953.

Schrock R.R., Rocklage S.M., Wengrovius J.H., Rupprecht G. and Feldmann J., *J.Mol. Catal.*, **1980**, 8, 73.

Schrock R.R., Murdzek J.S., Bazan G. C., Robbins J., DiMare M. and O'Regan M., *J. Am. Chem. Soc.*, **1990**, 112, 3875.

Schwab P., France M.B., Ziller J. W., Grubbs R.H., *Angew. Chem., Int. Ed. Engl.*, **1998**, 37, 1124.

Scholl M., Ding S., Lee C.W., Grubbs R.H., *Org. Lett.*, **1999**, 1, 953.

Smith A.B., III, Kozmin S.A., Adams C.M., Paone D.V., *J. Am. Chem. Soc.*, **2000**, 122, 4984.

Smith A.B., III, Adams C.M., Kozmin S.A., Paone D.V., *J. Am. Chem. Soc.*, **2001**, 123, 5925.

Smith D.W., Wagener K.B., *Macromolecules*, **1993**, 26, 1633.

Snapper M.L., Tallarico J.A., Randall M.L., *J. Am. Chem. Soc.*, **1997**, 119, 1478.

Steed J.W., Atwood J.L., *Supramolecular Chemistry, 2nd edition*, John Wiley & Sons, Ltd, **2009**.

Tallarico J.A., Bonitatebus P.J., Snapper M.L., *J. Am. Chem. Soc.*, **1997**, 119, 7157.

Teng X., Cefalo D.R., Schrock R.R., Hoveyda A.H., *J. Am. Chem. Soc.*, **2002**, 124, 10779.

Thoden van Velzen E.U., Engbersen J.F.J., Reinhoudt D.N., *J. Am. Chem. Soc.*, **1994**, 116, 3597.

Timmerman P., Verboom W., Reinhoudt D.N., *Tetrahedron*, **1996**, 52, 2663.

Tindall D., Pawlow J.H., Wagener K.B., in Topics in Organometallic Chemistry, Vol. 1 (Ed: A. Fürstner), SPRINGER-VERLAG, Berlin, **1998**, 183.

Truett W.L., Johnson D.R., Robinson I.M. and Montague B.P., *J. Am. Chem. Soc.*, **1960**, 82, 2337.

Trnka T.M., Morgan J.P., Sanford M.S., Wilhelm T.E., Scholl M., Choi T.L., Ding S., Day M.W. and Grubbs R.H., *J. Am. Chem. Soc.*, **2003**, 125, 2546.

Tsang W.C.P., Jernelius J.A., Cortez G.A., Weatherhead G.S., Schrock R.R., Hoveyda A.H., *J. Am. Chem. Soc.*, **2003a**, 125, 2591.

Tsang W.C.P., Hultzsch K.C., Alexander J.B., Bonitatebus P.J. and Schrock R.R., *J. Am. Chem. Soc.*, **2003b**, 125, 2652.

Tsuzuki S., Honda K., Uchimaru T., Mikami M., Tanabe K., *J. Am. Chem. Soc.*, **2000**, 122, 3746.

Tunstad L.M., Tucker J.A., Dalcanale E., Weiser J., Bryant J.A., Sherman J.C., Helgeson R.C., Knobler C.B., Cram D.J., *J. Org. Chem.*, **1989**, 54, 1305.

Vysotsky M.O., Bogdan A., Wang L., Böhmer V., *Chem. Commun.*, **2004**, 1268.

Volland M.A.O., Ansen S.M., Rominger F. and Hofmann P., *Organometallics*, **2004**, 23, 800.

Wagener K.B., Smith D. W., *Macromolecules*, **1991**, 24, 6073.

Wagener K.B., Boncella J. M., Nel J. G., *Macromolecules*, **1991a**, 24, 264.

Wagener K.B., Nel J.G., Duttweiler R. P., Hillmyer M. A., Boncella J.M., Konzelman J., Smith D. W., Puts R., Willoughby L., *Rubber Chem. Technol.*, **1991b**, 64, 83.

Wagener K.B., Brzezinska K., Anderson J.D., Younkin T.R., Steppe K., DeBoer W., *Macromolecules*, **1997,** 30, 7363.

Wakamatsu H., Blechert S., *Angew. Chem. Int. Ed.*, **2002a**, 41, 794.

Wakamatsu H., Blechert S., *Angew. Chem. Int. Ed.*, **2002b**, 41, 2403.

Wei A., *Chem. Commun.* **2006**, 1581.

Wengrovius J.H., Schrock R.R., Churchill M.R., Missert J.R. and Youngs W.J., *J. Am. Chem. Soc.*, **1980**, 102, 4515.

Wetskamp T., Schattenmann W.C., Herrmann W.A., *Angew. Chem. Int. Ed.*, **1998**, 37, 2490.

Yang Y., Swager T. M., *Macromolecules*, **2007**, 40, 7437.

Yu T., Guo M., *Prog. Polym. Sci.*, **1990**, 15, 825.

Zhang W., Kraft S., Moore J.S., *Chem. Commun.*, **2003**, 832.

Zhang W., Kraft S., Moore J.S., *J. Am. Chem. Soc.*, **2004a**, 126, 329.

Zhang W., Moore J.S., *J. Am. Chem. Soc.*, **2004b**, 126, 12796.

Part B

Basket-Resorc[4]arene 2b: Self-assembly Studies and Encapsulation Studies of Fullerenes C_{60} and C_{70}

Chapter B1

General Introduction

General Introduction

B1.1 Supramolecular Chemistry

In 1978, Jean-Marie Eehn introduced the modern concept of supramolecular chemistry which he defined as the "chemistry of molecular assemblies and of the intermolecular bond," although the term itself made a much earlier appearance (in *Webster's Dictionary* in 1903). Traditionally, phrases such as "chemistry beyond the molecule", "the chemistry of the non-covalent bond", and "on-molecular chemistry" or even "Lego chemistry" were also used to describe the field. In the beginning, supramolecules mainly comprised two components, a host and a guest, which interact with one another in a noncovalent fashion (Fig. 1.1).

The area rapidly evolved to encompass molecular devices and molecular assemblies. More recently, Lehn added a further functional definition: "Supramolecular Chemistry aims at developing highly complex chemical systems from components interacting by non-covalent intermolecular force" (Lehn et al., 2002). The current emphasis is thus on increasing complexity and, hence, increasingly sophisticated functionality, and on the information stored in molecular components that allows this complexity to be achieved.
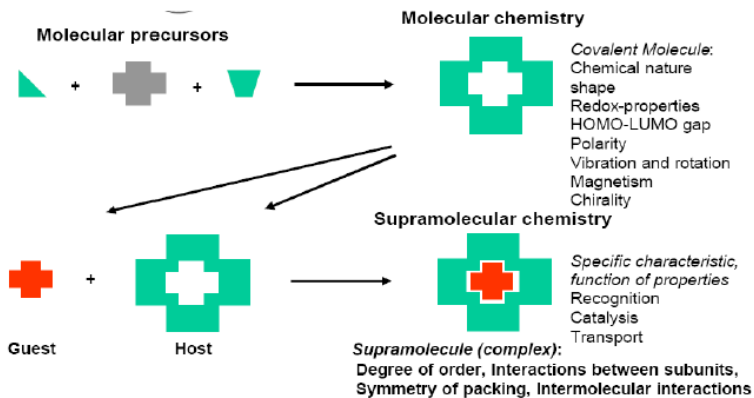
Figure 1.1 Comparison between the scope of molecular and supramolecular chemistry according to Lehn (Auld, 2001).

Fundamentally, supramolecular chemistry concerns the mutual interaction of molecules or molecular entities with discrete properties. This interaction is usually of a noncovalent type (an "intermolecular bond," such as a hydrogen bond, dipolar interaction or π-stacking). Key to many definitions of supramolecular chemistry is a sense of modularity (Steed and Atwood, 2009). Supramolecules, in the broad sense are aggregates in which a number of components (of one or more type) come together, either spontaneously or by design, to form a larger entity with properties derived from its components. These aggregates can be of the host-guest type in which one molecule encapsulates the other, or they

151

can involve mutually complementary, or self-complementary, components of similar size, in which there is no host or guest (Fig. 1.2).
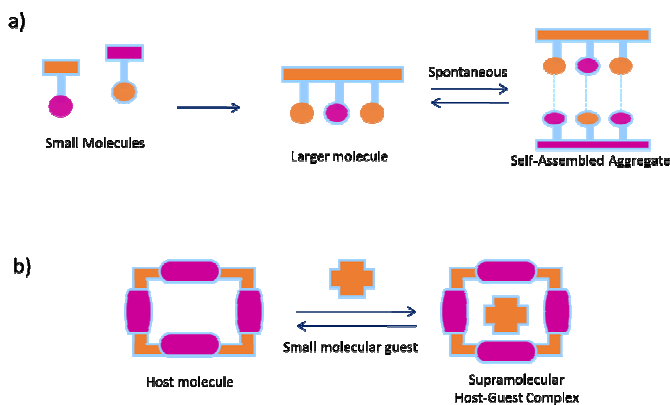

Figure 1.2 The development of a supramolecular system from molecular building blocks. (a) self-assembly between complementary species (circles represent binding sites) and (b) Host-guest complexation.

Biological systems have provided much of the inspiration for the development of supramolecular chemistry. Many synthetic supramolecular systems have been designed to mimic the structure or function of more complex biological processes (Steed and Atwood, 2009). Such artificial, abiotic (non-biological) molecules or

reaction mimics are termed models. By this we mean that, on a smaller scale, the artificial systems resemble, and help chemists to understand some or all of the properties of the real, biological chemistry.

The concept of a biological model has been summarised beautifully by Donald Cram in his Nobel Prize lecture:

"Few scientists acquainted with the chemistry of biological systems at the molecular level can avoid being inspired. Evolution has produced chemical compounds exquisitely organised to accomplish the most complicated and delicate of tasks. Many organic chemists viewing the crystal structures of enzyme systems or nucleic acids and knowing the marvels of specificity of the immune system must dream of designing and synthesising simpler organic compounds that imitate working features of these naturally occurring compounds" (Cram, 1988).

The beginnings of supramolecular chemistry, long before sophisticated artificial hosts such as carcerands, cryptands or self-assembling devices and systems were conceived, may be traced back to Fischer's lock and key model of enzymatic catalysis. This shape selection concept, coupled with Paul Erlich's work on antibodies, gives us the idea of a receptor. In biochemistry, receptor–substrate binding is of great importance and can be extremely selective.

153

B1.1.2 Interactions playing role in supramolecular chemistry

One of the most important aspects of supramolecular chemistry is its ability to utilize noncovalent interactions for the controlled, reversible assemblies of functional building blocks. Noncovalent interactions can be of attractive and repulsive intermolecular forces, with interaction energies ranging from 4-400 kJmol^{-1} as can be observed from Table 1.1. These are, in the order of decreasing strength, electrostatic interactions (ion-ion, ion-dipole and dipole-dipole interactions), hydrogen bonding, π–π stacking, solvent effects and van der Waals interactions.

Table 1.1 Average interaction energies of various noncovalenl interactions frequently used in sopramolecular chemistry[a].

Entry	Interaction	Energy/ kJmol^{-1}	Illustration/Example
1.	Ion-ion	50-400	
2.	Ion-dipole	50-200	
3.	Hydrogen bond	4-120	
4.	Dipole-dipole	4-40	
5.	π-π stacking	4-20	
6.	Solvent effects	4-40	
7.	van der Waals forces	<5	

[a]Cations (M), anions (X), electronegative element (D), elements with lone pair of electrons (Al (A), host (H) and guest (G).

In this Section, we will emphasize mainly the interaction due to the solvent (solvophobic effect), which play an important role in many

cases like folding of proteins, protein-protein interactions and tensioactives interactions. The aggregation of two molecules in a polar medium through their apolar sites is caused by the balancing of two forces:

a) the necessary energy to create a cavity in the solvent and so to win the coesion between the molecules of solvent;

b) the change of the solvating energy of the molecules participating to the process.

From a thermodynamic point of view, the process is favoured by entropic contribute. In fact, considering Frank and Evans' theory, the hydratation of a molecule which passes from a gaseous phase to solution is a process characterized by a negative entropy – and so unfavourable process- because a shell of solvent molecole around the molecules to solubilize is formed. Such entropic disadvantage is not filled either by the favourable enthalpy due to van der Waals interactions between solute and solvent. So aggregation of apolar particles follows and the molecules of solvent, which form the shell of solvation, are freed. Solvofobic interactions are directly proportional to the extension of the apolar area of the molecule, which represents the contact area of the complex. They are a good hint for the design of new

156

hosts. In fact, a new tendence is the synthesis of the so-called —*deep* cavitand (Rudkevich and Rebek, 1999), a macrocyclic compound with a deep hydrophobic cavity, which allows a better interaction with guest.

As an example, resorcinarene-based compounds like that depicted in Fig. 1.3 proved to be the first cavitand able to accomodate fullerene C_{60} within its hydrophobic cavity.
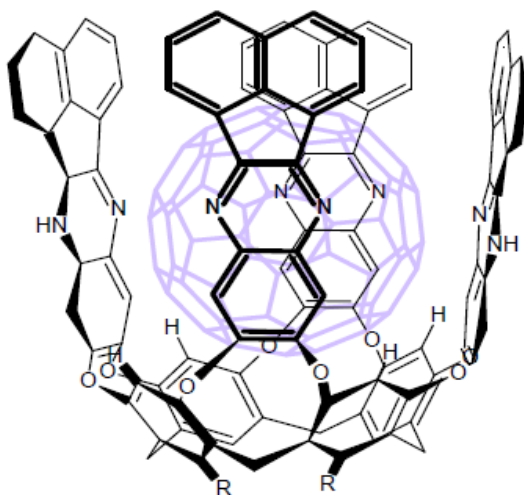

Figure 1.3 '*Deep*' cavitand interacting with fullerene C_{60} (Rudkevich and Rebek, 1999).

B1.2 Self-assembly

Self-assembly is one of the core concepts of supramolecular chemistry. It is often defined as the spontaneous formation of higher-ordered structures from molecular building blocks. This hypothesis first arose through research into biological systems. As the complex architectures found in living cells were delineated, the concept that such constructs were built by the convergent assembly of smaller subunits was increasingly invoked (Kushner, 1969). In particular, its relevance to one of the core principles of molecular biology soon became apparent. The central dogma holds that genetic information is stored, read, and duplicated by the nucleic acids DNA and RNA, and when required, this information is translated into the specific amino acid sequence of a protein, that then folds into its functional native form. As this model was developed, it became clear that it was underpinned by another assumption: that the final three-dimensional structure of a protein or a nucleic acid, is inherent in the linear sequence of its building blocks. In groundbreaking work on ribonuclease, the Nobel Laureate Christian Afinison labeled this supposition the "Thermodynamic Hypothesis", suggesting that, in physiological conditions, the native structure of a protein is the one in which the Gibbs free energy of the system is at its lowest (Afinson, 1973). This concept of self-assembly was then extended, as subsequent discoveries revealed

that, in many cases protein folding is facilitated by other factors (Ellis and Hemmingsen, 1989).

B1.2.1 Self-assembly processes classification

In an attempt to provide a general framework for discussion and research, Lindsey introduced a wideranging classification scheme, built upon the work of others, that encompasses self-assembly processes in biology and chemistry (Lindsey, 1991). This definitive scheme is broken up into seven broad, overlapping, classes.

Class 1. Strict Self-Assembly

The term "strict" emphasizes that the assembly process is reversible and the product forms spontaneously as a direct result of the structures of the component parts. Some of the classic examples of strict self-assembly include tobacco mosaic virus (Klug, 1999; Butler, 1999), oligomers of DNA, and metal chelates.

Class 2. Irreversible Self-Assembly

This class is the obverse of the previous case and is currently attracting much attention in synthetic organic chemistry (Bunce, 1995; McCarroll and Walton, 2001).

Unlike most self-assembly processes (vide infra), irreversible self-assembly is under kinetic control. Consequently, in most irreversible Multistep assembly processes, the initial architectures must be precisely located and aligned (McCarroll and Walton, 2001).

However, in some cases, highly complex architectures can result from apparently nontemplated, irreversible self-assembly (Gibb, 2000).

Class 3. Precursor Modification Followed by Self-Assembly

These processes involve the synthesis of precursors that are subsequently structurally modified. The synthesis of precursors in an assembly-inactive form permits their accumulation until ready for initiation of assembly. Whilst in biology there are many examples of such states (collagen, tubulin, fibrinogen), in chemistry this class would be merely viewed as completing the synthesis of the precursors for assembly.

Class 4. *Self-Assembly with Post-modification*

In this case, the self-assembly process precedes the final modifications that lead to the targeted architecture. Using this powerful methodology, self-assembled structures can be irreversibly locked into position within supramolecular chemistry: this strategy is most commonly employed in the elegant syntheses of catananes, rotaxanes, knots and other interlocked species (Kuehl et al., 2001).

Class 5. Assisted Self-Assembly

Here, external factors that are not part of the final assembly mediate the self-assembly process. This concept was developed as the function of molecular chaperones became apparent. Chaperones help in folding nascent polypeptide chains by preventing aggregation of peptide sequences, and they modulate refolding of denatured proteins. Chaperones do not affect the thermodynamics of folding-the ratio of folded and unfolded polypeptides is left unchanged-but they influence the kinetics of the process. It is thought that this is accomplished by stabilizing intermediates along the folding pathway, thus decreasing activation-energy barriers.

Class 6. Directed Self-Assembly

In Lindsey's original definition, this class includes processes in which a template participates as a structural element in the self-assembly process but does not appear in the final assembled architecture. An example from biology is the scaffolding protein directed assembly of viral capsids. External and internal scaffolding protein frameworks direct the construction of the protein coat that houses the viral DNA. Packaging of DNA is then accompanied by withdrawal of the internal scaffolding, and the final virion is produced after removal of the external scaffold (Dokland et al., 1997). Subsequently, within supramolecular chemistry, the term "directed self-assembly" has become more generally understood to include any templated process that brings together molecular components, even if the directing moiety is part of the final structure.

Class 7. Self-Assembly with Intermittent Processing

This final class incorporates elements from all the above classes. It includes all processes where there are sequential phases of self-assembly and irreversible modification. Such complex processes are still the exclusive domain of biology.

162

B1.2.2 Enthalpic and entropic factors in self-assembly process

With the exception of Class 1 self-assembly processes, the key steps in self-assembly tend to involve the interplay of dynamic, relatively weak, interactions. In these conditions, thermodynamic products, where free energy is maximized, will be favored. Consequently, entropic and enthalpic state functions must be considered.

Consider a simple hypothetical system, where 12 components can reversibly associate via a single weak enthalpically favored interaction into a discrete four membered cyclic structure; or alternatively, an open oligomeric structure (Fig. 1.4). Clearly, the formation of any oligomeric structure is enthalpically favored as new interactions are created, but as Lawrence et al. pointed out (Lawrence, 1995), discrete structures are slightly favored.
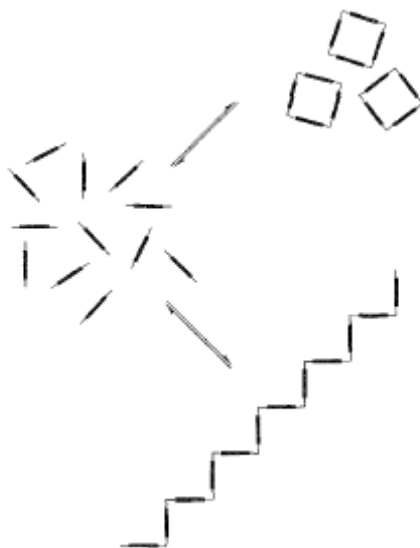
Figure 1.4 Subunits that call assemble into two possible products: a discrete four-membered cyclic structure or an open oligomeric structure.

The number of interactions per component created in the assembly of tetramers (one interaction per unit) is larger than that in the formation of the open oligomer (0.9167 interactions per unit). If there is more than one interaction between components, then assembly of the tetramer is even more advantageous. For example, if there are two interactions between individual components, then

164

the tetramer has two interactions per unit, while the oligomer only has 1.834 interactions per unit. While it is clear from an extension of such arguments that the enthalpic advantage of assembling tetramers over open polymeric structure incorporating a large number of components will rapidly become extremely small; it is also true that a cyclic structure with N components will be enthalpically favored over an open structure with N components.

Conversely, due to losses of translational and conformational degrees of freedom, the formation of any oligomeric structure is entropically unfavorable. Nevertheless, compared to self-assembly of discrete structures, generation of open oligomers (and especially polymers) is particularly unfavorable. Again, consideration of the system shown in Fig. 1.4 illustrates this argument. Relative to the tetramer: it seems likely that self-assembly of the less rigid, open oligomer results in a smaller change in conformational degrees of freedom. On the other hand, the formation of one oligomer particle, as opposed to three tetramer particles, will result in a much larger loss in translational degrees of freedom. If more components are incorporated within this polymer, the entropic disadvantage, relative to the tetramer, increases.

Seen in this light, preferential self-assembly of discrete architectures over open oligomeric structures is related to the widely studied phenomenon known as enthalpy-entropy compensation (Williams

165

and Westwell, 1998; Liu and Guo, 2001; Fujita et al., 1990; Fujita et al., 1996): the enthalpic benefits of interactions are balanced by the entropic costs in losing degrees of freedom.

B1.3 Host- Guest Chemistry

A host-guest complex was defined by Donald Cram (Cram, 1986) who shared the 1987 Nobel Prize in Supramolecular Chemistry, in the following way:

"Complexes are composed of two or more molecules or ions held together in unique structural relationships by electrostatic forces other than those of full covalent bonds...molecular complexes are usually held together by hydrogen bonding, by ion pairing, by π-acid to π-base interactions, by metal-to-ligand binding, by van der Waals attractive forces, by solvent reorganizing and by partially made and broken covalent bonds (transition states). High structural organisation is usually produced only through multiple binding sites. A highly structurated molecular complex is composed of at least one host and one guest component. A host-guest relationship involves a complementary stereoelectronic arrangement of binding sites in host and guest. The host component is defined as an organic molecule or ion whose binding sites converge in the complex." The guest component as any molecule or ion whose binding sites diverge in the complex. The key point here is the convergent

arrangement of binding sites on a host molecule. This disposition is deliberately introduced during the host synthesis and is an intrinsic property of the host. A preorganized host such as the spherand **1** (Fig. 1.5) will maintain a convergent arrangement of binding sites at all times, irrespective of the presence of guest species. More flexible hosts such as [I8]crown-6 (**2**) display some flexibility and may undergo a conformational change to a more convergent geometry upon guest complexation. Hosts such as **1** and **2** use their molecular cavity (whether preorganized or binding induced) to bind effectively to metal cations and were among the first modern host systems. The range of guest species is not limited to cations, however, and can include anions (Abouderbala et al., 2002) and neutral molecules (Cram et al.,1988).
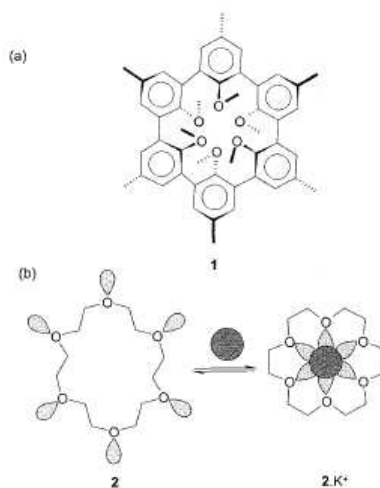
Figure 1.5 Molecular hosts (a) preorganized spherand, (b) flexible crown ether-in polar solvents, the oxygen lone pairs point outwards to interact with solvent but converge upon guest binding (lithium ion).

B1.3.1 Molecular recognition

Molecular recognition plays a crucial role in supramolecular chemistry, molecular engineering and structural biology. The first, simple but very effective model of molecular recognition has been proposed by Emil Fischer more than hundred years ago: "*... the intimate contact between the molecules ... is possible only with similar geometrical configurations. To use a picture, I would say that*

the enzyme and the substrate must fit together like a lock and key" (Fischer, 1984).

Associations between host (H) and guest (G) molecules are usually based on simultaneous non-covalent interactions between single binding sites, A (acceptor) and D (donor). Exceptions are solvent-driven equilibria and enforced guest encapsulations within closed host cavities. An important requirement for Multi-site binding is complementarity between binding sites of host and guest molecules. In other words, complexation will be more efficient when the shapes and arrangements of binding sites in host and guest molecules fit each other.

In order to bind, a host must have binding sites that are of the correct electronic character (polarity, hydrogen bond donor/acceptor ability, hardness or softness *etc.*) to complement those of the guest. Hydrogen bond donors must match acceptors, Lewis acids must match Lewis bases and so on. Furthermore, those binding sites must be spaced out on the host in such a way as to make it possible for them to interact with the guest in the binding conformation of the host molecule.

B1.3.2 Macrocyclic effect and preorganisation

Macrocyclic compounds are stabilised by what is traditionally termed the *macrocyclic effect* (Cram, 1986). This effect relates not only to the chelation of the guest by multiple binding sites, but also to the *organisation* of those binding sites in space prior to guest binding (*i.e. preorganisation*). Furthermore, the enthalpic penalty associated with bringing donor atom and lone pairs into close proximity to one another (with consequent unfavourable repulsion and desolvation effects) has been 'paid in advance' during the synthesis of the macrocycle. This makes macrocycles difficult to make but complexing agents stronger than analogous non-macrocyclic hosts. The macrocyclic effect was first elucidated by Cabbiness and Margerum who studied the Cu(II) complexes (a) and (b) depicted in Fig.1.6 (Cabbiness and Margerum, 1969). Both ions benefit from the stability associated with four chelating donor atoms. However, the macrocyclic complex (a) is about 104 times more stable than the acyclic analogue (b) as a consequence of the additional preorganisation of the macrocycle.
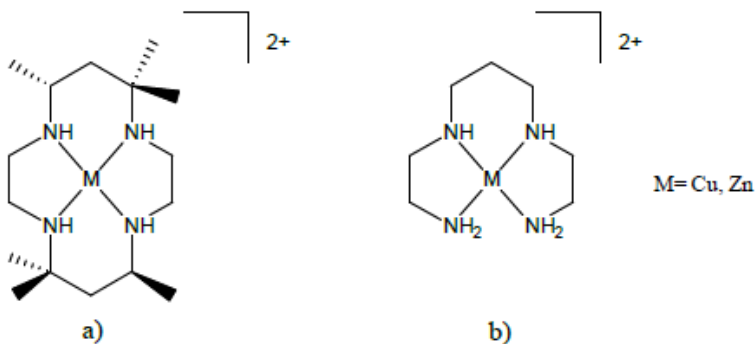
Figure 1.6 Ion complexes (Cabbiness and Margerum, 1969).

Thermodynamic measurements on the analogous (unmethylated) Zn^{2+} complexes reveal that the stabilisation by macrocyclic preorganisation has both enthalpic and entropic contributions. The enthalpic term arises from the fact that macrocyclic hosts are frequently less strongly solvated than their acyclic analogues. This is because they simply present less solvent-accessible surface area. As a result there are fewer solvent–ligand bonds to break than in the extended acyclic case. Entropically, macrocycles are less conformationally flexible and so lose fewer degrees of freedom upon complexation.

We can say that if a host molecule does not undergo a significant conformational change upon guest binding, it is *preorganised*. Host preorganisation is a key concept because it represents a major (in some cases decisive) enhancement to the overall free energy of guest complexation. Neglecting the effects of solvation, the host–guest binding process may be divided very loosely into two stages. First, there is an activation stage in which the host undergoes conformational readjustment; its binding sites must become complementary to the guest and at the same time unfavourable interactions between one binding site and another must be minimized. This is energetically unfavourable, and because the host must remain in this binding conformation throughout the lifetime of the host–guest complex, this energy is never paid back. In the second step, binding occurs; this is energetically favourable because of the enthalpically stabilising attraction between mutually complementary binding sites of host and guest. The overall free energy of complexation represents the difference between the unfavourable reorganisation energy and the favourable binding energy. If the reorganisation energy is reduced, destabilising the complex. If the host is preorganised, this rearrangement energy is small.

The preorganization principle states that 'the more highly hosts and guests are organized for binding and low solvation prior to

their complexation, the more stable will be their complexes'. (Cram, 1988). To sum up: both molecules will be optimally preorganized if (a) all complementary binding sites geometrically match; (b) in the complexed state they are in the same lowest free energy conformation as in the free state; and (c) polar binding sites need not to change solvation. In this case, all distortions will be negligible and the complexation will be energetically most favorable, including only the sum of intrinsic binding free energies. Although the general concept seems to be quite simple it is not easy to materialize it for every particular case and there is still only a limited number of highly efficient preorganized hosts.

An often applied strategy to preorganize a host molecule is rigidification with the purpose to obtain ideally a single conformation optimal for complexation. As a rule, creation of properly rigidified macrocycles requires complex synthetic routes. On the other hand, effective complexation requires primarily a sufficient number of complementary interaction sites, which in view of the usually minor entropy effects can also be linked by several flexible bonds.

The combined effects of preorganisation and complementarity are startlingly illustrated by a comparison of the binding constants

under standard conditions for the alkali metal complexes shown in Figure 1.7. All of the hosts bind through six ether oxygen atoms. The fairly hard (non-polarisable) oxygen donors are complementary to fairly hard alkali metal cations such as K^+. However, the stability constants range over nearly 14 orders of magnitude, refl ecting the increasing preorganisation of the oxygen atom donor array. The amine nitrogen atoms in some hosts do not signifi cantly enhance the binding because the softer amine is not complementary for alkali metal cations.

Thus replacing two oxygen atoms in [18]crown-6 with two secondary amine nitrogen atoms in diaza[18]crown-6 lowers the binding constant to below the value found for the podand EG5.
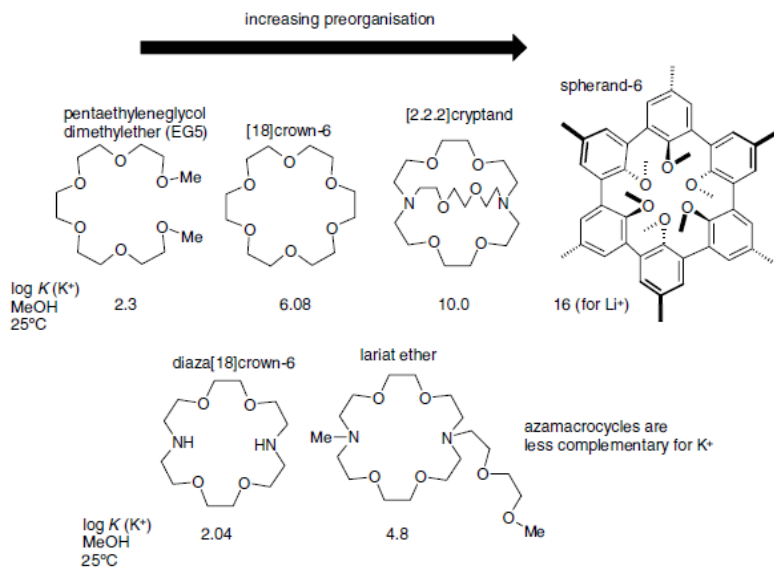
Figure 1.7 Comparison of the effects of preorganisation and complementarity on the magnitudes of the binding constant of polyether hosts for alkali metal cations. The fi gure for Li$^+$ is given for the highly preorganised spherand-6 since it is too small to accommodate K$^+$.

Chapter B2

Self-Assembly Studies

B2.1 Results and Discussion

B2.1.1 Supramolecular chirality

It is well know that chirality at the *molecular level* is displayed when the atoms of a molecule are arranged in one unique manner in space. Very frequently this may derive from the presence in the molecule of asymmetry elements (such as atoms, axes and/or planes of asymmetry) arranged in a way that excludes the emergence of planes or improper axes of symmetry. However, chirality may also be observed for molecules completely devoid of asymmetry elements but displaying particular molecular curvatures, such as those visible in helicenes. In this last typology of cases, it is commonly employed the term of "inherent chirality". Isomers that differ only for the spatial disposition of their atoms are called stereoisomers and they are divided in two categories: enantiomers (stereoisomers whose molecules are non superposable mirror images of each other) and diastereomers (stereoisomers whose molecular structures are not mirror images of each other). Similarly, chirality may also be expressed at *supramolecular level*. Supramolecular chirality involves the nonsymmetric arrangement of molecules in a noncovalent assembly. This can originate *i*) by the asymmetric nature of one or more of the interacting components; *ii*) by the particular way with which the interacting species

assemble, generating an adduct devoid of planes or improper axes of symmetry (Fig. 2.1) (Lehn, 1995). Therefore, suitable noncovalent synthesis may allow the preparation of supramolecules in either diastereomeric or enantiomeric form.
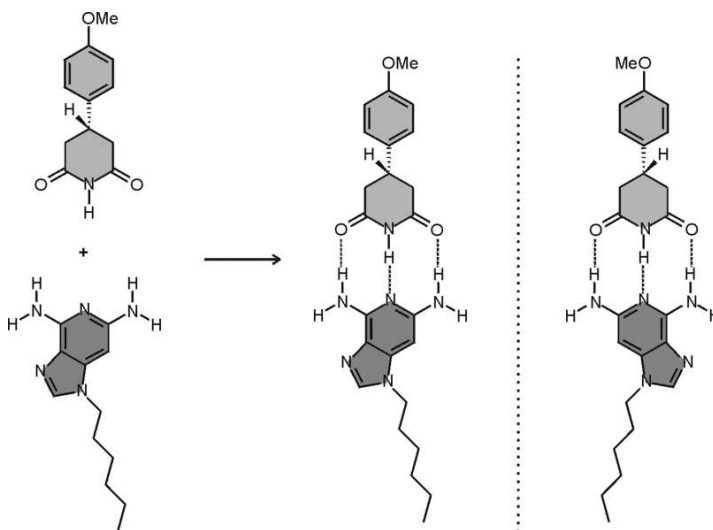

Figure 2.1 Assembly process of two achiral molecules (each of which endowed with a symmetry plane) leading to a chiral supermolecule devoid of any element of symmetry.

The term *molecular self-assembly* can be defined as the spontaneous association of two or more molecules under thermodynamic equilibrium resulting in the generation of well-

defined aggregates (strict self-assembly) or of extended polymolecular assemblies (self-organization) by means of noncovalent interactions such as hydrogen bonds, metal-coordination or π–π interactions (Philp and Stoddart, 1992; Lehn, 1995). The use of noncovalent bonds has the advantage that they are formed spontaneously and reversibly under thermodynamic equilibrium, with the possibility of error correction and without undesired side products. For these reasons, self-assembly is a valuable tool for the noncovalent synthesis of nanostructures such as helicates, grids, capsules, *etc*. To achieve this, kinetically labile reactants capable of suitable exchange reactions in solution are required, but this allows rapid racemization to occur. Consequently, the majority of the supramolecular architectures are formed of a racemic mixture, but for functional supramolecules (Schalley et al., 2001; Feringa and van Delden, 1999) it is important to control the stereoselectivity in the self-assembly process.

B2.1.2 Self-assembly in solid state: X-ray diffraction analysis of basket 3b

The molecular structure of basket **3b** is illustrated in Figure 2.2. Taking as a reference the weighed least squares plane, namely R, passing through the four bridging carbon atoms of the macrocycle, the calculated dihedral angles δ (collected in Table 2.1) show that the A and C aromatic rings are almost coplanar (8.46° below and 9.68° above, respectively) with the plane R, whereas B and D are almost orthogonal to it (82.25° and 80.05°, respectively). Following a procedure already reported, (Botta et al., 2007) the molecular conformation of the macrocycle was given by the conformational parameters ϕ and χ, which account without ambiguity for the reciprocal orientations between adjacent aromatic rings (see Table 2.1). The sequence of signs (+-,+-,+-,+-) of the calculated values of ϕ and χ suggested for basket **3b** a *flattened cone* conformation. As shown in Figure 2.2, the two ester bridging loops protruding above the resorcarene basket leave a large intramolecular space available for inclusion of other chemical species: the minimum interatomic distances between the carbon atoms of two opposite bridges are greater than 10 Å.
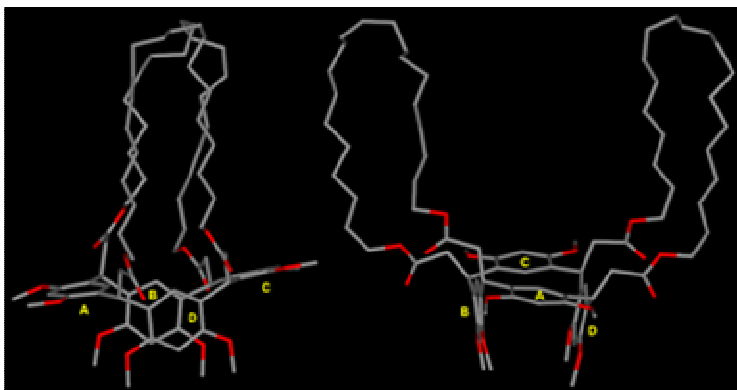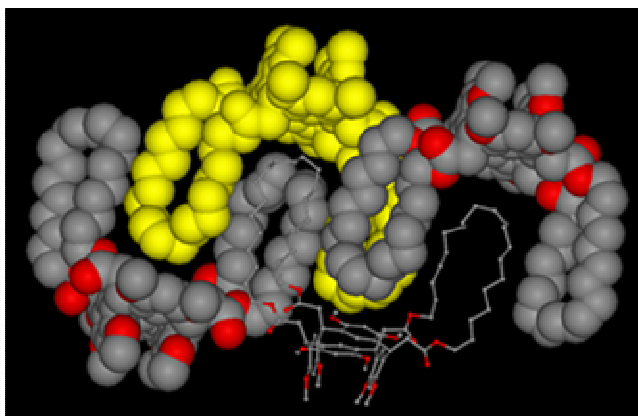
Figure 2.2 X-ray structure of basket resorc[4]arene **3b** showing the *flattened cone* conformation adopted by the macrocycle. Colors are as follows: C, grey; O, red. Hydrogen atoms are omitted for clarity.

Compound **3b**, upon crystallization, easily underwent a self-inclusion process yielding the supramolecular architectures shown in Figures 2.3 and 2.4. This "secondary structure" is built-up when each empty intramolecular space is filled by two ester arms of two neighbour resorcarenes, which produces zigzag one-dimensional ribbons, as those depicted in Figure 2.4.

181

Table 2.1 Dihedral Angles (δ) and Conformational Parameters (φ and χ) for Basket **3b**

Rings	δ (°)^a	Rings	ϕ (°)^a	χ (°)^a
R^A	171.54(5)	A–D	150.2(2)	-76.7(2)
R^B	82.25(5)	D–C	66.6(2)	-157.7(3)
R^C	189.68(5)	C–B	165.6(3)	-89.1(2)
R^D	80.05(4)	B–A	59.9(2)	-132.9(2)

^{a} Estimated standard deviations (ESD) are reported in parentheses. R is the weighed least squares plane passing through the four bridging carbon atoms of the macrocycle.

Figure 2.3 CPK and ball-and-stick views of the trimeric arrangement of basket resorc[4]arene **3b**.

182

A peculiar ''tertiary structure'' was indeed detected in the crystal lattice for basket resorc[4]arene **3b**, where a lamellar-type crystalline organization is built-up by the interdigitation of the methoxyl groups of one ribbon between those of the first adjacent ribbon. The layers are extended along the crystallographic *b* axis and bisect the crystallographic *ac* plane, as illustrated in Figure 2.4. On the other hand, when the crystal lattice is viewed orthogonally to the crystallographic *b* axis (i.e., orthogonally to the plane of Figure 2.4) it shows a Multilayered structure containing intercalated hydrophilic (ca. 9 Å thick) and hydrophobic (ca. 10 Å thick) layers.
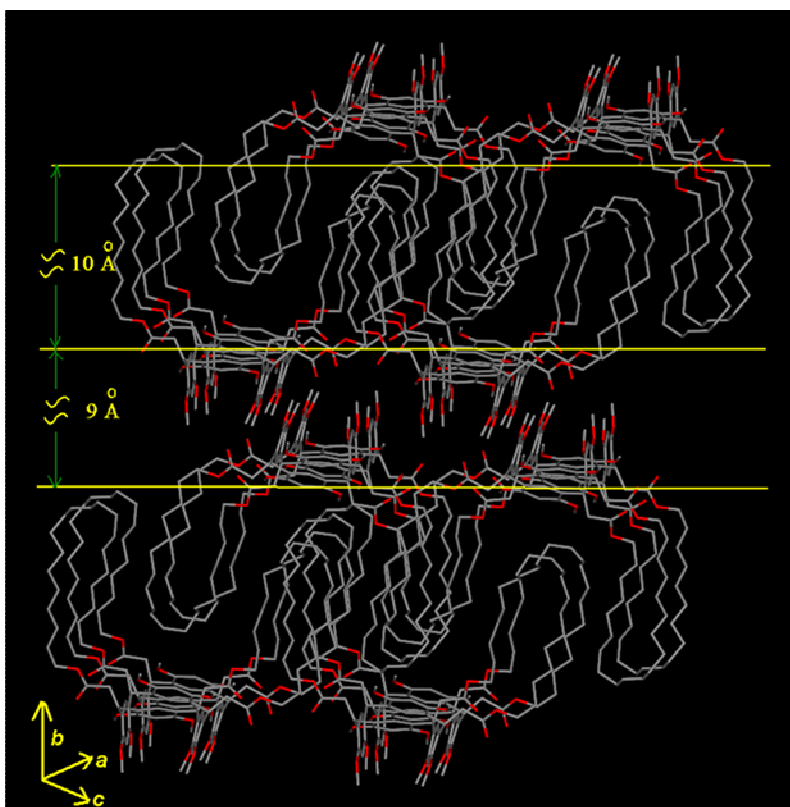
Figure 2.4 The self-assembly of the "zipped" ribbons in the crystal lattice of basket **3b** and its Multilayers structure.

From these considerations, it is reasonable to expect that this "nipper-like" resorc[4]arene molecule may give rise to a variety of non-covalent molecular assemblies in the solid state, allowing a rational evaluation of the structural requirements that a potential guest-partner should possess to achieve this purpose. In fact, the

presence of two alkenyl arms in **3b** endowed this new basket resorcarene structure with potential intriguing host properties. In the case of a similar basket compound armed with saturated bridge-chain (Botta et al., 2007), X-ray diffraction revealed an auto-complexing ability culminated in the formation of a supramolecular dimer. This time, for **3b** in its crystallized form, we observed the formation of a *trio* of molecules as the representative brick unit constituting the ripetitive fragment of the whole lattice. Notably, the threesome arrangement is responsible for a peculiar chiral behavior that originates from the reduction of symmetry coming from the particular relative folding assumed on self-assembly by the couple of the annular side chains (this folding, indeed, confers to a single **3b** molecule in the lattice a residual C_2 symmetry, as also visible in Figure 2.2).

B2.1.3 Study of the aggregation properties of 3b in solution

Nipper-like resorc[4]arene **3b** is characterized by wide hydrophobic regions, that should be prone to self-associate spontaneously in polar media. In the quite recent past a general protocol has been proposed (Angelini et al., 2001; Angelini et al., 2005) in view to prepare under controlled conditions both fully aqueous and water-organic solutions of some amphiphilic C_{60} fullerene derivatives (FD) in form of stable aggregates. The strong hydrophobic character of the spherical C_{60} carbon cage, indeed, hampers its solubilization in polar media such as water, thus slowing its possible direct use in biological applications. Up today, functionalization with hydrophilic addends has represented a possible direct strategy for making fullerenes relatively soluble in water. It has been found that these kind of derivatives can be effectively dissolved either in the form of monomers or as supramolecular aggregates (Nakamura and Isobe, 2003).

In particular, water-soluble C_{60} derivatives endowed with multiple hydrophilic substituting groups dissolve preferenzially as monomers in water and aqueous organic solvents, whereas monoderivatives on dissolution display a strong tendency to form clusters, depending upon both the particular hydrophilic/hydrophobic balance characterizing their molecular structures and the polarity of the used medium.

186

With regard to compound **3b,** a preliminary analysis showed that it is relatively soluble in organic solvents of moderate polarity (e.g. THF, CHCl$_3$, AcOEt), sparingly soluble in apolar or polar solvents (e.g. nC$_6$H$_{14}$, CH$_3$CN, CH$_3$OH) and virtually insoluble in water. On this base, resorting to the standardized procedure already described (Angelini et al., 2005), aqueous-organic solutions of aggregates of **3b** have been prepared starting from a stock solution in THF at which were progressively mixed increasing amounts of water employed as the co-solvent, always ensuring in the obtained mixtures a constant concentration of substrate (i.e. 8.8×10^{-4} M).

The generation of aggregates of **3b** in solution has been monitored by UV-spectroscopy measurements, in consideration of the clear differences emerged from the comparison among spectra obtained in solutions of **3b** solubilized in solvents of low polarity (e.g. nC$_6$H$_{14}$, THF, CHCl$_3$), where the resorcarenic substrate is certainly present in its monomeric form, and spectra registered in water-THF solutions.

In fact, the spectra of the solutions in which **3b** is only present as a monomer (aqueous-THF solutions with percentage (v/v) of THF > 52) display two quite sharp absorptions at 228.5 and 284.5 nm and a minimum of absorption at 261.0 nm (trace red in figure 2.5), while those in which **3b** is only present in aggregated form (aqueous-THF solutions with percentage (v/v) of THF < 40) clearly undergo a wide broadening of all the absorption bands, an absorption drift

187

increasing at the lower wavelengths (effects that typically originate from the generation of colloidal solutions, which trigger out dispersive phenomena of light) and the appearance of a shoulder at about 232 nm.
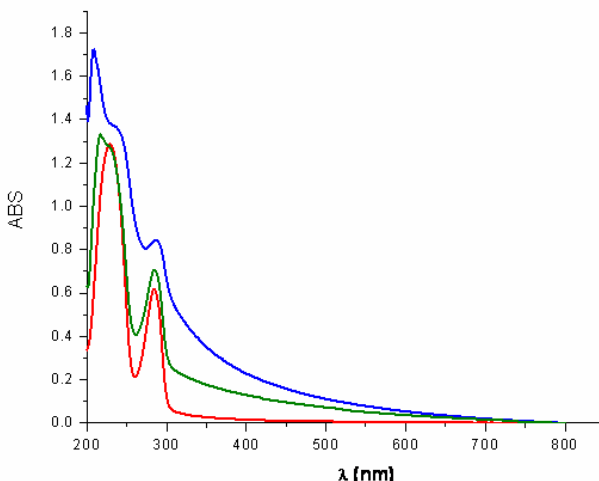

Figure 2.5. Modification of the absorption of compound **3b** in aqueous-THF solutions with different percentage (v/v) of THF.

According to these spectroscopical evidences, the autoaggregation process of **3b** has been effectively monitored by adopting the procedure already described (Angelini et al., 2005). At this purpose the quantity $\Delta ABS_{(261.0-284.5)norm}$, defined as reported in equation (1), was calculated from the UV spectrum registered at each analyzed water-THF mixture composition:

$$\Delta ABS_{(261.0-284.5)norm}=(\Delta ABS_{THFint}-\Delta ABS_{THFmin})/(\Delta ABS_{THFpure}-\Delta ABS_{THFmin}) \times 100 \qquad (1)$$

In equation (1) the subscripts THFint, THFmin and THFpure refer to differences in absorbance between 261.0 nm and 284.5 nm of **3b** in the investigated solvent mixtures at minimum (condition corresponding to a complete aggregation), maximum (condition corresponding to absence of aggregation) and intermediate (condition corresponding to incomplete aggregation) percentages of THF, respectively. A typical sigmoidal aggregation curve has been obtained for **3b** by plotting $\Delta ABS_{(261.0-284.5)norm}$ as a function of the the Hildebrand polarity index, δ_H, of the solvent mixtures water-THF (see Figure 2.6). We performed a regression analysis of the above sigmoidal plot by fitting the data points through equation (2) [rif2], from which the adjustable parameter API, an Aggregation Polarity Index useful to characterize the propensity of **3b** to self aggregate, has been derived:

$$\Delta ABS(254-430)norm = 100/[1+10^{\{(\delta H-API)/a\}}] \qquad (2)$$

More precisely, API represents the solvent polarity, expresses as δ_H index, at which the $\Delta ABS_{(261.0-284.5)norm}$ variation corresponds to 50% of the maximum. In general, at a given concentration of substrate, it is a reliable descriptor of the tendency to form molecular aggregates in a particular solvent mixture and its value is strictly related both to the hydrophilic/hydrophobic character possessed by the molecular structure prone to aggregate and, although to a

189

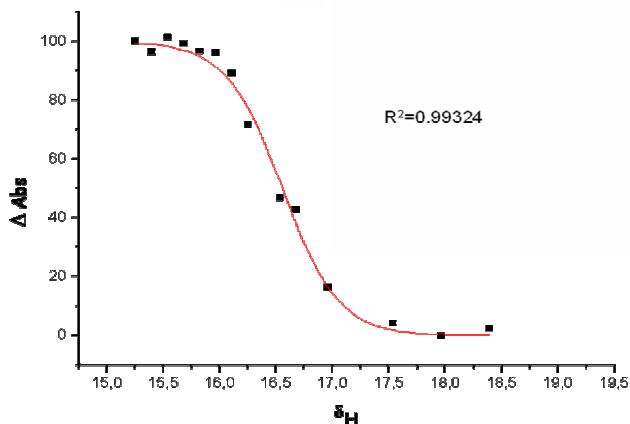lesser extent, to the particular organic co-solvent used along with the water.

Figure 2.6 Aggregation of **3b** in aqueous THF solutions: plots of $\Delta ABS_{(261.0-284.5)norm}$ against δH.

Since δ_H is directly related to the energy of cohesion of the solvent's molecules, higher API values point to a higher energy request for the formation of cavities within the solvent where the aggregate units can be hosted. Instead, always in equation (2) the variable a represents a futher adjustable parameter able to take into account the gradient of variation of $\Delta ABS_{(261.0-284.5)norm}$ as a function of the δ_H index.

For **3b**, at the analyzed concentration of $8.8 \times 10^{-4}M$, the above fitting afforded an API value of 16.56 ± 0.02 (which correspond to

190

solvent mixture composition of water_11.5%/THF_88.5% v/v) and a parameter a equal to 0.57. This means that the aggregation process of **3b** begins when the water-THF mixture achieve a composition characterized by a δ_H value of 15.99 and ends when the δ_H polatity of the solvent mixture become 17.13. As expected, the not particularly high value of API found as the aggregation index of **3b** suggests that enough intense solvophobic interactions among the molecules of substrate are already generated when the water achieve in the mixture the quite modest percentage of about 12. An effective assessment of the amount of solvophobic interactions taking place during the autoassociation of **3b** can be performed by resorting to equation (3) (Angelini et al., 2005):

$$\Delta\Delta G \text{cav} = (\kappa_2\gamma_2 - \kappa_1\gamma_1)A \qquad\qquad (3)$$

in which, $\Delta\Delta G$cav expresses the cavitation free-energy change due to the modification of the solvent-mixture composition before and after the aggregation of the substrate, the $\kappa_2\gamma_2$ and $\kappa_1\gamma_1$ terms represent the corrected surface tension values of the solvent-mixture before and after the induced aggregation of **3b** (Angelini et al., 2005), while A is the molecular surface of the same solute in its not aggregate form. Thus, exploiting the already known relationship existing between Hildebrand polarity index δ_H and corrected surface tension $\kappa\gamma$ for water-THF solvent mixtures (i.e. $\kappa\gamma = 9.00 \times 10^{-16} e^{(\delta H/0.78319)} + 2.00 \times 10^{-4} e^{(\delta H/6.27152)} + 5.61 \times 10^{-3}$, about this

see again ref 2), the difference $\kappa_2\gamma_2 - \kappa_1\gamma_1$ of equation (3) was assessed as 5.13×10^{-7} kcal/m^2. Next, the molecular surface A was evaluated by molecular mechanics calculations based on the MMFF force field, so that a molar surface area of 9.32×10^{6} m^2/mol has been derived. Finally, from the two above quantities, a $\Delta\Delta G$cav value of 4.78 kcal/mol has been estimated, an energy amount just identifiable with the solvophobic interactions leading to the observed aggregation of **3b**. In addition, through the corrected surface tension values of the solvent mixture that start and end the aggregation process (i.e. the $\kappa_2\gamma_2$ and $\kappa_1\gamma_1$ data), also the percentage of reduction of the solute surface area exposed to the solvent due to the association (i.e. $\%\Delta A$) can be calculated, this time by means of the new equation (4) (Angelini et al., 2005):

$$\%\Delta A = |(\kappa_1\gamma_1/\kappa_2\gamma_2 - 1)|\times100 \tag{4}$$

The obtained datum is $\%\Delta A$ = 5.9 %

At this point an interesting comparison may be performed between the API, $\Delta\Delta G$cav and $\%\Delta A$ values found for the structure of resorc[4]arene **3b** with those of the five amphiphilic fullerene derivatives (i.e. the structures symbolized as **FD1**-**FD5**) studied in the research work cited by (Angelini et al., 2005) and here reported in Table 2.2 for reasons of clarity.
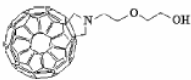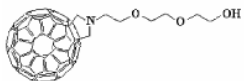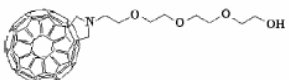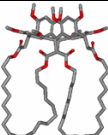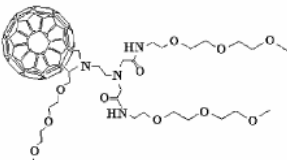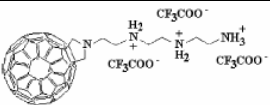
		API (at substate concentration of 8.8×10^{-4}M)	$\Delta\Delta G$cav (kcal/mol)	%ΔA
FD1		-	0.27	0.66
FD2		14.7	1.39	2.98
FD3		16.0	1.69	3.18
3b		16.56	4.78	5.90
FD4		-	12.55	13.11
FD5		-	21.42	23.02

Table 2.2 Comparison between the API, $\Delta\Delta G$cav and %ΔA values found for the structure of resorc[4]arene 3b with those of the five amphiphilic fullerene derivatives (i.e. the structures symbolized as FD1-FD5) (Angelini et al., 2005).

193

By inspection of such data it may be easily highlighted that, according to all the three above indexes, the hydrophilic/hydrophobic balance of **3b** ranks after that of **FD3** and before that of **FD4**.

B2.2 Experimental Section

General Remarks

All spectroscopic analysis were performed with the JASCO V-550 spectrometer with Peltier thermostat at 25 ° C using a quartz cuvette (cell length 1 mm). HPLC grade solvents $CHCl_3$ (chloroform, stabilized with ethanol), THF (tetrahydrofuran), ACN (acetonitrile), AcOEt (ethyl acetate), EtOH (ethanol) and H_2O (water) were obtained from Sigma Aldrich.

B2.2.1 Crystallographic data of basket resorc[4]arene 3b.

$C_{84}H_{120}O_{16}$, M = 1385.862, crystal system: triclinic, space group: P1, *a* = 15.775(5) Å, *b* = 22.923(5) Å, *c* = 12.270(5) Å, α = 99.920(5)°, β = 111.030(5)°, γ = 81.180(5)°, volume: 4059(2) Å^3, Z = 2, T = 293 K, ρ (calcd.) = 1.134 g cm^{-3}, 14527 total reflections collected, 13777 unique reflections (R_{int} = 0.06). These data can be obtained free of charge from The Cambridge Crystallographic Data Centre via www.ccdc.cam.ac.uk/data_request/cif.

B2.2.2 Solubility studies of basket 3b

Stock solutions of compound **3b** were prepared at room temperature and sonicated for 15 min. The saturated solutions of the same substrate were always prepared in flasks at room temperature and left to rest.

Procedure:

♣ Measurements of compound **3b** absorbance at 284 nm, using different concentrations according to the rule of progressive dilutions.

♣ Extrapolation of the relative calibration curves to determine the linear correlation between the intensity of absorption and concentration.

♣ Measurement of compound **3b** saturated solution absorption and extrapolation of the saturated concentration (CS_{3b}) from the corresponding calibration curve (Table 2.2).

Solvent	CS_{3b} (mol/dm^3)
water	insoluble
acetonitrile	3.2×10^{-3}
ethanol	4.5×10^{-5}
chloroform	1.6×10^{-2}
ethyl acetate	2.6×10^{-2}
tetraydrofuran	8.8×10^{-3}
n-hexane	insoluble

Table 2.2 Solubility of **3b** in solvents of different polarities

B2.2.3 Self-assembly studies in binary (THF/H$_2$O) solutions

Stock solutions of compound **3b** were prepared at room temperature and sonicated for 15min.

The 2.5 x10^{-3} M concentration of compound **3b** in the THF/H$_2$O (50:50 v/v) system showed interesting features: the solution was cloudy and after subsequent THF additions it became clear (THF/H$_2$O 6.43:3.58, 1.8 x 10^{-3} M of **3b**). Subsequent tests were performed with different amounts of the two solvents. The fixed concentration of compound **3b** was 8.9 x10^{-4} M and solutions with the following compositions were UV-Vis analyzed (Table 2.6)

250μl THF	THF/H$_2$O	THFμl	H$_2$Oμl	Conc.	Abs 284nm
1	5,7:4,3	320	430	$8,8 \cdot 10^{-4}$	0.61637
2	5,6:4,4	310	440	"	0.5934
3	5,5:4,5	300	450	"	0.5766
4	5,4:4,6	290	460	"	0.59852
5	5,3:4,7	280	470	"	0.6011
6	5,2:4.8	270	480	"	0.63149
7	5,1:4.9	260	490	"	0.68653
8	5:5	250	500	"	0.70505
9	4,8:5,2	230	520	"	0.43569
10	4,7:5,3	220	530	"	0.50205
11	4,6:5,4	210	540	"	0.93876
12	4,5:5,5	200	550	"	0.28756
13	4,1:5,9	160	590	"	0.9811
14	3,8:6,2	130	620	"	0.61558
15	3,5:6,5	100	650	"	0.95619

Table 2.6 Absorption of **3b** solutions (8.9 x10^{-4} M) in binary (THF/H$_2$O) systems with different percentages *v/v* of the two solvents.

Chapter B3

Encapsulation Studies of Fullerenes C$_{60}$ and C$_{70}$

B3.1 Results and discussion

B3.1.1 Complexation of fullerenes

A **fullerene** is any molecule composed entirely of carbon, in the form of a hollow sphere, ellipsoid, tube, and many other shapes. Spherical fullerenes are also called **buckyballs**, and they resemble the balls used in football (soccer). Cylindrical ones are called carbon nanotubes or buckytubes (Fig.3.1). Fullerenes are similar in structure to graphite, which is composed of stacked graphene sheets of linked hexagonal rings; but they may also contain pentagonal (or sometimes heptagonal) rings.

The first fullerene molecule to be discovered, and the family's namesake, buckminsterfullerene (C_{60}), was prepared in 1985 by Richard Smalley, Robert Curl, James Heath, Sean O'Brien, and Harold Kroto at Rice University. The name was a homage to Buckminster Fuller, whose geodesic domes it resembles. The structure was also identified some five years earlier by Sumio Iijima, from an electron microscope image, where it formed the core of a "bucky onion" (Iijima, 1980). Fullerenes have since been found to occur in nature (Buseck et al., 1992). More recently, fullerenes have been detected in outer space (Cami et al., 2010). According to astronomer Letizia Stanghellini, "It's possible that buckyballs from outer space provided seeds for life on Earth."
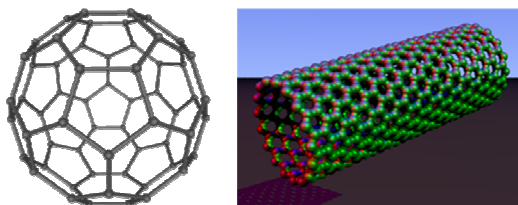
Figure 3.1 Buckminsterfullerene C_{60} (left) and carbon nanotubes (right) are two examples of structures in the fullerene family.

The fullerene family is one of the most intriguing classes of molecules and has received great attention due to potential applications in the fields of electrochemistry and material science. This is, indeed, testified by a large number of examples in which they demonstrated a strong attitude to be successfully used in the development of optoelectronic devices, hydrogen-storage materials and therapeutics for the treatment of cancer, AIDS and neurodegenerative diseases .

Commonly the chemical properties of fullerenes are modulated by chemical derivatization with suitable molecules, however correct modulation of their properties can also be achieved by promoting their supramolecular interaction with appropriate molecules hosts.

The design and synthesis of preorganized bowl-shaped macrocyclic hosts which can have applications in supramolecular and material chemistry has been of considerable interest in recent years. In particular, calix[n]arenes, resorcarenes, cyclodextrins, cyclotriveratrylenes, corannulenes, and similar macrocyclic frameworks have been studied, all providing efficient shape complementarity to spherical, mostly C_{60} fullerene, guests. From all of these investigations, it has become evident that a diversity of structures may be capable of associating with C_{60} at different extent and in various organic solvents. Progress of the studies of C_{60} complexes in host-guest chemistry, separation science, and molecular electronics has prompted synthetic chemists to construct well-designed host molecules possessing sizable bowl-, belt-, or cage-shaped cavities (Steed, 2004).

Summarized in Fig. 3.2 are the main types of host molecules, including cavitands, saddle-shaped molecules, porphyrins, siloxanes, curved-face tryptophanes and β,γ–cyclodextrins (Steed, 2004).
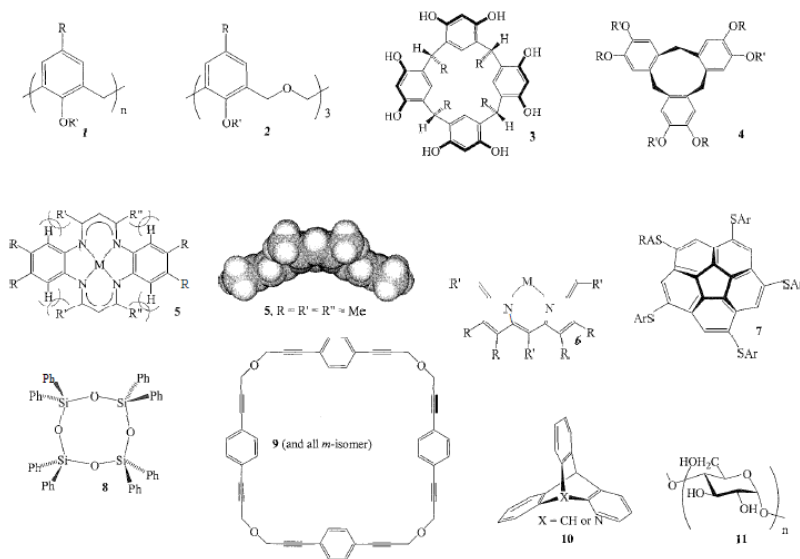
Figure 3.2 The main types of host molecules.

B3.1.2 Calixarenes and related molecules as hosts

Historically, complexation of fullerenes with p-Bu^t-calix[8]arene, (Fig. 3.2, 1 R = But. R' = H), was an important development in the field, independently reported in 1994 by Atwood and Shinkai, although there was an earlier report on the binding of a water-soluble calixarene bearing sulfonate groups on the lower (Atwood et al, 1994; Suzuki et al, 1994). p-Bu^t-calix[8]arene is effective in retrieving high-purity C$_{60}$ from toluene solutions of fullerite, which is a mixture of all the toluene-soluble fullerenes in carbon soot. This involves recrystallization of the precipitate from toluene followed

by decomposition of the 1: 1 complex when added to chlorinated hydrocarbons in which the fullerene is only sparingly soluble (Hardie and Raston, 1999).

The proposed structure of the final complex is a triangular arrangement of three fullerenes surrounded by a sheath of three calixarenes in the double-cone conformation. $[(C_{60})_3(p\text{-Bu}^t\text{-calix[8]arene})_3]$(Scheme 3.1).
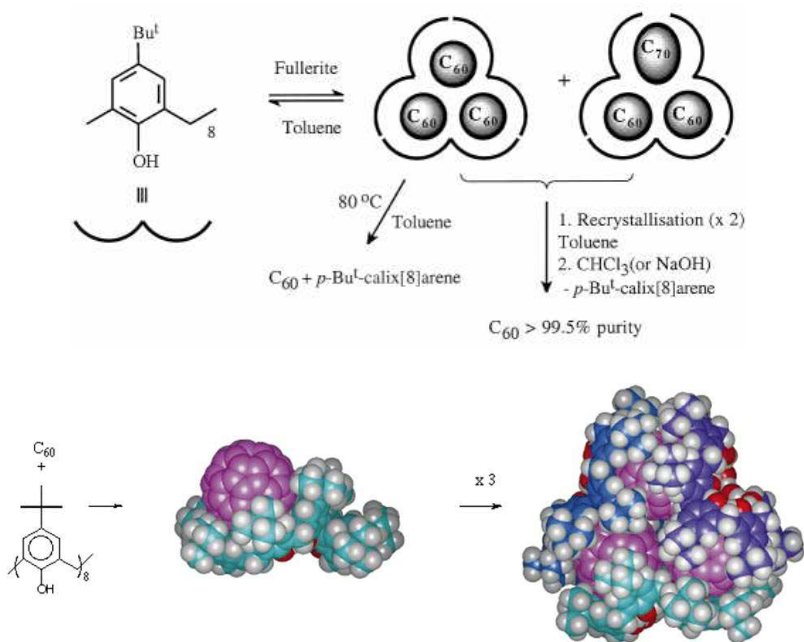
Scheme 3.1 Purification of C_{60} by complexation**:** formation of the micelle like species $[(C_{60})_3(p\text{-}tert\text{-butylcalix[8]arene})_3]$ *via* a monomeric transient 1 : 1 intermediate $(C_{60})(p\text{-}tert\text{-butylcalix[8]-arene})$.

Fullerene-rich calix[6]arene complexes, $(C_{60}$ or $C_{70})_2$ calix[6]arene, were structurally authenticated as isomorphous complexes (Hardie and Raston, 1999), showing the calixarene in the double-cone conformation with a fullerene perched in each of the shallow cavities, resembling the jaws of a pincer acting on two adjacent cage molecules. The extended structures have continuous three-dimensional interplay of the fullerenes close to the van der Waals limit (Fig. 3.3j).
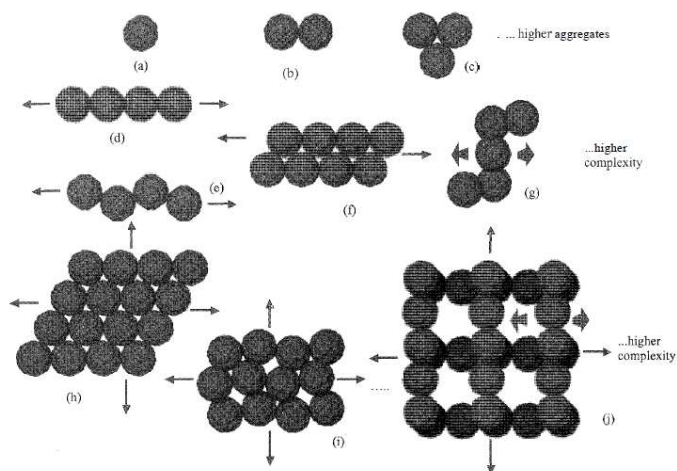

Figure 3.3 The types of arrangements of fullerenes (van der Waals contacts) in their host-guest complexes (host molecules not shown). These cover finite structures. (a) monomeric (encapsulated), b) dimeric and (c) the proposed trimeric complex involving p-Bu^t-calix[8]arene, and higher aggregates, and continuous structures, all of which were established in parts (d-j), with scope for structures of higher complexity.

p-Benzylcalix[5]arene and *p*-benzylhexahomooxacalix[3]arene form 2 : 1 complexes with C_{60} from toluene solutions, as the octa-toluene solvate in the case of the calix[5]arene (Hardie and Raston, 1999). In both structures the fullerene is shrouded by two staggered, *trans*-host molecules in cone conformations either with dangling benzyl groups, calix[5]arene, or edge on to the fullerene benzyl groups, oxacalix[3]arene, (Fig. 3.4) Either the benzyl groups are now directed away from the fullerene, $\theta = 180°$, or are such that there are C-H fullerene interactions, $\theta = 90°$. In both C_{60} structures, the alignment of the symmetry axis of the calixarene with the same symmetry element of C_{60}, C_5 and C_3, respectively, highlights the importance of symmetry matching in designing host molecules for fullerenes. This maximises the points of contact and efficiency of π–π interactions between the two interacting moieties.
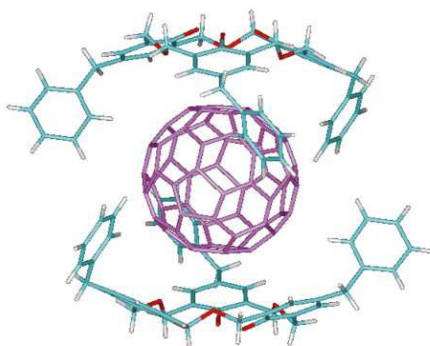
Fig. 3.4 The supermolecule [(C60)(*p*-benzylhexahomooxacalix[3]arene)$_2$]. The encapsulation of the fullerene by two oxacalix[3]arenes precludes the formation of extended supramolecular arrays *via* interfullerene interactions.

With regard to resorc[4]arenes, it has been described a molecular capsule derived from H-bonding of two resorcinarenes and propan-2-ol molecules, with the fullerenes also arranged in column (fig. 3.5) (Hardie and Raston, 1999).
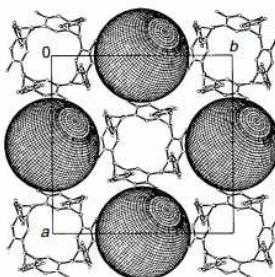

Figure 3.5 Packing diagram (only calix[4]resorcinarene and C$_{60}$ molecules are shown), parallel to the molecular columns.

A bis-calix[4]resorcinarene is effective in binding C_{60} (Wan et al., 2000) and calix[4]resorcinarenes bearing dithiocarbamate groups between the oxo group, R = alkyl chains, and with methylene groups between adjacent oxo-groups, form torus-shaped complexes comprised of three calixarenes with divalent cadmium and zinc ions, which effectively bind c_{60} (Fox et al., 2000) (Fig.3.6).
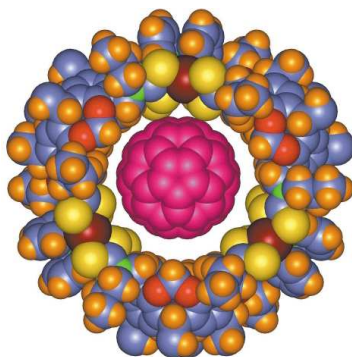

Fig. 3.6 Space filling model of host–C_{60} complex showing the proposed mode of fullerene binding by loop-shaped hosts.

B3.1.3 Encapsulation studies

In this Section we present an exhaustive study aimed to investigate the possible supramolecular recognition that the basket-like resorc[4]arene **3b** may exercise towards the fullerenes C_{60} and C_{70}. Encapsulation studies carried out by UV measurements showed that **3b** is able to efficiently encapsulate the cited pristine fullerenes. Consequently, the equilibrium constants of the relative **3b**:fullerene complexes were also determined.

As a final goal, molecular modeling studies (based on both Multi-conformational Molecular Docking and Molecular Dynamics approaches employed in integrated fashion) have provided results in satisfactory agreement with the experimental ones, so affording useful and interesting indications about the modalities with which the host-guest interaction can take place.

B3.1.3.1 UV measurements

Fullerenes and basket-like resorc[4]arene **3b**, as shown in Chapter B2, have a predominant hydrophobic character and exhibit a strong tendency to self-aggregation. The intermolecular forces that determined the formation of the fullerene self-aggregates , as well as in the basket self-assembly, are solvophobic. This type of interaction occurs between polar molecules in highly polar solvents like water. The solvent molecules are arranged on the

surface of the polar molecule to form a solvation shell in which water molecules are tightly organized, leading to a decrease of the system entropy (ΔS) unfavorable to the process. From an enthalpic (ΔH) standpoint, however, the process is favored because of the stability of Van der Waals interactions between solute molecules and water and due to the formation of hydrogen bonds between water molecules forming the solvation shell. The ΔG of the system (ΔG = ΔH-TΔS) is still positive, since the enthalpic contribution cannot exceed the entropic disadvantage. This means that in a polar solvent, apolar molecules tend to assemble, reducing the number of solvent molecules forming the solvation shell and increasing the number of free solvent molecules, which increases the entropy of the system.

In other words, to promote the complexation of fullerenes C_{60} and C_{70} with resorc[4]arene **3b**, it was necessary to increase the solvophobic intermolecular interaction with a higher percentage of the more-polar component of the solvent mixture.

The ability of C_{60} and C_{70} to successfully interact with **3b** has been experimentally demonstrated by UV measurements.

Compound **3b** is relatively soluble in organic solvents of moderate polarity as THF, sparingly soluble in apolar or polar solvents and insoluble in water. Since the fullerene C_{60} showed a low solubility

also in THF, decaline cis / trans was used as a cosolvent which did not interfere with the UV-vis measurements.

The measurements were performed within a binary and quite apolar solvent mixture (THF/decaline 50:1), selected with the aim of allowing a good solubility of both the interacting species (i.e. **3b** and the fullerenes C_{60} or C_{70}).

UV measurements (Figures 3.7 and 3.8) allowed us to obtain the relevant equilibrium constants of the formed complexes **3b**:C_{60} (Ks=135343, $\Delta G° = -6.88$) and **3b**:C_{70} (Ks=104907, $\Delta G° = -6.73$).

Figure 3.7 UV measurements performed within a binary and quite apolar solvent mixture (THF/decaline 50:1), with the aim of allowing a good solubility of the interacting species **3b** and the fullerene C_{60}.
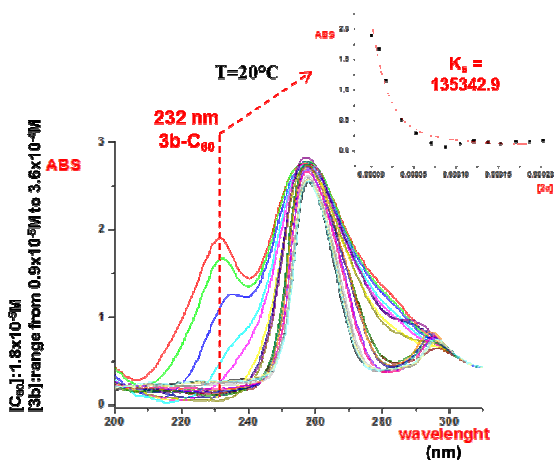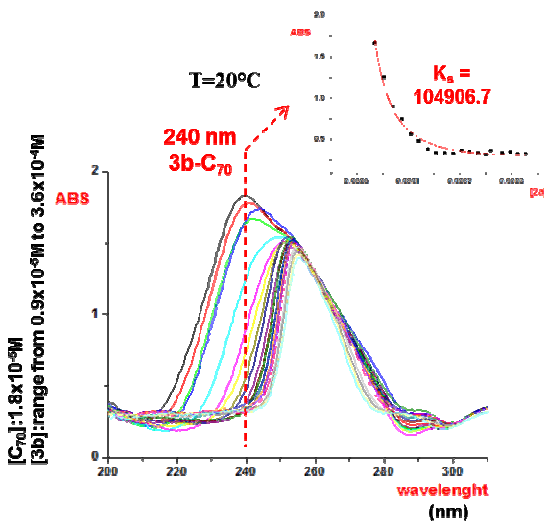
211

Figure 3.8 UV measurements performed within a binary and quite apolar solvent mixture (THF/decaline 50:1), with the aim of allowing a good solubility of the interacting species **3b** and the fullerene C_{70}.

For comparative purpose, the C_{60} sphere was also put in presence of the starting monomer (**M$_{3b}$**) (See section A2.2.2). As expected, the registered supramolecular interaction in this case was much weaker (adduct **M$_{3b}$**:C_{60}, Figure 3.9), thus confirming the role played by the solvophobic basket-like structure of **3b** in promoting the effective recognition of the considered fullerenes.
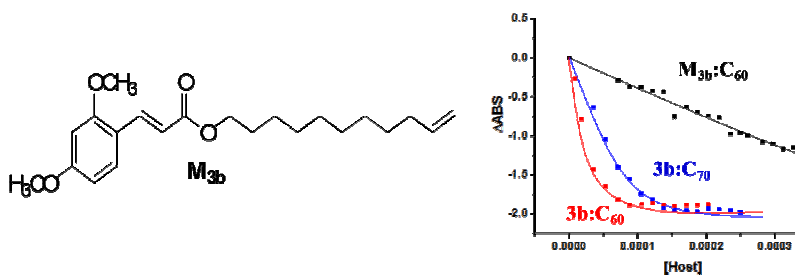
Figure3.9 Progressive complexation of the hosts M_{3b} and **3b** with C_{60} and C_{70}

B3.1.3.2 Molecular modeling studies

*STEP 1: Conformational Analysis of **3b***

A quite elaborated molecular modeling procedure has been employed in view to simulate the complexes formation between **3b** and the fullerene spheres C_{60} and C_{70}. In such a procedure, initially the structure of **3b** derived by X-rays has been submitted to conformational analysis (MM2 force field), using the random Monte Carlo method.

Among all the obtained conformations, we selected those included within an energy window of 6 Kcal from the global minimum, representative of the whole Boltzmann population (Fig.3.10).

213

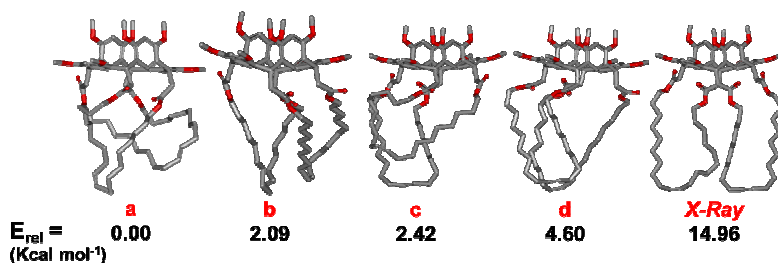**Figure 3.10** Conformations of **3b**

STEP 2: Docking Analysis

The conformations selected in step 1, together with the X-Ray conformation, were used to perform a Multi-conformational quasi-flexible automatic docking with the fullerene spheres C_{60} and C_{70}, through the lab-made computer program Moline (Alcaro et al., 2007), able to generate **3b**:C_{60} or **3b**:C_{70} adducts. This procedure afforded for both the complexes **3b**:C_{60} and **3b**:C_{70} 28600 rigid geometries of adducts, which were next conformationally relaxed (MM2 force field), in order to maximize the intermolecular interactions. Such ensembles of adducts were then clusterized on the base of both energy (by an energy window of 6 Kcal) and geometric criteria (RMS value set to 5), thus obtaining 75 configurations for **3b**:C_{60} and 88 configurations for **3b**:C_{70}, respectively; the most representatives are those shown in Fig.3.11.

214

3b:C$_{60}$ 3b:C$_{70}$
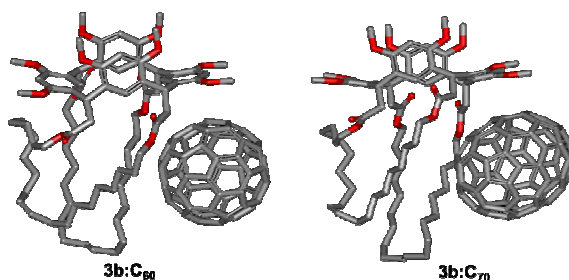
Figure 3.11 The most representative complexes derived from docking analysis.

STEP 3: Molecular Dynamics

With the aim of verifying the ability of host **3b** to improve the quality of its interaction with the fullerene guests by undergoing suitable conformational modifications (i.e. the effect commonly known with the term "guest-to-host induced fit") a further step based on molecular dynamic calculations has been designed (Fig.3.12). The molecular dynamics was carried out with Macromodel (Mohamadi et al., 1990) at a temperature of 350 K and dynamic time of 2 ns.

Figure 3.12 The most stable complexes obtained from molecular dynamics analysis.

B3.2 Experimental Section

General Remarks

All spectroscopic analysis were performed with the JASCO V-550 spectrometer with Peltier thermostat at 25 °C using a quartz cuvette (cell length 1 mm). HPLC grade THF (tetrahydrofuran) and decaline cis / trans were obtained from Sigma Aldrich.
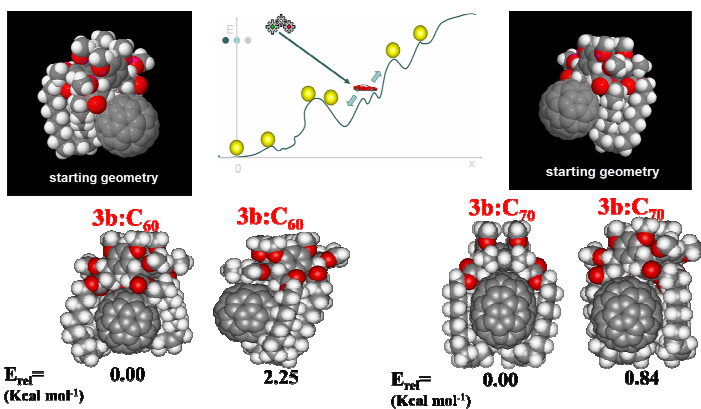
B3.2.1 Solubility studies in THF / Decaline 50:1

General procedure

The stock solutions were prepared at room temperature and sonicated for 3h. The saturated solutions of the same substrate were always prepared in flasks at room temperature and left to rest.

Procedure:

♣ Measurements of absorbance using different concentrations according to the rule of progressive dilutions.

♣ Extrapolation of the relative calibration curves to determine the linear correlation between the intensity of absorption and concentration.

♣ Measurement of saturated solution absorption and extrapolation of the saturated concentration (**CS**) from the corresponding calibration curve.

	λ (nm)	CS (M)
fullerene C_{60}	331	3.47×10^{-5}
fullerene C_{70}	240	6.84×10^{-5}
3b	284	4×10^{-3}

Table 3.1 Saturated concentration (**CS**) of C_{60}, C_{70} and **3b** in a binary and quite apolar solvent mixture (THF/decaline 50:1)

B3.2.2 Complexation studies in THF / Decaline 50:1

General procedure

A 1.8×10^{-3} M solution of guest (C_{60} or C_{70}) was prepared in a quite apolar solvent mixture (THF/decaline 50:1). A solution of the host was prepared using the guest solution as solvent medium in order to keep the concentration of the guest constant after each addition of host. Aliquots of the host solution were added stepwise to 2.00 mL of the guest solution in a 1.00 cm quartz cuvette. After each addition, a UV-Vis spectrum was acquired (Table 3.2 and 3.3).

Table 3.2

[C_{60}]	[BSK]	ABS (232 nm)
1.8×10^{-5}M	-	1.90015
1.8×10^{-5}M	8.95×10^{-6}M	1.167178
1.8×10^{-5}M	1.79×10^{-5}M	1.153
1.8×10^{-5}M	3.56×10^{-5}M	0.508274
1.8×10^{-5}M	5.3×10^{-5}M	0.287582
1.8×10^{-5}M	7×10^{-5}M	0.118741
1.8×10^{-5}M	8.8×10^{-5}M	0.0546412
1.8×10^{-5}M	1.05×10^{-4}M	0.11626
1.8×10^{-5}M	1.21×10^{-4}M	0.152427
1.8×10^{-5}M	1.38×10^{-4}M	0.138031
1.8×10^{-5}M	1.55×10^{-4}M	0.117387
1.8×10^{-5}M	1.71×10^{-4}M	0.151482
1.8×10^{-5}M	1.87×10^{-4}M	0.149401
1.8×10^{-5}M	2.03×10^{-4}M	0.16494
1.8×10^{-5}M	2.19×10^{-4}M	0.189663
1.8×10^{-5}M	2.35×10^{-4}M	0.188303
1.8×10^{-5}M	2.51×10^{-4}M	0.220873
1.8×10^{-5}M	2.66×10^{-4}M	0.230062
1.8×10^{-5}M	2.82×10^{-4}M	0.258064
1.8×10^{-5}M	2.97×10^{-4}M	0.265613
1.8×10^{-5}M	3.12×10^{-4}M	0.267489
1.8×10^{-5}M	3.27×10^{-4}M	0.271465

Table 3.3

$[C_{70}]$	$[BSK]$	ABS (240nm)
1.8×10^{-5}M	-	1.83067
1.8×10^{-5}M	8.95×10^{-6}M	1.77240
1.8×10^{-5}M	1.79×10^{-5}M	1.64464
1.8×10^{-5}M	3.56×10^{-5}M	1.66158
1.8×10^{-5}M	5.3×10^{-5}M	1.25469
1.8×10^{-5}M	7×10^{-5}M	0.900045
1.8×10^{-5}M	8.8×10^{-5}M	0.746175
1.8×10^{-5}M	1.05×10^{-4}M	0.564775
1.8×10^{-5}M	1.21×10^{-4}M	0.481308
1.8×10^{-5}M	1.38×10^{-4}M	0.384494
1.8×10^{-5}M	1.55×10^{-4}M	0.338368
1.8×10^{-5}M	1.71×10^{-4}M	0.340334
1.8×10^{-5}M	1.87×10^{-4}M	0.332291
1.8×10^{-5}M	2.03×10^{-4}M	0.373209
1.8×10^{-5}M	2.19×10^{-4}M	0.357498
1.8×10^{-5}M	2.35×10^{-4}M	0.337331
1.8×10^{-5}M	2.51×10^{-4}M	0.318818
1.8×10^{-5}M	2.66×10^{-4}M	0.36716
1.8×10^{-5}M	2.82×10^{-4}M	0.337954
1.8×10^{-5}M	2.97×10^{-4}M	0.351802
1.8×10^{-5}M	3.12×10^{-4}M	0.328652
1.8×10^{-5}M	3.27×10^{-4}M	0.32638

Chapter B4

References

Abouderbala L.O., Belcher W.J., Boutelle M.G., Cragg P.J., Fabre M., Dhaliwal J., Steed J.W., Turner D.R., Wallace K.J., *Chem. Commun.*, **2002**, 358.

Afinson C.B., *Science*, **1973**, 181, 223.

Alcaro S., Gasparrini F., Incani O., Caglioti L., Pierini M., Villani C., *J. Comput. Chem*., **2007**, *28*, 1119.

Angelini G., De Maria P., Fontana A., Pierini M., Maggini M.*,* Gasparrini F., Zappia G., *Langmuir*, **2001,** 17, 6404.

Angelini G., Cusan C., De Maria P., Fontana A., Maggini M., Pierini M., M Prato M., Schergna S.,Villani C., *Eur. J. Org. Chem.* **2005**, 1884.

Auld D.S., Zinc Sites in Metalloenzymes and Related Proteins. In Handbook on Metalloproteins; Bertini I., Sigel A., Sigel H. Eds.: Marcel Dekker, Inc.: New York, **2001**, 881.

Atwood J.L., Koutsantonis G.A. and Raston C.L., *Nature*, **1994**, 368, 229.

Bunce R.A., *Tetrahedron*, **1995**, 48, 13103.

Buseck P.R.; Tsipursky S.J., Hettich R., *Science*, **1992,** 257, (5067), 215.

Butler P.J.G., *Phil. Trans. R. Soc. Lond. B.*, **1999**, 354, 537.

Cami J., Bernard-Salas J., Peeters E., Malek S. E., *Science*, **2010**, 329, (5996), 1180.

Cabbiness D.K., Margerum D.W., *J. Am. Chem. Soc*, **1969**, 91, 6540.

Cram D.J., *Angew. Chem. Int. Ed.*, **1986**, 25, 1039.

Cram D.J., *Angew. Chem. Int. Ed.*, **1988**, 27, 1009.

Cram D.J., Karbach S., Kim H.E., Knobler C.B., Maverick E.F., Ericson J.L., Helgeson R.C., *J. Am. Chem. Soc.*, **1988**, 110, 2229.

Dokland T., McKenna R., Ilag L.L., Bowman B.R., Incardona K.L., Fane B.A., Rossmann M.G., *Nature* **1997**, 389, 308.

Ellis R.J., Hemmingsen S.M., TIBS, **1989**, 14, 339.

Feringa B.L. and van Delden R.A., *Angew. Chem. Int. Ed.*, **1999**, 38, 3418.

Fischer E., *Ber. Dtsch. Chem. Ges.,* **1894**, 27, 2985.

Flurry R.L., *J. Phys. Chem.*, 69, **1965**.

Fox G.D., Dremr M.G.B., Wilkinson E.J.S., Beer P.D., *Chem. Commun.*, **2000,** 391.

Frank H.S., Evans M.W., *J. Chem. Phys.* **1945**, 13, 507.

Fujita M., Yazaki J., Ogura K., *J. Am. Chem. Soc.*, **1990**, 112. 5467.

Fujita M., Sasaki Q.M., Mitsuhashi T., Fujita T., Uazaki J., Yarnaguchi K., Ogura K., *Chem. Commun.*, **1996**, 1535.

Gibb C.L.D., Stevens E.D., Gibb B.C., *Chem. Commun.*, **2000**, 363.

Hardie M.J., Raston C.L., *Chem. Commun.*, **1999**,1153.

Iijima S., *Journal of Crystal Growth*, **1980**, 50, 675.

Klug A., *Phil. Trans. R. Soc. Lond. B.*, **1999**, 354, 531.

Kushner D.J., *Bacteriol. Rev.* **1969**, 33, 302.

Kuehl C.J., Huang S.D. and Stang P.J., *J. Am. Chem. Soc.*, **2001**, *123*, 9634.

Lindsey J.S. *New J. Chem.* A review., **1991**, 15, 153

Lehn J.-M., *Supramolecular Chemistry.* 1 ed.; VCH: Weinheim, **1995**.

Lehn J.-M., *Proc. Natl. Acad. Sci*., **2002**, 99, 4763.

Lawrence D.S., Jiang T., Levett M., *Chem. Rev.*, **1995**, 95, 2229.

Liu L., Guo Q.-X., *Chem. Rev.*, **2001**, 101, 673.

McCarroll A.J., Walton J.C., *Angew. Chem. Int. Ed.*, **2001**, 40, 2224.

Mohamadi F., Richards N.G.J., Guida W.C., Liskamp R., Lipton M., Caufield C., Chang G., Hendrickson T., Still W.C., *J. Comput. Chem.*, **1990**, 1, 440.

Nakamura E., Isobe H., *Acc. Chem. Res.,* **2003**, 36, 807.

Philp D. and Stoddart J.F., *Angew. Chem., Int. Ed.*, **1996**, 35, 1154.

Rudkevich D.M., Rebek J.Jr.; *Eur. J. Org. Chem.*,**1999**, 1991.

Schalley C.A., Beizai K. and Vögtle F., *Acc. Chem. Res.*, **2001**, 34, 465.

Suzuki T., Nakashima K. and Shinkai S., *Chem. Lett.*, **1994**, 699.

Steed J.W., *Encyclopedia of supramolecular chemistry*, **2004**, 1401.

Steed J.W., Atwood J.L., *Supramolecular Chemistry, 2nd edition*, John Wiley & Sons, Ltd, **2009**.

Wan U., Mitltin 0., Barnhurst L.: Kurchan A., Kutateladre A., *Org. Lett.*, **2000**, *2,* 3817.

Williams D.H., Westwell M.S., *Chem. Soc. Rev.*, **1998**, 27, 57.

Conclusions

Resorc[4]arenes endowed with long side chains ending with a vinylidene group can be considered as intriguing substrates for metathesis reactions. The three undecenyl derivatives **1a**, **1b**, and **1c** were synthesized by a classical procedure and submitted to olefin metathesis by exposure to a 2nd-generation Grubbs complex as a catalyst. The different spatial orientations of the axial undecenyl substituents can be foreseen as the source of unexpectedly varying results.

In the *chair* stereoisomer **1a** the four substituents have an *rctt* distribution pattern, *i. e.* the hydrocarbon chains point independently two by two in opposite directions. Under partially optimized conditions of solvent, concentration and catalyst %, **1a** underwent two separate contemporary intramolecular ring-closing metathesis (RCM) reactions to give the bicyclic alkene **2a** in 46% yield and with an *E* : *Z* ratio = 3 : 1.

Regarding the formation of a new double bond in a metathesis reaction, no definitive rule per type of reaction, substrate and catalyst can be found in the literature. Experimentally, we obtained always a mixture *E/Z* of products in an approximate ratio 3:1 (by NMR integration) for both intra- and inter-molecular links. The

geometrical isomerism of the double bonds affects in some cases the quality of ^{1}H and ^{13}C NMR spectra by the presence of satellite signals. However, the different intensities allow the assignment of the major geometrical isomer. Moreover, the reduction (10% H_2/Pd) of the products led to complete saturation of the alkyl chains and to the obtainment of clean NMR spectra. The relatively low yield of **2a** was attributed to a co-occurring ADMET-like polymerization, which, although under unfavorable conditions, afforded in comparable yield (44%) an insoluble polymer product **P1a**, as suggested by the solid state ^{13}C CPMAS NMR spectrum. Actually, resorc[4]arene **1a**, under typical ADMET reaction conditions, gave an insoluble polymerization material with almost coincident NMR features. We supposed that in the case of linear intermolecular polymerization every terminal alkene could react independently with the single terminal alkene of diverse (upper or lower) moieties of different neighbor molecules. As a result, the polymer will be formed by a complex connection of the same macrocyclic units.

A third minor (%) product, the linear dimer **3a**, was isolated from the reaction mixture and it was shown to be formed from two molecules of **2a**, reasonably by the opening of one intramolecular double bond and the reaction of its activated chain with another molecule of **2a** via ROM and then CM. The dimer **3a** has still two reactive alkenes, which could likely give similar trimers or tetramers.

The formation of such compounds was suggested by very minor spots in the TLC plate of the reaction mixture, but was not supported by the material isolation. In summary, we have shown that undecenyl resorc[4]arene **1a** (*chair* stereoisomer), with a relatively simple arrangement of the chains, may give different metathesis products by exposure to ruthenium catalysts, depending on the reaction conditions.

X-Ray diffraction analysis of **1a** (see section A2.1.2) shown a peculiar type of self-assembly that suggested us to study its tendency to exhibit strong gelation characteristics in organic solvents to afford gel materials. Gel networks find extensive use in everyday life ranging from applications in cosmetics through to complex pharmaceutical formulations that exhibit tunable drug release profiles. Preliminary gelation studies are in progress.

In the *cone* stereoisomer **1b** the four axial substituents are all-*cis* (rccc) and the side chains crowd together in the lower rim of the macrocycle. Under the same conditions (time, temperature and catalyst) as those used for **1a** (see A3.2.2 Section) resorc[4]arene **1b** gave the following products in the order: **2b** (yellow solid, 15% yield), **3b** (white solid, 50% yield), **4b** (white solid, 9% yield), and **5b** (white solid, 5% yield). Compounds **2b** (hemi-basket) and **3b** (basket) proceed from the partial and the double intramolecular ring closure, respectively. Notably, the second one produces a

change in the cone conformation of **1b**, which is frozen in a partial cone arrangement. The other products of the metathesis reaction, the linear dimer **4b** and the linear trimer **5b**, derive from intramolecular links formed after the reopening of two alkene rings along the pathway **3b → 4b → 5b**, where the first step is equal to the passage **2a + 2a → 3a** discussed above, while the second one corresponds to a similar **3b** + **4b** reaction. Consideration of the new structures suggests that some products could function as host of suitable molecular guest in supramolecular recognition.

For instance X-ray diffraction analysis of compound **3b**, endowed with a large solvophobic basket-like cavity defined by two C_{20} hydrocarbon chain loops, revealed an auto-complexing ability culminated in the formation of a *trio* of molecules as a brick unit.

To indentify the supramolecular interaction involved, the aggregates have been investigated by UV-vis spectroscopy in solution and in binary (THF/H_2O) solution, **3b** exhibits a strong tendency to self-aggregation, provided that the Hildebrand polarity index, δ, of the solvent is higher than about 15.

The optimal behavior of the resorc[4]arene **3b** in the self-assembly process suggested us to promote its supramolecular interaction with fullerenes C_{60} and C_{70} as guests.

Preliminary studies on the ability of **3b** to form as host stable complexes with C_{60} and C_{70} revealed that the resocarene has to

undergo crucial conformational modifications to allow the insertion of the fullerene spheres inside the solvophobic cavity. The energetic data, coming from a molecular modeling investigation, are in agreement with the experimental results obtained by UV measurements. The small gap of -3 Kcal mol^{-1} is probably due to the fact that vibrational contributions have been omitted (see Table 3.5). Notably, if we consider the difference of stability between the two **3b**:C$_{60}$ and **3b**:C$_{70}$ complexes (i.e., ΔΔG° (**3b**:C$_{60}$)-(**3b**:C$_{70}$), the gap between theoretical and experimental values is reduced to only 0.2 Kcal mol^{-1}.

Table 3.5 Theoretical and experimental values of the difference of stability between the two **3b**:C$_{60}$ and **3b**:C$_{70}$ complexes (i.e., ΔΔG° (**3b**:C$_{60}$)-(**3b**:C$_{70}$).

	3b:C$_{60}$	3b:C$_{70}$	ΔΔG°(3b:C$_{60}$)-(3b:C$_{70}$)	
			Calculated	Experimental
ΔH° (Kcal mol^{-1})	-22.76	-22.36		
ΔS° (Kcal mol^{-1} K^{-1})	-0.0653	-0.0652	-0.38	-0.15
ΔG° (Kcal mol^{-1})	-3.62	-3.24		

In the *1,2-alternate* stereoisomer **1c** the four substituents have an *rctc* distribution pattern, *i. e.* three hydrocarbon chains (at C-2, C-8 and C-20) form the lower rim of the macrocycle together with the aromatic rings *C* and *D*, whereas the fourth one (at C-14) points up as *A* and *B* aromatic rings do.

Two products, **2c** (yellow solid, 15% yield) and **3c** (white solid, 26% yield) were isolated, after the usual metathesis reaction. The former showed in proton and carbon NMR spectra the chemical changes, which accounted for a successful metathesis reaction, and the same distribution pattern of the remaining signals as in the starting **1c**, which excluded conformational changes. In the EIMS spectrum of **2c** the two main monoisotopic monocharged peaks at 1408 $[M + Na]^+$ and 2793 $[2M + Na]^+$ which correspond to M = 1384 D. These same peaks are shifted in the mass spectrum of the reduction (10% H_2/Pd) product **2cr** to 1412 and 2781, respectively, in agreement with M = 1388. These findings, as compared with those of the dimer **3a** and **4b** or the trimer **5b**, obtained from the other stereoisomers, suggest that **2c** is a linear polymer of n units, where the two peaks represent the pseudo-molecular ions of one and two units. The molecular weight of **2c** remains anyway undetermined as nM, where n is >4 (*vide infra*). The absence of proton and/or carbon signals of the terminal $=CH_2$ requires that n is so large that these signals become insignificant or that **2c** is a cyclic oligomer. The mass spectrum of **3c** (main peaks again at 1408 and 2793 *m/z*) is apparently coincident with that of **2c**. By contrast in the NMR spectra the signals for the aromatic rim (including the methoxyl groups) are doubled, as well as the equivalent resonances for the C-8/C-20 methine bridges and relative CH_2COOCH_2 residue. These findings testify the loss of the

symmetry plane (passing through C-2 and C-14 carbons) of the molecule, a result that can be easily envisaged by the formation of an alkene ring between the C-2/C-8 or C-2/C-20 chains. The two uncyclized chains (C-20 and C-14 or C-8 and C-14) of these **4c**-type intermediates, enantiomeric each other, lie approximately in perpendicular planes (defined by C-2/C-14 and by C-8/C-20 pairs) and can be imagined at the origin of a similar polymerization that we may define angular. Looking again at the mass spectrum, we discovered a small cluster of peaks relative to a monoisotopic double charged ion at 2100 *m/z* corresponding to $[3M + 2Na]^{+2}$. The ion is flanked by the expected isotopic peaks (at 0.5 *m/z* distances) and by peaks corresponding to the loss of CH_2 (at 7 *m/z* distances). We assigned thus **3c** (mw 4152 D) the structure of a macro-triangle having at each summit the 1,2-alternate aromatic rim, decorated with a 20-elements alkene ring, and as sides a 20-elements alkene line connection.

Elucidation structure studies are in progress.

Acknowledgements